



Review

Fundamental Aspects and Comprehensive Review on Physical Properties of Chemically Grown Tin-Based Binary Sulfides

Sreedevi Gedi ¹, Vasudeva Reddy Minnam Reddy ^{1,*}, Tulasi Ramakrishna Reddy Kotte ², Chinho Park ¹ and Woo Kyoung Kim ^{1,*}

¹ School of Chemical Engineering, Yeungnam University, 280 Daehak-ro, Gyeongsan 38541, Korea; drsrvi9@gmail.com (S.G.); chpark@ynu.ac.kr (C.P.)

² Department of Physics, Sri Venkateswara University, Tirupati 517 502, India; ktrkreddy@gmail.com

* Correspondence: drmvasudr9@gmail.com (V.R.M.R.); wkim@ynu.ac.kr (W.K.K.)

Abstract: The rapid research progress in tin-based binary sulfides ($\text{Sn}_x\text{S}_y = \text{o-SnS}$, c-SnS , SnS_2 , and Sn_2S_3) by the solution process has opened a new path not only for photovoltaics to generate clean energy at ultra-low costs but also for photocatalytic and thermoelectric applications. Fascinated by their prosperous developments, a fundamental understanding of the Sn_xS_y thin film growth with respect to the deposition parameters is necessary to enhance the film quality and device performance. Therefore, the present review article initially delivers all-inclusive information such as structural characteristics, optical characteristics, and electrical characteristics of Sn_xS_y . Next, an overview of the chemical bath deposition of Sn_xS_y thin films and the influence of each deposition parameter on the growth and physical properties of Sn_xS_y are interestingly outlined.

Keywords: o-SnS; c-SnS; SnS_2 ; Sn_2S_3 ; CBD; solar cells



Citation: Gedi, S.; Minnam Reddy, V.R.; Kotte, T.R.R.; Park, C.; Kim, W.K. Fundamental Aspects and Comprehensive Review on Physical Properties of Chemically Grown Tin-Based Binary Sulfides. *Nanomaterials* **2021**, *11*, 1955. <https://doi.org/10.3390/nano11081955>

Academic Editor: Vlad Andrei Antohe

Received: 20 June 2021
Accepted: 26 July 2021
Published: 29 July 2021

Publisher's Note: MDPI stays neutral with regard to jurisdictional claims in published maps and institutional affiliations.



Copyright: © 2021 by the authors. Licensee MDPI, Basel, Switzerland. This article is an open access article distributed under the terms and conditions of the Creative Commons Attribution (CC BY) license (<https://creativecommons.org/licenses/by/4.0/>).

1. Introduction

To make a significant contribution to the energy needs of society with low production cost, thin film photovoltaic (TFPV) technology has been developed. Currently, the CdTe/CdS and Cu(In,Ga)Se₂(CIGS)/CdS heterojunction TFPV technologies have received worldwide attention because these solar cells achieved record efficiencies of 22.1% [1] and 23.35% [2], respectively. However, their wider impact is hindered due to major concerns raised on the presence of harmful elements (Cd and Se) and scarcity of constituent elements (Te, In and Ga). In view of that, considerable efforts have been made to develop environmentally friendly absorbers and buffers that are free from the aforementioned toxic and inadequacy elements. Along this path, the tin-based binary sulfides (Sn_xS_y) such as tin monosulfide (orthorhombic (ORT)-SnS and cubic (CUB)-SnS), tin disulfide (SnS_2), and tin sesquisulfide (Sn_2S_3) have drawn much attention because these are abundant, inexpensive, and nontoxic [3]. According to the merits of Sn_xS_y (see Table 1), the o-SnS, c-SnS, and Sn_2S_3 are strongly expected as potential and alternative absorbers to the conventional CdTe and CIGS, and SnS_2 is expected as an appropriate and alternative buffer to the regular CdS. Furthermore, their simple composition and promising physical properties made them suitable for other applications such as photocatalytic, thermoelectric, etc. (see Figure 1). Among Sn_xS_y , o-SnS, SnS_2 , and Sn_2S_3 occur naturally, whereas c-SnS was synthesized in the laboratory. The historical information and the applications of Sn_xS_y available in the literature are presented in Table 2.

The deposition of Sn_xS_y in thin film form became prominent owing to their wide applications. The selection of deposition technique along with the growth conditions is critical because the properties of Sn_xS_y thin films are susceptible to their growth method. Sn_xS_y films should be prepared by low-cost techniques such as solution processes to further reduce the production cost of TFPV devices. The preparation of Sn_xS_y thin films via chemical methods, especially by chemical bath deposition (CBD), includes a slightly

low cost and is, in fact, unchallenging on the preparation side. In addition, CBD provides several experimental flexibilities such as non-vacuum thin-film deposition, a wide selection of various substrates, easy doping of elements, and room temperature film growth, which are suitable for the large-scale fabrication of flexible devices for industrial applications.

The deposition of Sn_xS_y thin films using CBD is relatively new, and their process–property relationships must be understood for the desired application. Further, the formation of single-phase o-SnS, c-SnS, SnS_2 , and Sn_2S_3 thin films in CBD is highly dependent on preparative conditions. In addition, identification and separation of the o-SnS, c-SnS, SnS_2 , and Sn_2S_3 phases are also critical criteria. However, there is a lack of comprehensive studies on the optimization of growth parameters until now. Therefore, extensive research studies on the growth, deposition mechanism, and preparative parameters that affect phase separation and the physical properties of Sn_xS_y thin films are crucial to a successful device design in the production of clean energy.

In this scenario, the present article provides an overview of the bulk properties of Sn_xS_y and a comprehensive review of the deposition, growth mechanism, and effect of growth parameters on the physical properties of Sn_xS_y thin films. According to the authors' knowledge, this is the first review of Sn_xS_y thin films by CBD.

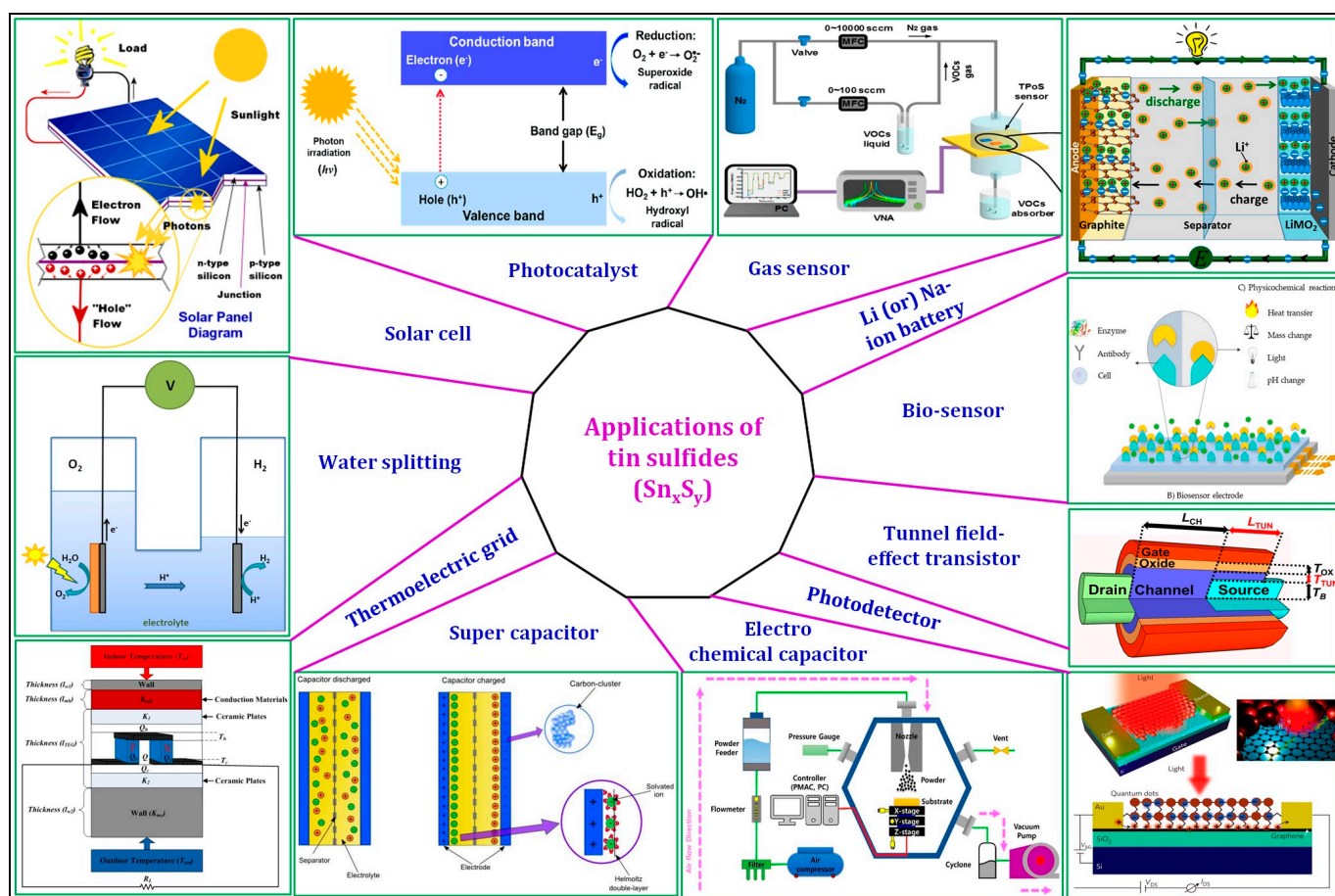





Figure 1. Applications of Sn_xS_y [4–12]. Solar cell (o-SnS, c-SnS, Sn_2S_3 as light absorber and SnS_2 as buffer); photodetector (o-SnS, c-SnS, Sn_2S_3 as light absorber and SnS_2 as buffer); Li- and Na-ion batteries (o-SnS, c-SnS, and SnS_2 as anode materials); gas- and bio sensors (o-SnS, c-SnS, and SnS_2 as sensing materials); tunnel field-effect transistors (TFET) (o-SnS, c-SnS, and SnS_2 as top or back gates); electrochemical and super capacitors (o-SnS, c-SnS, and SnS_2 as electrode materials); capacitor; thermoelectrics (o-SnS, c-SnS, and Sn_2S_3 as grids); and water-splitting (o-SnS, c-SnS, and SnS_2 as photocathodes).

Table 1. The advantages of Sn_xS_y compared to the conventional absorbers (CdTe, CIGS, and CZTS) and the buffer (CdS).

Characteristics	PV Absorbers					PV Buffers		
	CdTe	CIGS	CZTS	o-SnS	c-SnS	Sn_2S_3	CdS	SnS_2
Earth abundance	No	No	Yes	Yes	Yes	Yes	Yes	Yes
Eco-friendly	No	No	Yes	Yes	Yes	Yes	No	Yes
Band gap (eV)	1.45–1.5 eV [13]	1.1–1.5 [14]	1.0–1.5 [15]	1.16–1.79 [16–23]	1.64–1.75 [24–29]	0.95–2.03 [30–34]	2.35–2.50 [14,35]	2.04–3.30 [36–41]
Absorption coefficient	$>10^4$	10^5	$>10^4$	10^5	10^5	10^4	–	–
Conductivity type	p-type	p-type	p-type	p-/n-type	p-type	p-/n-type	n-type	n-type
Carrier density (cm^{-3})	10^{14} – 10^{17} [35]	10^{12} – 10^{18} [14]	10^{16} – 10^{18} [42]	10^{11} – 10^{18} [43–49]	10^{11} – 10^{18} [29,50,51]	10^{14} – 10^{16} [45,52,53]	10^{12} – 10^{18} [14,35]	10^{13} – 10^{17} [54–56]
Structure	Zinc blend [13]	Chalcopyrite [14]	Kesterite [57]	Orthorhombic [58,59]	Cubic [60]	Orthorhombic [51]	Hexagonal [35]	Hexagonal [61]
Maximum theoretical efficiency (%)	~29	~29	31 [62]	31 [63]	>25 [64]	–	–	–

Table 2. The historical information and the applications of Sn_xS_y .

Tin Sulfides	Mineral Form [65–67]	Appearance [68]	Other Names	Discovered/Reported [69,70]	Applications [24,71–91]
o-SnS	 Herzenbergite	Black color with dark red–brown internal reflections.	Kolbeckine	Reported by Ramdohr from the Maria-Teresa mine (Oruro, Bolivia) in 1934.	PV, photodetectors [24], photocatalysts [71], water splitting [72], supercapacitors [83], field-effect transistors [85], sodium-ion and lithium-ion batteries [86,87], gas sensors [88], biosensors [89] thermoelectric [90], and electro chemical capacitors [91].
SnS_2	 Berndtite	Pale yellow with intense brownish to yellow–orange internal reflections.	Mosaic gold	Discovered at the Stiepelmann mine in Arandis, Namibia, as described by Ramdohr in 1935.	PV, photocatalysts [73], water splitting [74], supercapacitors [75], field-effect transistors [76], lithium-ion and sodium-ion batteries [77,78], gas sensors [79], thin film diodes [80], and high-speed photodetectors [81].
Sn_2S_3	 Ottemanite	Gray with orange–brown internal reflections.	–	Reported by Moh from the Cerro de Potosi mine (Bolivia) in 1964.	PV, optoelectronic [82], thermoelectric and IR detectors [84].

2. Physical Properties of o-SnS, c-SnS, SnS_2 , and Sn_2S_3

The physical properties such as structural, optical, and electrical properties of Sn_xS_y can significantly influence the device's performance. The crystal structure of a material can influence its optical and electrical properties, which can affect the material-related device performance [92]. Understanding and obtaining knowledge on the electronic band structure and optical characteristics of Sn_xS_y is essential before using them for device applications because the main optical parameter, band gap energy (E_g), is very sensitive to the crystal structure and defects, which directly influences the performance of a PV device. Electrical characteristics such as conduction type, resistivity, carrier concentration, and mobility of Sn_xS_y play a key role in achieving high-performance photovoltaic devices. These electrical properties critically depend on the formation of defects in Sn_xS_y . There-

fore, a good understanding of the physical properties is required for the development of effective devices.

2.1. Crystal Structure and Structural Characteristics

In o-SnS, c-SnS, SnS₂, and Sn₂S₃, Sn exhibits '2+' (divalent Sn(II)) or/and '4+' (tetravalent Sn(IV)) oxidation states (Table 3). The capability of Sn to elect different oxidation states is the origin of structural diversity/different structures (Figure 2a) of resulting compounds [93]. o-SnS (α -SnS, space group, Pnma- D_{16}^{2h}) and c-SnS (π -SnS, space group, P2₁3) are the two polymorphic forms of SnS, resulting from distortions in the crystal lattice depending on growth conditions. The o-SnS consists of a double layer of Sn and S atoms (two-dimensional SnS sheets) with zigzagged chains in which each Sn atom bonds to two S atoms in the b–c plane of the layer with a bond length of 2.671 Å and one additional S atom at a short bond length of 2.633 Å perpendicular to the plane (along a-axis) in the layer stack. The interlayer bond length of Sn–Sn atoms is 3.48 Å, and the distance between the layer stacks is 2.79 Å. The lone pair of 5s² in the Sn atom occupies the fourth coordination site and weakens interaction along the b-axis. In the case of c-SnS, each Sn atom bonds with three nearest S atoms at 2.7 Å and forms a trigonal pyramidal environment, with the Sn–S bond at the trigonal base and the 5s² lone pair pointing toward the apex. The stereo chemical activity of Sn(II) 5s² lone pair creates a highly distorted internal structure of c-SnS. The local coordination in c-SnS is similar to o-SnS; however, a three-dimensional network is formed by a covalent bond [60]. Additionally, SnS also exhibits some of other polymorphs [94] such as, β -SnS (formed at T > 880 K), γ -SnS [95], δ -SnS [96,97], RS-SnS (rock salt-SnS, Fm $\bar{3}$ m) [98]. One key point is that c-SnS and RS-SnS belong to the cubic crystal system. Further, c-SnS is a simple cubic lattice type, and RS-SnS is a face-centered cubic lattice (important note: the structure of c-SnS was incorrectly assigned as ZB-SnS previously in the literature. To avoid confusion in the literature, the readers should replace ZB-SnS with c-SnS in previous literature). More details can be found in the literature clarifying these assignments [28,93,99,100]. Furthermore, the weak interactions between distorted lone pair of 5s² in Sn and neighboring S form the metastable SnS crystals or polymorphs of SnS [101].

Next, the SnS₂ adopts a layered hexagonal structure with P $\bar{3}$ m1 space group, similar to the structure of the CdI₂ system. In this structure, the layers are arranged in the b–c plane, which is perpendicular to the a-axis, and each layer is composed of S, Sn, and S atomic parallel monolayers. Each Sn atom forms bonds in an octahedral environment with six S atoms, similar in rutile SnO₂ structure [93]. It has a symmetric edge-sharing Sn(IV)S₆ octahedral with 2D planes that are separated by weak van der Waals interaction between 3.6 Å distant S atoms [61]. Finally, the Sn₂S₃ exhibits an orthorhombic crystal structure similar to o-SnS with the same space group of Pnma. It contains tetravalent (4+) and divalent (2+) Sn atoms in equal proportions, and they form Sn(IV)S₆ octahedral 1D chains covered by Sn(II) tetrahedral [51]. The lone pair in Sn(II) occupies one coordination site as in the ground state form of o-SnS. These lone pairs are responsible for weak interchain interactions. The optimized theoretical lattice parameters along with experimental values for all these Sn_xS_y phases are presented in Table 3. The structural characterization of Sn_xS_y thin films is generally performed by X-ray diffraction (XRD). The standard XRD patterns of o-SnS, c-SnS, SnS₂, and Sn₂S₃ (Figure 2b) showed the highest intensity for peaks located at 2 θ of: 31.53°, 26.63°/30.84°, 15.03°, and 21.49°, arising from diffraction from (111), (222)/(400), (001), and (130) planes, respectively [25,28,102–104].

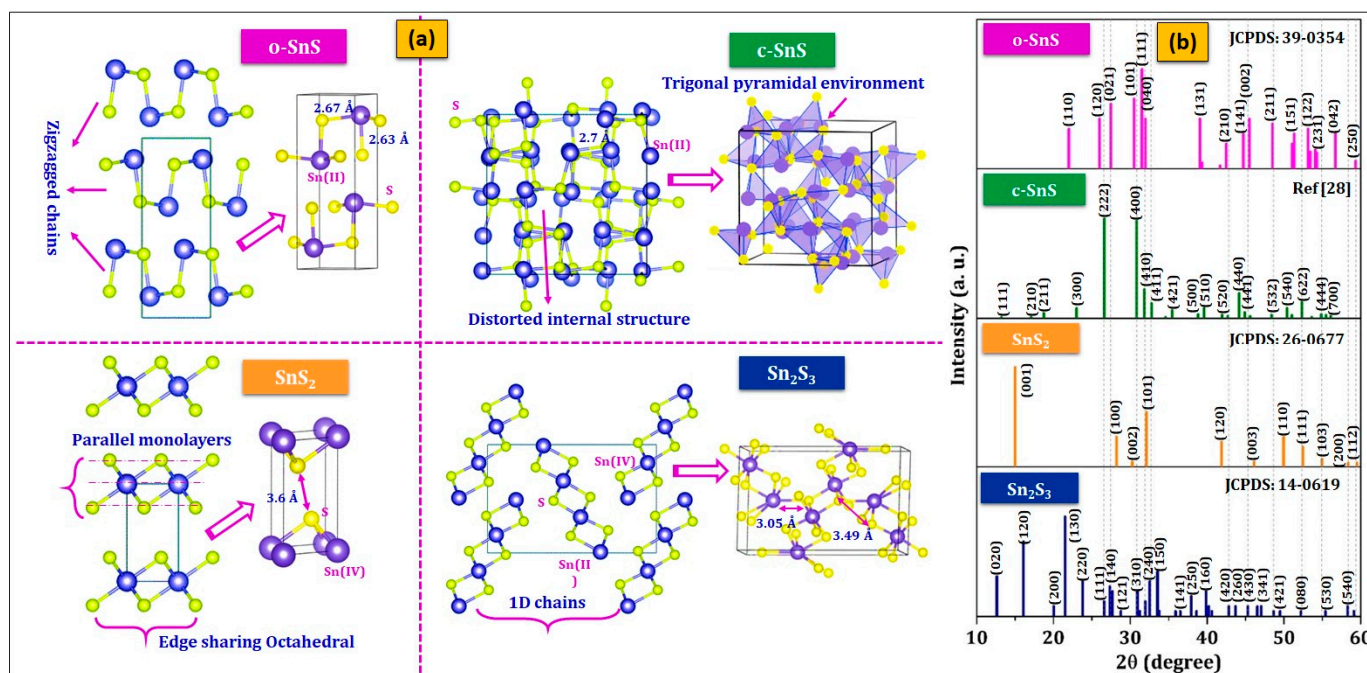


Figure 2. (a). Crystal structures of ground state Sn_xS_y forms (reprinted with permission [51] © 2017, Royal Society of Chemistry) and (b) standard powder diffraction patterns for Sn_xS_y .

The o-SnS, c-SnS, SnS₂, and Sn₂S₃ thin films have similarities in XRD patterns (Figure 3a). Thus, clear differentiation of one phase to another is difficult by using diffraction analysis alone. In this respect, it is preferable to identify these phases in pure form using a complementary method such as Raman spectroscopy because the Raman spectrum is sensitive to mainly crystal quality, structural symmetry, and strength of the chemical bond between atoms [105]. The o-SnS has 21 optical vibrational modes with the irreducible representation of $\Gamma = 4A_g + 2B_{1g} + 4B_{2g} + 2B_{3g} + 2A_u + 4B_{1u} + 2B_{2u} + 4B_{3u}$ [106,107]. In these phonons, two are inactive ($2A_u$), seven are infrared-active ($3B_{1u}$, $3B_{3u}$, and $1B_{2u}$), and twelve are Raman-active ($4A_g$, $2B_{1g}$, $4B_{2g}$, and $2B_{3g}$). In the case of c-SnS, there are 189 optic branches, and they can be reduced to 3 in the form of $\Gamma = 16A + 16E + 47T$ [51]. Next, the SnS₂ has six vibrational modes with the irreducible representation, $\Gamma = A_{1g} + E_g + 2A_{2u} + 2E_u$ [108]. The six optic modes are divided into two Raman-active modes (A_{1g} and E_g), two infrared-active (A_{2u} and E_u), and two acoustic modes (A_{2u} and E_u). Additionally, the Sn₂S₃ has 57 optic modes with reduced form of $\Gamma = 10A_g + 5A_u + 5B_{1g} + 9B_{1u} + 10B_{2g} + 4B_{2u} + 5B_{3g} + 9B_{3u}$ [51,109]. The simulated Raman spectra [51] (Figure 3b) clearly showed the significant differences in frequencies and spectral intensities because the o-SnS, c-SnS, SnS₂, and Sn₂S₃ phases have differences in structure and bonding. The Raman spectrum of the o-SnS showed three prominent peaks at 160 cm^{-1} (narrow mode, B_{2g}), 189 cm^{-1} (highest intensity mode, A_g), and 220 cm^{-1} (narrow mode, A_g). The spectrum also showed a weak A_g mode at approximately 92 cm^{-1} , which has a narrow line width up to room temperature. In the case of c-SnS, there are three strong A phonon modes at 174 cm^{-1} , 187 cm^{-1} , and 202 cm^{-1} and two prominent E modes at 166 cm^{-1} and 183 cm^{-1} along with a group of weak modes in between the ranges of $50\text{--}125\text{ cm}^{-1}$ and $200\text{--}250\text{ cm}^{-1}$. Next, the SnS₂ showed a single and strong mode at 305 cm^{-1} (A_g), which has a constant line width with the temperature. Furthermore, the Sn₂S₃ showed a significantly high-intensity A_g mode at 291 cm^{-1} and a moderate-intensity A_g mode at 300 cm^{-1} with a narrow line width. Its spectrum also showed weak modes at 182 cm^{-1} , 210 cm^{-1} , 226 cm^{-1} , 244 cm^{-1} , and 252 cm^{-1} , which are observed at high temperatures. Notably, the Raman mode of Sn₂S₃ (307 cm^{-1}) overlaps marginally with the active mode of SnS₂ (310 cm^{-1}). However, the phase can be easily identified based on the band width of modes. Sn₂S₃ has a band width that is significantly

greater than that of SnS₂ (Figure 3b). From the experimental Raman spectra (Figure 3c), o-SnS, c-SnS, SnS₂, and Sn₂S₃ films showed Raman active modes at 93 cm⁻¹, 161 cm⁻¹, 192 cm⁻¹, and 218 cm⁻¹ [110]; 59 cm⁻¹, 71 cm⁻¹, 90 cm⁻¹, 112 cm⁻¹, 123 cm⁻¹, 176 cm⁻¹, 192 cm⁻¹, 202 cm⁻¹, and 202 cm⁻¹ [111]; 224 cm⁻¹ and 310 cm⁻¹ [112]; and 61 cm⁻¹, 91 cm⁻¹, 179 cm⁻¹, 220 cm⁻¹, and 307 cm⁻¹ [113], respectively, which matched well with theoretically calculated data. The Raman results suggested that o-SnS, c-SnS, SnS₂, and Sn₂S₃ phases have distinct modes. Moreover, S-rich impurity phases can easily be found in SnS due to the sharp Raman mode of SnS₂ (310 cm⁻¹).

2.2. Electronic Band Structure and Optical Characteristics

According to the electronic band structures of Sn_xS_y (Figure 3d), the valence band maxima (VBM) of o-SnS, c-SnS, and Sn₂S₃ are formed mostly of S 3p and Sn 5s hybrid states with a tiny contribution from Sn 5p states, whereas SnS₂ is primarily composed of S 3p orbitals. The conduction band minimum (CBM) of SnS₂ and Sn₂S₃ is formed by the Sn 5s bands, whereas SnS is mainly composed of Sn 5p orbitals. The VBM of SnS₂ is lower than those of o-SnS, c-SnS, and Sn₂S₃; however, the CBMs of all o-SnS, c-SnS, SnS₂, and Sn₂S₃ are almost aligned. The partial hybridizations with S 3s and Sn 5p states result in SnS polymorphs due to the change in density of state.

On the other hand, the band-edge positions deviated from the special points in the reciprocal space except for the CBM of Sn₂S₃. However, they fall between the Brillouin zone center and the zone boundaries [64,114]. From the ab initio band-structure calculations and Kohn–Sham density-functional theory, o-SnS and c-SnS exhibited the indirect and direct energy gaps of 1.6 eV and 1.8 eV; and 1.72 eV and 1.74 eV, respectively, which is due to an inherent error in calculating band structure [58]. The energy difference between direct and indirect band gaps is small; thus, the change in the nature of the band gap could be due to the effect of temperature through thermal expansion and electron-phonon coupling [64]. According to the band-structure calculations from the Hartree–Fock exchange HSE06 functional technique, o-SnS, SnS₂, and Sn₂S₃ showed indirect energy gaps of 1.11 eV, 2.24 eV, and 1.09 eV, respectively [115]. The optical characterization of Sn_xS_y thin films is generally studied by a UV-Vis-NIR spectrometer. Although theoretical calculations showed the indirect band gap energy of Sn_xS_y, most of the experimental studies (Figure 3e) proved that Sn_xS_y thin films have direct band gap energies, with the following ranges (Tables 4 and 5): 1.16–1.79 eV; 1.64–1.75 eV; 2.04–3.30 eV; 0.95–2.03 eV; for o-SnS, c-SnS, SnS₂, and Sn₂S₃, respectively. The band gap energies of these phases depend on various factors such as strain, sulfur impurities, and Sn vacancies [116–122].

2.3. Conduction Type and Electrical Characteristics

In Sn_xS_y, three types of defects, namely, (i) Sn and S vacancies (V_{Sn} and V_S), (ii) Sn and S interstitials (Sn_i and S_i), and (iii) Sn on S antisites (Sn_S) and S on Sn antisites (S_{Sn}) are commonly formed, as shown in Figure 4a. According to the defect energy concepts (Figure 4b), the formation energy of vacancies (V_{Sn(II) or Sn(IV)}, V_S) depends on the coordination number, i.e., it generally increases with increasing coordination number. Thus, V_{Sn(II)} has lower formation energy compared to V_{Sn(IV)} because the coordination number is three for Sn(II) and six for Sn(IV). As a result, V_{Sn(II)} becomes a major defect that acts as an acceptor and contributes to the p-type conducting nature to SnS. In SnS, the primary defects are V_{Sn} and V_S, whereas Sn_i and S_i have higher energies. SnS exhibits the p-type at the Sn-poor condition, whereas the n-type at the Sn-rich condition. The defect-formation energies in SnS₂ differ from those in SnS. The major defects are V_S, S_i, and S_{Sn(II)}, which are inert to carrier generation. The defect-formation energies in Sn₂S₃ are typically interpreted as a mixture of those in SnS and SnS₂. On the other hand, the formation energy of interstitials (Sn_i, S_i) associates with the gap of interlayer free spaces, and that gap follows the notation of SnS > Sn₂S₃ > SnS₂. Sn_i always prefers to locate at the center of the gaps, whereas S_i likes to make a covalent bond with neighboring S atoms. The tin interstitial, Sn_i in both SnS₂ and Sn₂S₃, has lower formation energy compared to SnS, and it acts as a deep

donor in SnS_2 and Sn_2S_3 and contributes to an n-type conductivity. All the antisites in Sn_xS_y have higher formation energies because they are correlated with chemical bonds. Therefore, these defects do not play a major role in the conduction type of Sn_xS_y phases. The electrical characterization of Sn_xS_y thin films is generally performed by the popular van der Pauw–Hall method.

From the reported electrical parameters of Sn_xS_y films (Table 3), the o-SnS has a hole density in the order of 10^{11} – 10^{18} cm^{-3} , hole mobility in the range of 4 – 500 $\text{cm}^2 \text{V}^{-1} \text{s}^{-1}$, and electrical resistivity in the range of 13 – 10^5 Ωcm . In contrast, the c-SnS has a hole density in the order of 10^{11} – 10^{18} cm^{-3} , hole mobility in the range of 10^{-2} – 78 $\text{cm}^2 \text{V}^{-1} \text{s}^{-1}$, and electrical resistivity in the range of 70 – 10^7 Ωcm . In the case of the SnS_2 , it has a carrier concentration of the order of 10^{13} – 10^{17} cm^{-3} , electron mobility in the range of 15 – 52 $\text{cm}^2 \text{V}^{-1} \text{s}^{-1}$, and electrical resistivity in the range of 1.11 – 10^7 Ωcm , whereas the Sn_2S_3 has a carrier density in the order of 10^{14} – 10^{16} cm^{-3} and resistivity in the range of 0.4 – 10^5 Ωcm , and a very little information related to Sn_2S_3 carrier mobility value is available in the literature. The reported variation in electrical parameters is expected due to the differences in the growth process and chemical composition.

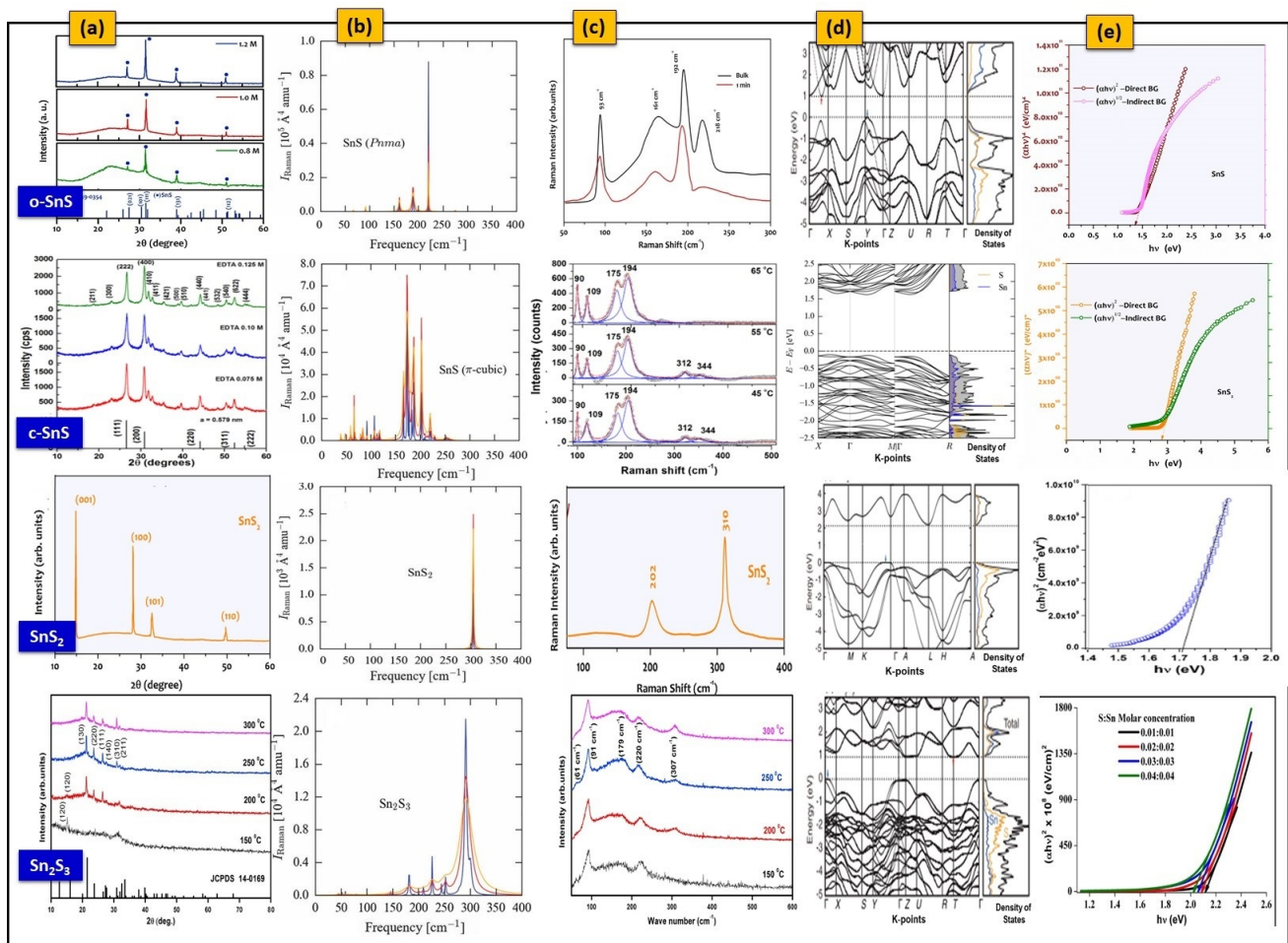


Figure 3. (a) XRD profiles of o-SnS and c-SnS (reprinted with permission [26]. © 2016, Elsevier), hexagonal SnS_2 (reprinted with permission [123]. © 2016, Elsevier), and orthorhombic Sn_2S_3 (reprinted with permission [113]. © 2016, Elsevier). (b) Simulated Raman spectra for Sn_xS_y at different temperatures of 10 K, 150 K, and 300 K (reprinted with permission [51]. © 2017, Royal Society of Chemistry). (c) Experimental Raman spectra of o-SnS (reprinted with permission [110]. © 2017, Elsevier), c-SnS (reprinted with permission [26]. © 2016, Elsevier), hexagonal SnS_2 (reprinted with permission [123]. © 2016, Elsevier), and orthorhombic Sn_2S_3 (reprinted with permission [113]. © 2016, Elsevier). (d) Band structures of Sn_xS_y (reprinted with permission [114]. © 2016, American Physical Society), and (e) bandgap estimation of o-SnS (reprinted with permission [123]. © 2016, Elsevier), c-SnS (reprinted with permission [26]. © 2016, Elsevier), hexagonal SnS_2 (reprinted with permission [123]. © 2016, Elsevier), and orthorhombic Sn_2S_3 (reprinted with permission [124]. © 2016, Sciendo).

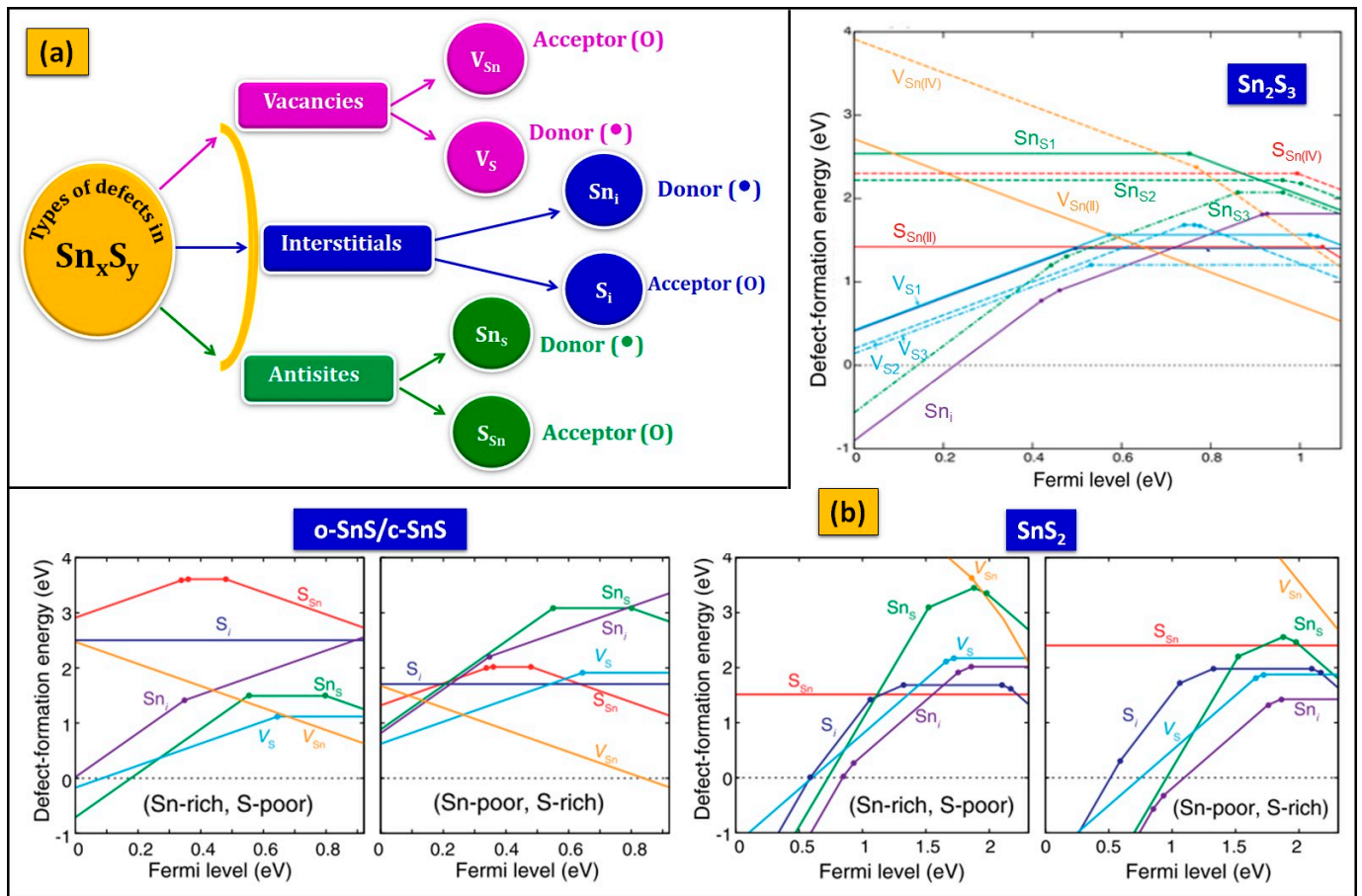


Figure 4. (a) Possibility of different defect formation in Sn_xS_y , and (b) defect formation energies in Sn_xS_y as a function of Fermi energy under Sn-rich (S-poor) and Sn-poor (S-rich) conditions (reprinted with permission [114]. © 2016, American Physical Society).

Table 3. Optimized theoretical and experimental lattice parameters, reported optical bandgaps, and electrical parameters of Sn_xS_y (Th: theoretical, Exp: experimental).

Sn _x S _y Phase	Structural Properties					Optical Properties		Electrical Properties		
	Structure (Space Group)	Oxidation State of Sn	Angles and Rule	Parameters of unit cell		Optical Band Gap (eV)	Carrier Concentration (cm ⁻³)	Mobility (cm ² V ⁻¹ s ⁻¹)	Resistivity (Ω-cm)	
				Intercepts a (Å), b (Å), c (Å)						
				Theoretical [51]	Experimental [111,125,126]					
o-SnS	Orthorhombic (Pnma)	2+	α = β = γ = 90° a ≠ b ≠ c	4.251, 11.082, 3.978	4.33, 11.18, 3.98	1.16 [16], 1.30 [17], 1.32 [18], 1.35 [19], 1.42 [20], 1.43 [20], 1.48 [21], 1.70 [22], 1.79 [23].	1 × 10 ¹¹ [43], 3.6 × 10 ¹² [44], (1–1.2) × 10 ¹⁵ [21,45], 1.5 × 10 ¹⁶ [46], (1–1.16) × 10 ¹⁷ [47,48], (1–3) × 10 ¹⁸ [49].	3.7 [20], 15.3 [46], 90 [43,49], 228 [44], 385 [19], 400–500 [17].	12.98 [17], 14.49 [20], 30 [16], 33.33 [18], 0.63 × 10 ³ [43], 2.1 × 10 ⁴ [44], (0.16–0.25) × 10 ⁵ [127,128].	
c-SnS	Cubic (P2 ₁ 3)	2+	α = β = γ = 90° a = b = c	11.506	11.603	1.64 [24], 1.66 [25], 1.67 [26], 1.73 [27], 1.74 [28], 1.75 [29].	5.87 × 10 ¹¹ [29], 7.93 × 10 ¹² [50], 6 × 10 ¹⁸ [51].	1.47 × 10 ⁻² [51], 75 [50], 77.7 [29].	70 [51], 1 × 10 ⁴ [50], 1.37 × 10 ⁵ [29], 1 × 10 ⁶ [25], 1 × 10 ⁷ [28].	
SnS₂	Hexagonal (P3ml)	4+	α = β = 90°; γ = 120° a = b ≠ c	3.651, 3.651, 6.015	3.638, 3.638, 5.880	2.04 [36], 2.12 [39], 2.14 [129], 2.18 [37], 2.30 [38], 2.35 [130], 2.40 [131], 2.41 [39], 2.44 [132], 2.45 [133] 2.50 [134], 2.67 [135], 2.75 [136], 2.80 [56], 3.08 [40], 3.30 [41].	1 × 10 ¹³ [54], 2 × 10 ¹⁷ [55], 6.8 × 10 ¹⁷ [56].	15 [54], 48 [56], 51.5 [55].	1.11 [55], 11.2 [56], 0.77 × 10 ² [137], 0.42 × 10 ⁵ [54], 0.26 × 10 ⁷ [138].	
Sn₂S₃	Orthorhombic (Pnma)	2+ and 4+	α = β = γ = 90° a ≠ b ≠ c	a ≠ b ≠ c	8.11, 3.76, 13.83	8.878, 3.751, 14.020	0.95 [30], 1.16 [31], 1.2 [139], 1.65 [32], 1.9 [33], 1.96 [140], 2.0 [141], 2.03 [34].	9.4 × 10 ¹⁴ [52] 1 × 10 ¹⁵ [45], 4.0 × 10 ¹⁶ [53].	20.5 [53]	0.359 [124], 7.57 [53], 0.66 × 10 ² [45], (0.22–0.36) × 10 ³ [52,141], (0.4–2.5) × 10 ⁵ [137].

3. Influence of Deposition Parameters on Sn_xS_y Thin Film Growth and Properties

In CBD, the selection of tin source precursor, sulfur source precursor, complexing agent, and their concentrations is crucial to prepare the high-quality Sn_xS_y thin films using CBD. Moreover, the selection of suitable activation conditions such as solution/bath temperature, solution/bath pH (acidic or basic medium), deposition time, and stirring speed is also important [36,142] because they significantly affect the phase formation, growth, and properties of Sn_xS_y films. In addition to the above parameters, the nature of the substrate and its cleaning procedure also affect the phase formation, growth, and properties of Sn_xS_y films. Therefore, the understanding of the influence of all those parameters on the growth process of Sn_xS_y films and their physical properties is necessary to deposit the quality films for device applications. In Tables 4 and 5, the deposition parameters used for different thin films of tin sulfides made from chemical methods were summarized.

3.1. Overview of CBD Process of Sn_xS_y Thin Films

The CBD refers to “a typical synthesis employing mild conditions [143]”. As schematically illustrated in Figure 5a, the experimental setup of CBD consists of the following parts: (i) magnetic stirrer with thermostat (to stir the mixed reactant solution continuously), (ii) oil bath (to maintain the desired temperature), (iii) substrate holder (to keep the substrates stable), (iv) stock chemical solutions to compose the reaction bath (mixture of different reagent solutions and its level always remains below the outer oil level), and (v) cleaned substrates [144]. The deposition of o-SnS, c-SnS, SnS_2 , and Sn_2S_3 by CBD was reported in 1987 [145], 2006 [146], 1990 [36,130], and 2012 [34], respectively. Sn_xS_y films were deposited using various Sn precursors such as tin (II) chloride dihydrate ($\text{SnCl}_2 \cdot 2\text{H}_2\text{O}$), tin(IV) chloride pentahydrate ($\text{SnCl}_4 \cdot 5\text{H}_2\text{O}$), and tin ingots; various S precursors such as sodium sulfide (Na_2S), ammonium sulfide ($(\text{NH}_4)_2\text{S}$), sodium thiosulfate ($\text{Na}_2\text{S}_2\text{O}_3$), thioacetamide ($\text{C}_2\text{H}_5\text{NS}$), and thiourea ($\text{CH}_4\text{N}_2\text{S}$); and various complexing agents such as triethanolamine ($\text{C}_6\text{H}_{15}\text{NO}_3$), ammonia (NH_3)/ammonium hydroxide (NH_4OH), ammonium fluoride (NH_4F), ammonium citrate ($\text{C}_6\text{H}_{17}\text{N}_3\text{O}_7$), trisodium citrate ($\text{Na}_3\text{C}_6\text{H}_5\text{O}_7$), citric acid ($\text{C}_6\text{H}_8\text{O}_7$), tartaric acid ($\text{C}_4\text{H}_6\text{O}_6$), ethylenediaminetetraacetic acid ($\text{C}_{10}\text{H}_{16}\text{N}_2\text{O}_8$), and disodium ethylenediaminetetraacetate ($\text{C}_{10}\text{H}_{14}\text{N}_2\text{Na}_2\text{O}_8$). Among the above-mentioned chemicals, tin (II) chloride, thioacetamide, and triethanolamine, along with ammonia, were widely used as Sn precursor, S precursor, and complexing agents, respectively (Figure 5b). Other types of Sn precursors such as tin ingots [130,147] and tin (IV) chloride [131] were employed to deposit the SnS_2 films. Except for the above reports, tin (II) chloride was used as an Sn source. In the case of S precursors, sodium thiosulfate was used as a second alternative to the regularly used thioacetamide.

The preparation of Sn_xS_y thin films by CBD occurs when a substrate is immersed in the solution mixture of Sn ion (Sn^{2+} or Sn^{4+})-source, S ion (S^{2-})-source, and an appropriate complexing agent. In the deposition process, the $\text{Sn}^{2+}/\text{Sn}^{4+}$ ions are complexed through the coordinated bond formation by the complexing agent, which controls the rate of reaction [148]. At super saturation condition (Ionic product, $Q_{\text{ip}} > \text{Solubility product } K_{\text{sp}}$), Sn_xS_y films can be deposited (Figure 5c). However, simply maintaining supersaturation condition in the bath will not provide acceptable quality Sn_xS_y films; managing the solubility product of tin hydroxides is required because when an Sn precursor is dissolved in water, it rapidly binds with hydroxide ions, creating $\text{Sn}(\text{OH})_2$ and $\text{Sn}(\text{OH})_4$. The differences in K_{sp} values between SnS ($1 \times 10^{-25} \text{ mol}^2 \text{ dm}^{-6}$), irrespective of the polymorphs, and SnS_2 ($1 \times 10^{-46} \text{ mol}^3 \text{ dm}^{-9}$) are very close to those between their hydroxides ($\text{Sn}(\text{OH})_2$ ($1 \times 10^{-28} \text{ mol}^3 \text{ dm}^{-9}$) and $\text{Sn}(\text{OH})_4$ ($1 \times 10^{-56} \text{ mol}^5 \text{ dm}^{-15}$)). Therefore, it is vital to monitor supersaturation with respect to an individual phase as well as the growth kinetics. In addition, the K_{sp} of Sn_xS_y is affected by the concentration of precursor, solvent type, bath temperature, and bath pH [148,149]. Therefore, the optimum condition for the deposition of Sn_xS_y thin film can be achieved by manipulating the above deposition parameters.

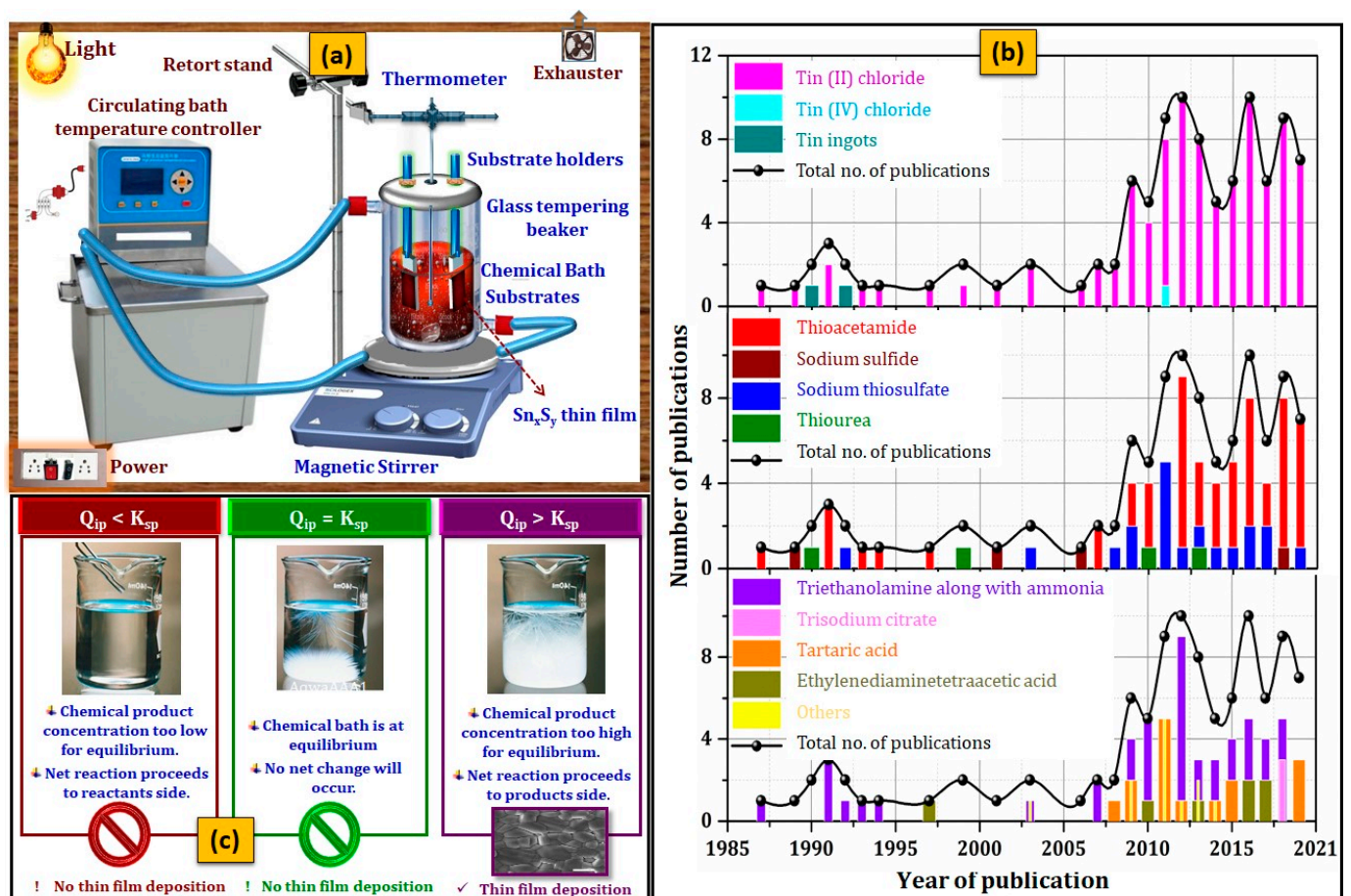
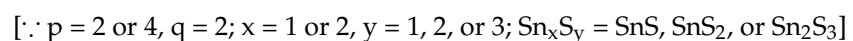
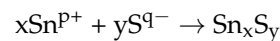


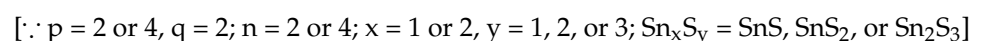
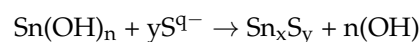
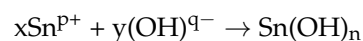
Figure 5. Schematic representation of (a) CBD, (b) main chemical reagents used for the preparation of Sn_xS_y thin films from 1987 to the present, and (c) importance of K_{sp} and Q_{ip} relation on the films by CBD.

According to previous reports, the formation of o-SnS, c-SnS, SnS₂, and Sn₂S₃ thin films is achieved through either an ion-by-ion mechanism (Figure 6a) or a simple cluster (hydroxide) mechanism (Figure 6b) based on the reaction process and parameters maintained in the bath [150]. The formation reaction of Sn_xS_y thin films through the ion-by-ion mechanism and cluster (hydroxide) mechanism is as follows:

Ion-by-ion mechanism:



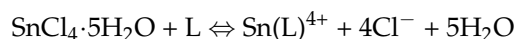
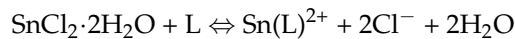
Cluster (hydroxide) mechanism:



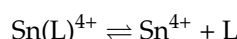
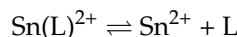
The physical properties of the CBD-deposited o-SnS, c-SnS, SnS₂, and Sn₂S₃ thin films can be affected by the growth mechanism, level of supersaturation, and surface energy of the complexing agents [17]. Therefore, it is crucial to understand the actual mechanism undertaken in the solution for tuning the properties of the deposited films. Moreover, in the process of o-SnS, c-SnS, SnS₂, and Sn₂S₃ thin film deposition, controlling the reaction to reduce or remove the spontaneous precipitation is essential, which can only be achieved by complexing the tin ions using an appropriate complexing agent (L). The

kinetics of o-SnS, c-SnS, SnS₂, and Sn₂S₃ thin film formation can be comprehended through the following reactions.

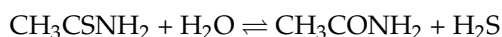
The complexing reactions in an aqueous Sn precursor solution are as follows:



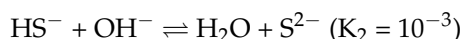
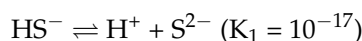
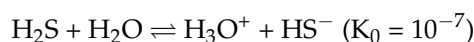
The free Sn²⁺/Sn⁴⁺ ions are slowly released by the tin complex in a controlled way. As the tin complex dissociates, then



Here, the concentration of complex tin ions in the solution, Sn(L)²⁺ or Sn(L)⁴⁺, can be controlled by adjusting the concentration of the complexing agent and bath temperature [151]. If these ions can be generated, then the deposition of Sn_xS_y thin films can be achieved. On the other hand, controlling the reaction by a slow and uniform generation of sulfur ions in the solution is also a significant factor when thin films are deposited. Thioacetamide (C₂H₅NS) is one of the most frequently employed S precursors. The hydrolysis of the S precursor can produce H₂S and then S²⁻ ions by the following reactions [152]:

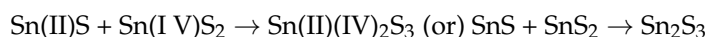
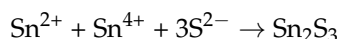


When the reaction attains an equilibrium [153], the following reactions are expected at a temperature of 25 °C:



At low pH values (<2.5), the reaction is controlled by the rate of hydrolysis of S precursor leading to the formation of hydrogen sulfide (H₂S), whereas at higher pH values (>2.5), the reaction is controlled by the formation and decomposition of the tin-thioacetamide complex. Therefore, the pH of the bath and metal-thioacetamide complexes are also considered as the growth rate- and growth mechanism-determining components in the film formation [154].

The Sn ions react with the S ions and initiate the formation of tin sulfides (o-SnS, c-SnS, SnS₂, and Sn₂S₃). The generation rate of Sn and S ions is controlled primarily by the source concentration, pH, and solution temperature. When the precursor concentration is changed, multiphase or other single-phase films can be formed by the following reactions [155,156]:



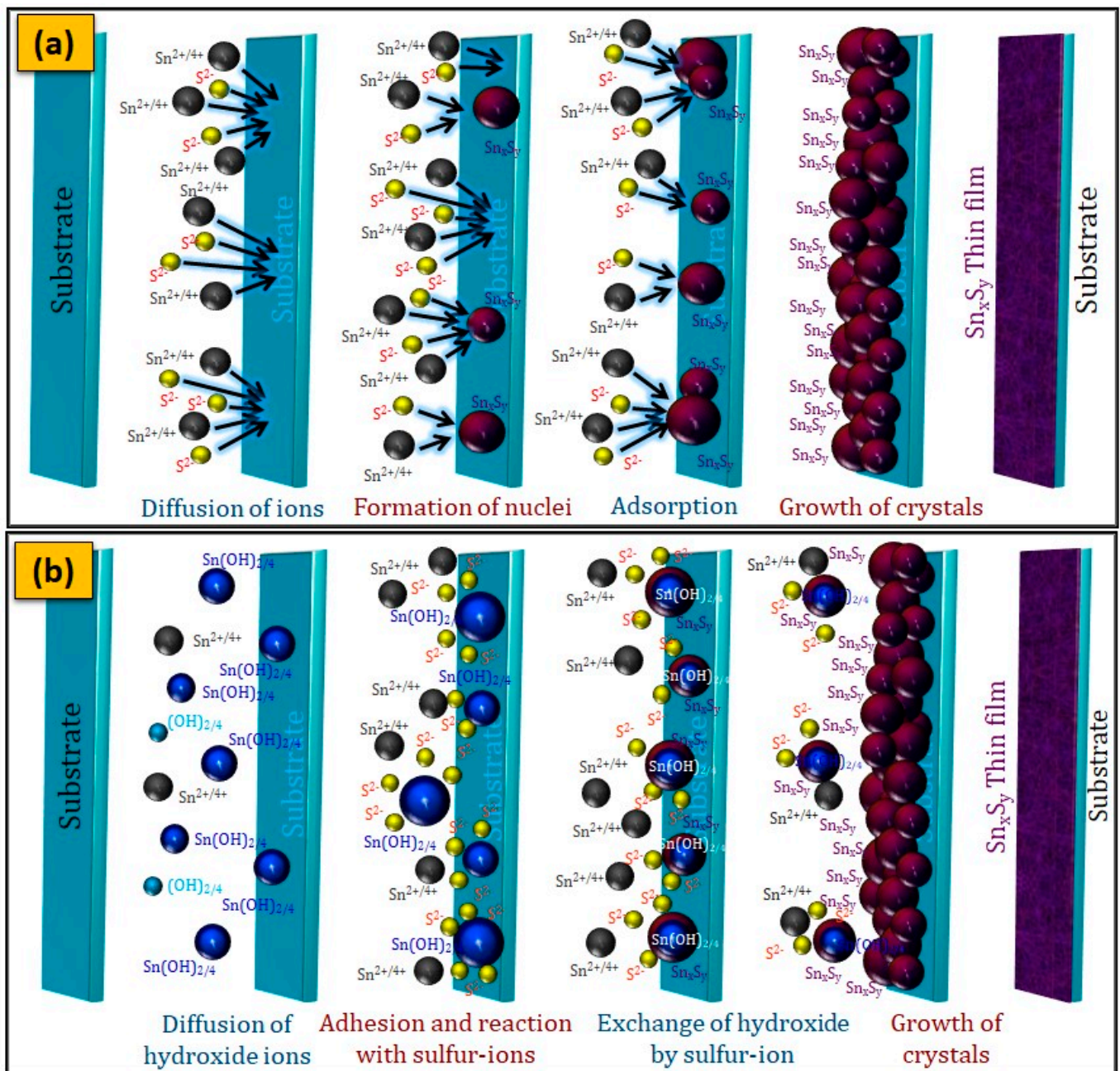


Figure 6. Schematic representation of (a) ion-by-ion mechanism and (b) cluster-by-cluster (hydroxide) mechanism.

Table 4. Deposition conditions and the physical properties of ORT- and c-SnS films grown by CBD.

Sn _x S _y Phase	Precursors	Complexing Gent	Deposition Parameters	Structure	Band Gap (eV)	Electrical Parameters				Ref
						Type	R (Ωcm)	μ (cm ² V ⁻¹ S ⁻¹)	N (cm ⁻³)	
o-SnS										
o-SnS	T(II)C = 0.1 M TA = 0.1 M	TEA = 15 mL NH ₃ = 8 mL	T _b = 27 °C t _d = 20 h pH = 10.5 ± 1	Amorphous	1.51 (i)	n	–	–	–	1987 [145]
o-SnS	T(II)C = 0.025 mol SDS/AS = 0.025 mol	–	T _b = – t _d = – pH = 3,10,12	ORT(013)	1.08	p	10 ⁷ –10 ³	–	–	1989 [36]
o-SnS	T(II)C = – TU = –	–	T _b = – t _d = – pH = –	Polycrystalline	1.3 (i)	–	–	–	–	1990 [157]
o-SnS	T(II)C = 1 g TA = 1 M	TEA = 12 mL NH ₃ = 10 mL	T _b = 75 °C, 25 °C t _d = 5 h, 40 h pH = –	Polycrystalline	1.3	p	–	–	–	1991 [128]
o-SnS	T(II)C = 2 mL TA = 1 mol L ⁻¹	TEA = 0.5 mL NH ₃ = –	T _b = 50 °C, 25 °C t _d = 2–4 h, 5–10 h pH = –	Crystalline	–	–	–	–	–	1991 [158]
o-SnS	T(II)C = 1 g TA = 4 mL, 8 mL	TEA = 12 mL NH ₃ = 12 mL	T _b = 75 °C, 25 °C t _d = 5 h, 40 h pH = –	–	–	–	–	–	–	1991 [159]
o-SnS	T(II)C = 1 g TA = 1 M	TEA = 12 mL NH ₃ = 10 mL	T _b = 60 °C t _d = 7 h 30 min pH = –	ORT(111)	–	–	–	–	–	1992 [160]
o-SnS	T(II)C = 1 g TA = 1 M	TEA = 12 mL NH ₃ = 10 mL	T _b = 60 °C t _d = 7 h 30 min pH = 9.5	ORT(111)	–	p	–	–	–	1993 [161]
o-SnS	T(II)C = 1 g TA = 1 M	TEA = 12 mL NH ₃ = 13 mL	T _b = 50–75 °C, t _d = 1.5 h, 20 h pH = –	ORT(111)	–	p	–	–	–	1994 [162]

Table 4. Cont.

Sn _x S _y Phase	Precursors	Complexing Gent	Deposition Parameters	Structure	Band Gap (eV)	Electrical Parameters				Ref
						Type	R (Ωcm)	μ (cm ² V ⁻¹ S ⁻¹)	N (cm ⁻³)	
o-SnS										
o-SnS	T(II)C = 15 g TU = 5 g, 10 g	-	T _b = - t _d = 5 min pH = 3 S _p = 1.33 mm/s	ORT(040)	1.4	-	-	-	-	1999 [163]
o-SnS	T(II)C = 0.1 M SDS = 0.05 M	-	T _b = 80 °C t _d = - pH = 12	-	-	p	-	-	-	2001 [164]
o-SnS	T(II)C = 1.125 g ST = 2 M	AF	T _b = T _r t _d = 18 h pH = 7	ORT(111)	1.38 (d) 0.96–1.14 (i)	-	-	-	-	2003 [165]
o-SnS	T(II)C = 1 g TA = 8 mL	TEA = 12 mL NH ₃ = 10 mL	T _b = 35 °C t _d = 15 h pH = 9.5	ORT(111)	1.18 (d)	p	10 ⁷ –10 ⁴	-	-	2003 [166]
o-SnS	T(II)C = 0.56 g SS = 0.025 M	-	T _b = 80 °C t _d = - pH = 12	ORT(111)	-	-	-	-	-	2006 [167]
o-SnS	T(II)C = 1.13 g TA = 0.1	TEA = 30 mL NH ₃ = 16 mL	T _b = RT 293–298 K t _d = 5–6 h pH = -	ORT(111)	1.17 (d) 1.12 (i)	-	10 ⁸ –10 ⁶	-	-	2007 [168]
	T(II)C = 1 g TA = 1 M	TEA = 12 mL NH ₃ = 10 mL	T _b = 308 K t _d = 20 h pH = -							
o-SnS	T(II)C = 1 g TA = 1 M	TEA = 10 mL NH ₃ = 5 mL	T _b = 45 °C t _d = - pH = -	ORT(111)	1.33–1.39 (d)	-	-	-	-	2007 [169]
o-SnS	T(II)C = 1 g TA = 8 mL	TEA = 12 mL NH ₃ = 10 mL	T _b = 55 °C t _d = 8 h pH = -	ORT(111)	-	p	10 ³	90	10 ¹¹	2008 [43]

Table 4. Cont.

Sn _x S _y Phase	Precursors	Complexing Gent	Deposition Parameters	Structure	Band Gap (eV)	Electrical Parameters				Ref
						Type	R (Ωcm)	μ (cm ² V ⁻¹ S ⁻¹)	N (cm ⁻³)	
o-SnS										
o-SnS	T(II)C = 1.12 g ST = 0.5 M	TTA = 10 mL	T _b = T _r t _d = 24 h pH = 7	ORT(111)	1.1 (d)	-	10 ⁶	-	-	2008 [170]
o-SnS	T(II)C = 1 g TA = 8 mL	TEA = 12 mL NH ₃ = 10 mL	T _b = 313 K t _d = 8–22 h pH = -	ORT(111)	1.2–1.7 (d)	p	-	-	-	2009 [171]
o-SnS	T(II)C = 0.15 M ST = 2 M	NH ₄ OH = 6 mL	T _b = 30 °C t _d = 24 h pH = 7	ORT(040)/(141)	1.31 (d)	-	-	-	-	2009 [172]
o-SnS	T(II)C = 2 × 10 ⁻² M TA = 1 × 10 ⁻² –8 × 10 ⁻² M	-	T _b = 80 °C t _d = 60 min pH = 1.87	Amorphous	-	-	-	-	-	2009 [142]
o-SnS	T(II)C = 1 g TA = 8 mL	TEA = 12 mL NH ₃ = 10 mL	T _b = 55 °C t _d = 8 h pH = -	ORT(111)	1.12 (i)	-	-	-	-	2009 [173]
o-SnS	T(II)C = 0.15 M ST = 2 M	AH = 6 mL	T _b = T _r t _d = 24 h pH = 7	ORT(111)	-	-	-	-	-	2009 [174]
o-SnS	T(II)C = - TA = -	TEA = - NH ₃ = -	T _b = 75 °C t _d = - pH = -	ORT(111)	0.82–1.22 (i)	-	-	-	-	2009 [175]
o-SnS	T(II)C TA = 0.1 M	TEA = 30 mL NH ₄ OH = 16 mL	T _b = - t _d = 5 h pH = -	ORT(111)/(040)	1.76 (i)	-	-	-	-	2010 [176]
o-SnS	T(II)C = 1 M TA = 1 M	TEA = 10 mL TSS = 5 mL NH ₃ /NH ₄ Cl = 5 mL	T _b = 60 °C t _d = 2–10 h pH = 9.31	ORT(111)/(040)	1.30–1.97 (d) 0.83–1.36 (i)	p	9.9–12.3	-	-	2010 [177]

Table 4. Cont.

Sn _x S _y Phase	Precursors	Complexing Gent	Deposition Parameters	Structure	Band Gap (eV)	Electrical Parameters				Ref
						Type	R (Ωcm)	μ (cm ² V ⁻¹ S ⁻¹)	N (cm ⁻³)	
o-SnS										
o-SnS	T(II)C = 1 M TA = 1 M	TEA = 10 mL TSS = 5 mL NH ₃ /NH ₄ Cl = 5 mL	T _b = 27 °C t _d = 24 h pH = 10.7	ORT(110)	1.37 (d) 1.05 (i)	p	10 ⁵	9 × 10 ⁵	–	2010 [178]
o-SnS	–	TEA = 12.5 M, 13 M	T _b = – t _d = – pH = –	–	1.93–2.16 (d)	–	–	–	–	2010 [179]
o-SnS	T(II)C = 0.95 g TA = 0.1 M	TEA = 8 mL NH ₃ = 6 mL	T _b = 75 °C t _d = 1 h pH = –	ORT(111)/(040)	1.3 (i)	p	–	–	–	2010 [180]
o-SnS	T(II)C = – TA = –	TEA, NH ₃ TTA	T _b = T _r , 90 °C t _d = 24 h, 3 h pH = –	ORT(400)	1.1–1.9 (d)	–	–	–	–	2011 [181]
o-SnS	T(II)C = 0.2 M ST = 0.2 M	Na ₂ EDTA = 25 mL of 0.2 M	T _b = 40–80 °C t _d = 30 h pH = 1.5	–	1.2–1.5 (d)	–	–	–	–	2011 [182]
o-SnS	T(II)C = 0.15 M ST = 0.15 M	Na ₂ EDTA = 25 mL of 0.2 M	T _b = 75 °C t _d = 150 min pH = –	–	1.2–1.6 (d)	–	–	–	–	2011 [183]
o-SnS	T(II)C = 0.1 M ST = 0.25 M	AC = 50 mL of 0.2 M	T _b = 35 °C t _d = 10 h pH = 5, 6	ORT(111)	1.75 (d) 1.12 (i)	–	–	–	–	2011 [184]
o-SnS	T(II)C = 0.1 M ST = 0.25 M	AC = 50 mL of 0.2 M	T _b = 35 °C t _d = 10 h pH = 5	ORT(111)	1.75 (d) 1.15 (i)	–	420	–	–	2011 [185]
o-SnS	T(II)C TA	TEA = – NH ₃ = –	T _b = 20–50 °C t _d = – pH = –	ORT(111)	1.15 (i) 1.35(d)	p	6.3 ± 0.1	11 ± 7	10 ¹⁶ –10 ¹⁷	2011 [186]

Table 4. Cont.

Sn _x S _y Phase	Precursors	Complexing Gent	Deposition Parameters	Structure	Band Gap (eV)	Electrical Parameters				Ref
						Type	R (Ωcm)	μ (cm ² V ⁻¹ S ⁻¹)	N (cm ⁻³)	
o-SnS										
o-SnS	T(II)C = 0.1 M ST = 0.25–0.75 M	AC = 50 mL of 0.3 M	T _b = 60–80 °C t _d = 3 h pH = 5	ORT(111)/(040))	1.01–1.26 (i)	p	10 ³	–	–	2012 [187]
o-SnS	T(II)C = – TA = –	TEA = – NH ₄ Cl = –	T _b = 45 °C t _d = 5 h pH = –	ORT(111)	0.7–1.3 (i)	–	–	–	–	2012 [188]
o-SnS	T(II)C = 1 g TA = 1 M	TEA = 12 mL NH ₃ = 10 mL	T _b = 60 °C t _d = 6 h pH = 6	ORT(111)/(101)	0.9–1.1	–	10 ⁶ –10 ¹	–	–	2012 [189]
o-SnS	T(II)C = 1 M TA = 1 M	TEA = 10 mL NH ₃ = 2 mL	T _b = RT = 27 °C t _d = 24–72 h pH = 9.7	ORT(111)	1.14–1.18 (i) 1.32–1.44 (d)	–	–	–	–	2012 [190]
o-SnS	T(II)C = 0.06 M–0.12 M TA = 0.1 M	TEA = 1.85 M NH ₃ = 1.5 M	T _b = 30 °C t _d = 90 min pH = –	ORT(040)/(111)	1.5–1.95 (d)	–	–	–	–	2012 [191]
	T(II)C = 0.1 M TA = 0.1 M	TEA = 1.75–1.90 M NH ₃ = 1.5 M	T _b = 30 °C t _d = 90 min pH = –							
	T(II)C = 0.1 M TA = 0.1 M	TEA = 1.85 M NH ₃ = 1.5 M	T _b = 40–60 °C t _d = 90 min pH = –							
o-SnS	T(II)C = 1 g TA = 1 M	TEA = 12 mL NH ₄ OH = 10 mL	T _b = 60 °C t _d = 6 h pH = –	ORT(111)	1.9 (d) 1.1 (i)	–	–	–	–	2013 [192]
o-SnS	T(II)C = 0.1 M TA = 0.6 M	TTA = 1 M	T _b = 50–70 °C t _d = 50 min pH = 1.5	ORT(111)	1.30–1.35 (d)	–	–	–	–	2013 [193]

Table 4. Cont.

Sn _x S _y Phase	Precursors	Complexing Gent	Deposition Parameters	Structure	Band Gap (eV)	Electrical Parameters				Ref
						Type	R (Ωcm)	μ (cm ² V ⁻¹ S ⁻¹)	N (cm ⁻³)	
o-SnS										
o-SnS	T(II)C = 0.05–0.2 M TA = 0.4–0.7 M	Na ₂ EDTA = 20 mL of 0.1 M	T _b = 50–80 °C t _d = 0.5–3 h pH = 9–12	ORT(200)	–	–	–	–	–	2013 [194]
o-SnS	T(II)C = 0.1 M ST = 0.3 M	Na ₂ EDTA = 5 mL of 0.1 M TSC = 5 mL of 0.66 M	T _b = T _r t _d = 24 h pH = 10	–	1.50–1.90 (d)	–	–	–	–	2013 [195]
o-SnS	T(II)C = 0.5 M TU = 1 M	NH ₃ = 3 M	T _b = T _r t _d = 60–180 min pH = –	–	1.98–2.01 (d) 1.82–1.98 (i)	p	–	–	–	2013 [196]
o-SnS	T(II)C TA = 0.1 M	TEA = 30 mL NH ₄ OH = 16 mL	T _b = – t _d = 5 h pH = –	ORT(111)/(200)	1.64–1.7 (f)	–	–	–	–	2013 [197]
o-SnS	T(II)C = 0.1 M TA = 0.1 M	EDTA = 0.05 M–0.08 M NH ₃ = 1.4 M	T _b = – t _d = 3–4 h pH = –	ORT(111)/(101)	1.5–1.60 (d)	p	400	–	–	2013 [198]
o-SnS	T(II)C = 1 g TA = 1 M	TEA = 6 mL NH ₃ = 10 mL	T _b = – t _d = – pH = –	ORT(240)	1.78–1.75 (d)	–	10 ⁹ –10 ⁸	–	–	2014 [199]
o-SnS	T(II)C = 1 g TA = 1 M	TEA = 12 mL NH ₃ = 10 mL	T _b = 20–40 °C t _d = 24 h pH = 11	ORT(111)	ORT 1.1 (i)	p	10 ⁷ –10 ²	–	–	2014 [146]
o-SnS	T(II)C = 0.5 g TA = 1 M	TEA = 6 mL TSC = 0.006–0.008 M NH ₃ = 5 mL	T _b = 30 °C t _d = 24 h pH = –	ORT(111)	1.17–1.40 (d)	–	10 ⁴	148–228	10 ¹²	2014 [44]
o-SnS	T(II)C = – TA = –	TSC = –	T _b = 50 °C t _d = 2.5 h pH = 5	ORT(111)	1.25–1.83 (d) 1.1–1.65 (i)	n	10 ³	–	–	2014 [200]

Table 4. Cont.

Sn _x S _y Phase	Precursors	Complexing Gent	Deposition Parameters	Structure	Band Gap (eV)	Electrical Parameters				Ref
						Type	R (Ωcm)	μ (cm ² V ⁻¹ S ⁻¹)	N (cm ⁻³)	
o-SnS										
o-SnS	T(II)C = 0.03 M ST = 0.03 M	TTA = 0.44 M	T _b = T _r t _d = 24 h pH = 7	ORT(400)	1.49–1.39 (i) 1.28–1.5 (i)	–	–	–	–	2014 [201]
o-SnS	T(II)C = 1 g TA = 1 M	TEA = 12 mL NH ₃ = 10 mL	T _b = 40 °C t _d = 17 h pH = –	ORT(111)	1.25–1.1 (i)	–	10 ³	–	–	2015 [202]
o-SnS	T(II)C = 0.1 M TA = 0.1 M	TEA = 15 mL NH ₃ = 8 mL	T _b = 26 °C t _d = 22 h pH = –	ORT(021)	1.76–3.32 (d)	–	–	–	–	2015 [203]
o-SnS	T(II)C = – ST = 0.01–0.09 M	TTA	T _b = 22 °C t _d = 24 h pH = 7	–	–	–	–	–	–	2015 [204]
o-SnS	T(II)C = 20 mL TA = 20 mL	TTA = 1 M	T _b = 40–80 °C t _d = 50 min pH = 1.5	–	1.33–1.41 (d)	–	–	–	–	2015 [17]
o-SnS	T(II)C = 0.1 M TA = 0.15 M	TSC = 0.2 M NH ₃ = –	T _b = 80 °C t _d = 4 h pH = 7	ORT(040)	1.65 (d)	p	–	–	–	2016 [205]
o-SnS	T(II)C = 1 g TA = 8 mL	TEA = 12 mL NH ₃ = 10 mL	T _b = 40 °C t _d = 10 h pH = 11	ORT(111)	ORT = 1.1 (i)	p	10 ⁶	–	–	2016 [25]
o-SnS	T(II)C = 0.1 M TA = 20 mL	TTA = 1 M	T _b = 70 °C t _d = – pH = –	ORT(111)	1.31–1.26 (d)	p	6–38	124	10 ¹⁵ –10 ¹⁶	2016 [144]
o-SnS	T(II)C = 1 g TA = 0.3 g	TEA = 5.5 mL NH ₃ = 5 mL	T _b = 70 °C t _d = – pH = –	ORT(002)	1.14–1.75 (d)	–	–	–	–	2016 [206]

Table 4. Cont.

Sn _x S _y Phase	Precursors	Complexing Gent	Deposition Parameters	Structure	Band Gap (eV)	Electrical Parameters				Ref
						Type	R (Ωcm)	μ (cm ² V ⁻¹ S ⁻¹)	N (cm ⁻³)	
o-SnS										
o-SnS	T(II)C = -- TA = --	TTA = 1 M	T _b = 70 °C t _d = -- pH = --	ORT(111)	1.3 (d)	p	38–14.2	55–23	10 ¹⁵ –10 ¹⁹	2016 [123]
o-SnS	T(II)C = 0.1 M TA = 0.15 M	TSC = 0.15–0.21 M	T _b = 80 °C t _d = 4 h pH = 5.8	ORT(111)	1.64–1.1 (d)	–	–	–	–	2017 [207]
o-SnS	T(II)C = 0.1 M TA = 0.15 M	TSC = 0.2 M	T _b = 80 °C t _d = 4 h pH = 6.5–7.5	ORT(111)	1.51 (d)	–	–	–	–	2018 [27]
o-SnS	T(II)C = 1 g TA = 1 M	TEA = 312 mL NH ₃ = 10 mL	T _b = 40 °C t _d = 17 h pH = 1.5	ORT(111)	1.1 (i)	–	–	–	–	2018 [208]
o-SnS	T(II)C = 4 mmol TA = 4–8 mmol	TSC = 0.15–0.21 M	T _b = 80 °C t _d = 1–2 h pH = 0.4–1.0	ORT(111)	1.39–1.41 (d)	–	–	–	–	2018 [209]
o-SnS	T(II)C = 0.1 M TA = 0.15 M	TEA = --	T _b = 343 K t _d = 120, 240, 369 min pH = 4	ORT(013)	–	–	–	–	–	2018 [210]
o-SnS	T(II)C = 20 mL TA = 20 mL	TTA = 0.6–1.6 M	T _b = 70 °C t _d = 50 min pH = --	ORT(111)	1.28–1.45 (d)	p	38–62	29–108	1.92 × 10 ¹⁵ – 4.12 × 10 ¹⁵	2019 [211]
o-SnS	T(II)C = 0.1 M TA = 0.6 M	TTA = 1 M	T _b = 40–80 °C t _d = 50 min pH = 1.5	ORT(111)	1.30–1.41 (d)	p	38	55	1.5 × 10 ¹⁵ – 3.4 × 10 ¹⁵	2019 [212]

Table 4. Cont.

Sn _x S _y Phase	Precursors	Complexing Gent	Deposition Parameters	Structure	Band Gap (eV)	Electrical Parameters				Ref
						Type	R (Ωcm)	μ (cm ² V ⁻¹ S ⁻¹)	N (cm ⁻³)	
o-SnS										
o-SnS	T(II)C = 1 g TA = 1 M	TEA = 18 mL NH ₃ = 10 mL	T _b = 40–70 °C t _d = 3 H pH = 10	ORT(040)	1.32–2.08 (d)	–	–	–	–	2019 [213]
o-SnS	T(II)C = 0.2 M TA = 0.4 M	TTA = 0.5 M	T _b = 50–80 °C t _d = 90 min pH = 1.5	ORT(040)	1.55–1.92 (d)	–	–	–	–	2019 [214]
o-SnS	T(II)C = 0.1 M TA = 0.15 M	TSC = 0.2 M	T _b = 80 °C t _d = 4 h pH = 5.0–6.5	ORT(111)	1.34–1.51 (d)	–	–	–	–	2019 [215]
o-SnS	T(II)C = 4 mmol TA = 6 mmol	–	T _b = 80 °C t _d = 120 min pH = 0.7	ORT(111)	1.41–1.49 (d)	–	–	–	–	2019 [216]
o-SnS	T(II)C = 2 g ST = 0.2 M	TEA = 70 mL CA = 0.4 M NH ₃ = 10 mL	T _b = 55 °C t _d = 4 h pH = 11	ORT(111)	1.33 (i)	–	–	–	–	2019 [217]
o-SnS	T(II)C = 20 mL TA = 10 mL PVA = 2 g	TTA = 0.5 M	T _b = 80 °C t _d = 45–90 min pH = 10	ORT(040)	1.55–1.79 (d)	–	–	–	–	2019 [218]
o-SnS	T(II)C = 0.1 M TA = 1 M	TEA = 10 mL TSC = 0.66 M	T _b = – t _d = – pH = 9.2–9.6	ORT(102)	1.36–1.99 (d)	–	–	–	–	2020 [219]
o-SnS	T(II)C = 0.1 mol TA = 0.4 mol	AA = 0.8 mL	T _b = 75 °C t _d = 70 min pH = 9.2–9.6	ORT(110)	–	–	–	–	–	2020 [220]
o-SnS	T(II)C = – TA = 0.1 M	TEA = – NH ₃ = 15 mL	T _b = 25 °C t _d = 4 h pH = – 200–600 °C	–	1.5–1.7 (d)	–	–	–	–	2021 [221]

Table 4. Cont.

Sn _x S _y Phase	Precursors	Complexing Gent	Deposition Parameters	Structure	Band Gap (eV)	Electrical Parameters				Ref
						Type	R (Ωcm)	μ (cm ² V ⁻¹ S ⁻¹)	N (cm ⁻³)	
o-SnS										
o-SnS	T(II)C = 1 g TA = 0.6 g	TEA = 12 mL NH ₃ = 15 mL	T _b = 70 °C t _d = 2 h pH = 10.93	ORT(111)	1.38 (d)	-	-	-	-	2021 [222]
o-SnS	T(II)C = 4 m mol TA = 6 m mol	-	T _b = 80 °C t _d = 120 min pH = 0.7	ORT(111)	0.78–1.13 (d)	-	-	-	-	2021 [223]
o-SnS	-	-	T _b = 65 °C t _d = 3 h pH = 5.5–8.5	ORT(111)	1.41–1.75 (d)	-	-	-	-	2021 [224]
c-SnS										
c-SnS	T(II)C = 2.26 g TA = 10 mL	TEA = 30 mL NH ₃ = 16 mL	T _b = 25 °C t _d = 6 h pH = -	CUB (111)/(200)	1.64–1.73 (d)	p	10 ⁵	10 ⁴	10 ⁹	2008 [43]
c-SnS	T(II)C = 2.26 g TA = 10 mL	TEA = 30 mL NH ₃ = 16 mL	T _b = 25 °C t _d = 6 h pH = -	CUB (111)/(200)	1.7 (d)	-	-	-	-	2009 [171]
c-SnS	T(II)C = 2.26 g TA = 10 mL	TEA = 30 mL NH ₃ = 16 mL	T _b = 25 °C t _d = 6 h pH = -	CUB (111)/(200)	1.7 (d)	-	-	-	-	2009 [173]
c-SnS	T(II)C = - TA = 0.1 M	TEA = 8964 g NH ₄ OH = 15 M	T _b = 25 °C t _d = 2–4 h 30 min pH = -	CUB (111)/(200)	1.7 (d)	-	-	-	-	2011 [225]
c-SnS	T(II)C = - TA = 0.1 M	TEA = - NH ₄ OH = 15 M	T _b = 25 °C t _d = - pH = -	-	-	-	-	-	-	2011 [226]
c-SnS	T(II)C = - TA = 0.1 M	TEA = 8964 g NH ₄ OH = 15 M	T _b = 25 °C t _d = - pH = -	CUB (111)/(200)	1.76 (d) 1.44–1.51 (d)	-	-	-	-	2012 [227]

Table 4. Cont.

Sn _x S _y Phase	Precursors	Complexing Gent	Deposition Parameters	Structure	Band Gap (eV)	Electrical Parameters				Ref
						Type	R (Ωcm)	μ (cm ² V ⁻¹ S ⁻¹)	N (cm ⁻³)	
c-SnS										
c-SnS	T(II)C = -- TA = 0.1 M	TEA = 8964 g NH ₄ OH = 15 M	T _b = 25 °C t _d = -- pH = --	CUB (111)/(200)	1.76 (d)	-	-	-	-	2012 [228]
c-SnS	T(II)C = 1 g TA = 1 M	TEA = 12 mL NH ₃ = 10 mL	T _b = 20–40 °C t _d = 24 h pH = 11	CUB (111)/(200)	1.67 (d)	p	10 ⁷ –10 ²	-	-	2014 [146]
c-SnS	T(II)C = 2.26 g TA = 0.1 M	TEA = 30 mL NH ₃ = 16 mL	T _b = 17 °C t _d = 10 h pH = --	CUB (222)/(400)	1.74 (d)	-	-	-	-	2015 [28]
c-SnS	T(II)C TA = 0.1 M	TEA = 0.1 M NH ₄ OH = 15 M	T _b = 25 °C t _d = -- pH = --	CUB(111)/(200)	1.70 (d)	-	-	-	-	2015 [229]
c-SnS	T(II)C = 2.26 g T(II)C = 0.1 M	TEA = 30 mL NH ₃ = 16 mL	T _b = 17 °C t _d = 15 h pH = 11	CUB(222)/(400)	1.73 (d)	-	10 ³	-	-	2016 [230]
c-SnS	T(II)C = 2.26 g TA = 10 mL	TEA = 30 mL NH ₃ = 16 mL	T _b = 17 °C, 10 °C t _d = 4 h, 18 h pH = 11	CUB(222)/(400)	1.66–1.72 (d)	p	10 ⁶	-	-	2016 [25]
c-SnS	T(II)C = 0.1 M TA = 0.1 M	TEA = 30 mL NH ₃ = 16 mL	T _b = 25 °C t _d = 6 h pH = 11	CUB(222)/(400)	-	-	-	-	-	2016 [231]
c-SnS	T(II)C = 2.26 g TA = 0.1 M	TEA = 30 mL NH ₃ = 16 mL	T _b = 17 °C t _d = 10 h pH = 11	CUB(222)/(400)	-	-	-	-	-	2016 [232]
c-SnS	T(II)C = 2.26 g ST = 1 M	EDTA = 20 mL of 0.5 M	T _b = 25–65 °C t _d = 6 h pH = 10.5	CUB(222)/(400)	1.74–1.68 (d)	p	10 ⁵ –10 ⁴	8.98–28.6	10 ¹² –10 ¹³	2016 [50]

Table 4. Cont.

Sn _x S _y Phase	Precursors	Complexing Gent	Deposition Parameters	Structure	Band Gap (eV)	Electrical Parameters				Ref
						Type	R (Ωcm)	μ (cm ² V ⁻¹ S ⁻¹)	N (cm ⁻³)	
c-SnS										
c-SnS	T(II)C = 2.26 g ST = 1 M	EDTA = 15–25 mL of 0.5 M NH ₃ = 5 mL	T _b = 45 °C t _d = 6 h pH = 10.5 S _p = -	CUB(222)/(400)	1.67–1.73 (d)	p	10 ⁵ –10 ⁴	0.34–28.6	10 ¹⁴ –10 ¹²	2016 [26]
c-SnS	T(II)C = 0.1 M TA = 0.15 M	TSC = 0.2 M	T _b = 80 °C t _d = 4 h pH = 7	CUB(222)/(400)	1.64 (d)	-	-	-	-	2017 [24]
c-SnS	T(II)C = 0.1 M TA = 0.1 M	TEA = 30 mL NH ₃ = 16 mL	T _b = 17 °C, 80 °C t _d = 3 h, 21 h pH = -	-	-	-	-	-	-	2017 [233]
c-SnS	T(II)C = 0.1 M ST = 0.125 M	EDTA = 0.1 M	T _b = 45 °C t _d = 6 h pH = -	CUB(222)/(400)	1.67–1.75 (d)	p	10 ⁵ –10 ⁴	5.22–77.7	10 ¹¹ –10 ¹³	2017 [29]
c-SnS	T(II)C = 0.1 M TA = 0.15 M	TSC = 0.2 M	T _b = 80 °C t _d = 4 h pH = 6.5–7.5	CUB(222)/(400)	1.64–1.73 (d)	-	-	-	-	2018 [27]
c-SnS	T(II)C = 0.1 M TA = 0.15 M	TSC = 0.2 M	T _b = 80 °C t _d = 4 h pH = 7	CUB(222)/(400)	1.5 (d)	-	-	-	-	2018 [234]
c-SnS	T(II)C = 0.5 M TA = 0.5 M	TEA = 30 mL NH ₃ = 16 mL	T _b = 35 °C t _d = 4 h pH = 9.78	CUB(222)/(400)	1.74 (d)	-	-	-	-	2018 [235]
c-SnS	T(II)C = 2.26 g TA = 0.1 M	TEA = 30 mL NH ₃ = 16 mL	T _b = 17 °C, 80 °C t _d = 3 h, 21 h pH = -	CUB(222)/(400)	1.76 (d)	-	-	-	-	2018 [236]
c-SnS	T(II)C = 2.26 g TA = 10 mL	TEA = 30 mL NH ₃ = 16 mL	T _b = 17–8 °C t _d = 3–21 h pH = -	CUB(222)/(400)						2019 [217]

Table 4. Cont.

Sn _x S _y Phase	Precursors	Complexing Gent	Deposition Parameters	Structure	Band Gap (eV)	Electrical Parameters				Ref
						Type	R (Ωcm)	μ (cm ² V ⁻¹ S ⁻¹)	N (cm ⁻³)	
c-SnS										
c-SnS	T(II)C = 0.04 M TA = 0.08 M	TEA = 1.1 M NH ₃ = 9.5 mL	T _b = 30 °C t _d = 4 h pH = -	CUB(222)/(400)	1.74 (d)	-	-	-	-	2020 [237]
c-SnS	T(II)C = 0.1 M TA = 0.15 M	TSC = 0.2 M	T _b = - t _d = - pH = -	CUB(222)/(400)	-	-	-	-	-	2020 [238]
c-SnS	T(II)C = 1 g TA = 0.3 g	TEA = 5.5 mL NH ₃ = 5 mL	T _b = 24 °C t _d = 4.25 h pH = 9.25	CUB(222)/(400)	1.70–1.74 (d)	-	10 ³ –10 ⁴	-	-	2020 [239]
c-SnS	T(II)C = 0.2 M TA = 0.1 M	TEA = 5.5 mL NH ₃ = 5 mL	T _b = 17–8 °C t _d = 3–21 h pH = 11	CUB(222)/(400)	1.76 (d)	p	10 ⁸	-	-	2020 [240]
c-SnS	T(II)C = 2.25 g ST = 0.1 M	EDTA = 0.5 M NH ₃ = 5–7.5 mL	T _b = 50 °C t _d = 6 h pH = 10.3	CUB(222)/(400)	1.75–1.8 (d)	p	10 ³ –10 ⁴	15–75	10 ¹² –10 ¹³	2020 [241]
c-SnS	T(II)C = 1 g TA = 0.6 g	TEA = 12 mL NH ₃ = 15 mL	T _b = 70 °C t _d = 2 h pH = 8.24	CUB(200)	1.72 (d)	-	-	-	-	2021 [222]
c-SnS	T(II)C = 1.21 g TA = 0.5 M	TTA = 1 M	T _b = 80 °C t _d = 2–6 h pH = 5–8	CUB(222)/(400)	1.72–1.90 (d)	-	10 ⁷ –10 ⁸	-	-	2021 [242]
c-SnS	T(II)C = 0.5 g TA = 1 M	NTA = 0.6 M	T _b = 40 °C t _d = 90–182 min pH = 10	CUB(222)/(400)	1.77–1.81 (d)	-	10 ⁶	-	-	2021 [243]
c-SnS	T(II)C = 0.01 mol TA = 0.1 M	TEA = 0.6 M	T _b = 17–8 °C t _d = 3–21 h pH = 10	CUB(222)/(400)	1.70–1.80 (d)	-	-	-	-	2021 [244]

Table 5. Deposition conditions and the physical properties of SnS₂ and Sn₂S₃ films grown by CBD.

Sn _x S _y Phase	Precursors	Complexing Agent	Deposition Parameters	Structure	Band Gap (eV)	Electrical Parameters			Ref	
						Type	R (Ωcm)	μ (cm ² V ⁻¹ S ⁻¹)		N (cm ⁻³)
SnS₂										
SnS ₂	T(II)C = 0.025 mol SDS/AS = 0.025 mol	-	T _b = - t _d = - pH = 3, 10, 12	-	2.04	SnS ₂ -n	10 ⁷ -10 ³	-	-	1989 [36]
SnS ₂	Tin-ingots (99.9%) ST = 10 mL	-	T _b = T _r t _d = 2 h pH = -	Amorphous	2.35 (d)	n	10 ³ -10 ⁴	-	-	1990 [130]
SnS ₂	Tin ingots (99.9%) ST = 10 mL	-	T _b = 27 °C t _d = - pH = 1.4	Amorphous	2.20 (i)	n	10 ⁷ -10 ⁸	-	-	1992 [147]
SnS ₂	T(II)C = 1.13 g TA = 0.1 M	EDTA = 25 mL NH ₃ = 15 mL	T _b = T _r t _d = 10-120 min pH = 10	-	2.3 (d)	n	4 × 10 ⁻¹	-	-	1997 [38]
SnS ₂	T(II)C = 15 g TU = 5 g, 10 g	-	T _b = - t _d = 5 min pH = 3 S _p = 1.33 mm/s	HEX(001)	2.05 (i)	-	-	-	-	1999 [163]
SnS ₂	TC(IV) = 0.02 mol TA = 0.5 mol L ⁻¹	CA = 0.375, 0.5, 0.625 mol/L	T _b = 35 °C t _d = - pH = 1.3	-	2.40 (d)	-	-	-	-	2011 [131]
SnS ₂	T(II)C = 1 g TA = 0.5 M	TEA = 24 mL NH ₃ = 12 mL-20 mL	T _b = 60 °C t _d = 2 h pH = -	HEX(001)	3.3-3.7 (d)	-	-	-	-	2012 [41]
SnS ₂	T(II)C = 0.8 M TA = 0.5 M	TEA = 3.75 M NH ₃ = 12 mL	T _b = 60 °C t _d = - pH = -	HEX(001)	2.8-3.0 (d)	-	-	-	-	2013 [245]
SnS ₂	T(II)C = 2.26 g ST = 1 M	EDTA = 20 mL of 0.5 M NH ₃ = 5 mL	T _b = 45 °C t _d = 6 h pH = -	HEX(001)	2.58 (d)	-	-	-	-	2017 [246]

Table 5. Cont.

Sn _x S _y Phase	Precursors	Complexing Agent	Deposition Parameters	Structure	Band Gap (eV)	Electrical Parameters			Ref	
						Type	R (Ωcm)	μ (cm ² V ⁻¹ S ⁻¹)		N (cm ⁻³)
SnS₂										
SnS ₂	T(II)C TA	TTA = 1 M	T _b = - t _d = 30–120 min pH = -	HEX(001)	2.95–2.80 (d)	n	11.2	48	10 ¹⁷	2017 [56]
SnS ₂	T(II)C = 0.84 g TA = 0.5 M	TEA = 24 mL NH ₃ = 16 mL	T _b = 60 °C t _d = 2 h pH = -	-	-	-	-	-	-	2018 [247]
SnS ₂	T(II)C = 0.1 M TA = 0.1 M	TTA = 0.1 M	T _b = 60 °C t _d = 6 h pH = -	HEX(001)	2.25–2.53 (d)	-	-	-	-	2019 [248]
Sn₂S₃										
Sn ₂ S ₃	T(II)C = 1 M TA = 1 M	TEA = 10 mL	T _b = 30 °C t _d = 20–24 h pH = 10.7	ORT(131)	2.03–2.12 (d)	-	-	-	-	2012 [34]
Sn ₂ S ₃	T(II)C = 1.4 g TA = 1 M	TEA = 30 mL NH ₃ = 50 mL	T _b = RT t _d = 24 h pH = -	ORT(211)	1.2 (d)	-	-	-	-	2012 [139]
Sn ₂ S ₃	T(II)C = 0.05 M SDS = 0.05 M	-	T _b = - t _d = - pH = -	ORT(021)	1.3 (d)	-	-	-	-	2018 [249]
Sn ₂ S ₃	T(II)C = 0.1 M TA = 0.1 M	TEA = 30 mL NH ₃ = 16 mL	T _b = 17 °C t _d = 15 h 450 °C (S-powder: 15 mg), 5–75 min	ORT(211)	1.75 (d)	p	10 ⁴	6 × 10 ⁻⁶	-	2020 [250]

3.2. Sn and S Precursors and Their Concentration Effect

The selection of Sn precursor and its concentration plays a vital role in the growth, phase formation, crystallinity, preferred orientation, morphology, band gap, and other properties of Sn_xS_y thin films [251]. This is because the releasing rate of Sn ions strongly depends on the selection of Sn precursors. As mentioned in Section 3.1, the $\text{SnCl}_2 \cdot 2\text{H}_2\text{O}$ (T(II)C) has been considerably utilized as an Sn precursor for the deposition of Sn_xS_y films. According to the literature (Tables 4 and 5), until recently, there have been no reports related to the study of different types of Sn precursors on the formation of Sn_xS_y films and the Sn precursor concentration effects on the formation of SnS_2 and Sn_2S_3 films and their properties. However, there have been very few quantitative analyses of Sn precursor concentration effect on the formation of o-SnS films and their properties. The primary report related to the effect of Sn precursor concentration ($[\text{T(II)C}] = 0.06\text{--}0.12\text{ M}$) on the growth of o-SnS films was made in 2012 [191]. A lower T(II)C concentration stimulates the formation of multi phases with a dominant SnS_2 phase, whereas a higher T(II)C concentration reduces the crystallinity. The T(II)C concentration of 0.1 M is beneficial for the deposition of pure, good crystalline o-SnS with (111) preferred orientation (Figure 7a). A small variation in T(II)C concentration (at 0.15 M) changes the preferred orientation of o-SnS from (111) to (200) [194]. Moreover, the change in T(II)C concentration can increase the grain size and decrease the band gap (1.95–1.5 eV) (Figure 7b,c) [191]. Therefore, the manipulation of preferred orientation, crystallinity, and band gap can be achieved by the change in Sn precursor concentration.

In addition to the suitable Sn precursor selection, the choice of S precursor and its concentration are highly desirable to obtain good quality Sn_xS_y films. In CBD, the releasing rate (or reaction rate) of S ions greatly affect the growth kinetics and phase formation, and it can be controlled by the S precursor concentration. According to the previous reports (Tables 4 and 5), TA and ST have been chiefly used as S ion sources (Figure 5b). In those, TA is preferable compared to ST because it works in both acidic and alkaline bath conditions. The influence of TA concentration on o-SnS film growth (thickness) was initially reported in 1987 [145]. An extremely low or high TA concentration produces the o-SnS films of smaller terminal thickness, whereas a moderate TA concentration promotes the growth of maximum thickness (Figure 7d). The reason for the lower film thickness obtained at a lower S precursor concentration is the insufficient number of S ions in the reaction bath that can combine with all the available Sn ions. At a higher S precursor concentration, the releasing rate of S ions is high enough to stimulate the precipitation process, which also results in a lower film thickness [145].

Furthermore, the S precursor concentration can influence the morphology and phase formation of o-SnS films (Figure 7e). A higher TA concentration stimulates the formation of multi phases such as Sn_2S_3 and Sn_3S_4 ($\text{Sn}_2\text{S}_3 + \text{SnS} \rightarrow \text{Sn}_3\text{S}_4$) [209] and a lower TA concentration assists the growth of single-phase o-SnS films, but with lower crystallinity [142,198]. A TA concentration of 0.1 M is preferable for the deposition of a single-phase, polycrystalline o-SnS with (101) preferred orientation [198], and a ST concentration of 0.75 M is advisable for (111)/(040) preferred orientation (Figure 7f). The effect of changes in the S source concentration on the band gap of o-SnS films is controversial until the present. A reduction in band gap from 1.70 eV to 1.25 eV with increasing TA concentrations was reported in [200], although no significant change in band gap was found with TA concentration in [198]. On the other hand, no studies in the literature have focused on the influence of S precursor concentration on the properties of c-SnS, SnS_2 , and Sn_2S_3 films.

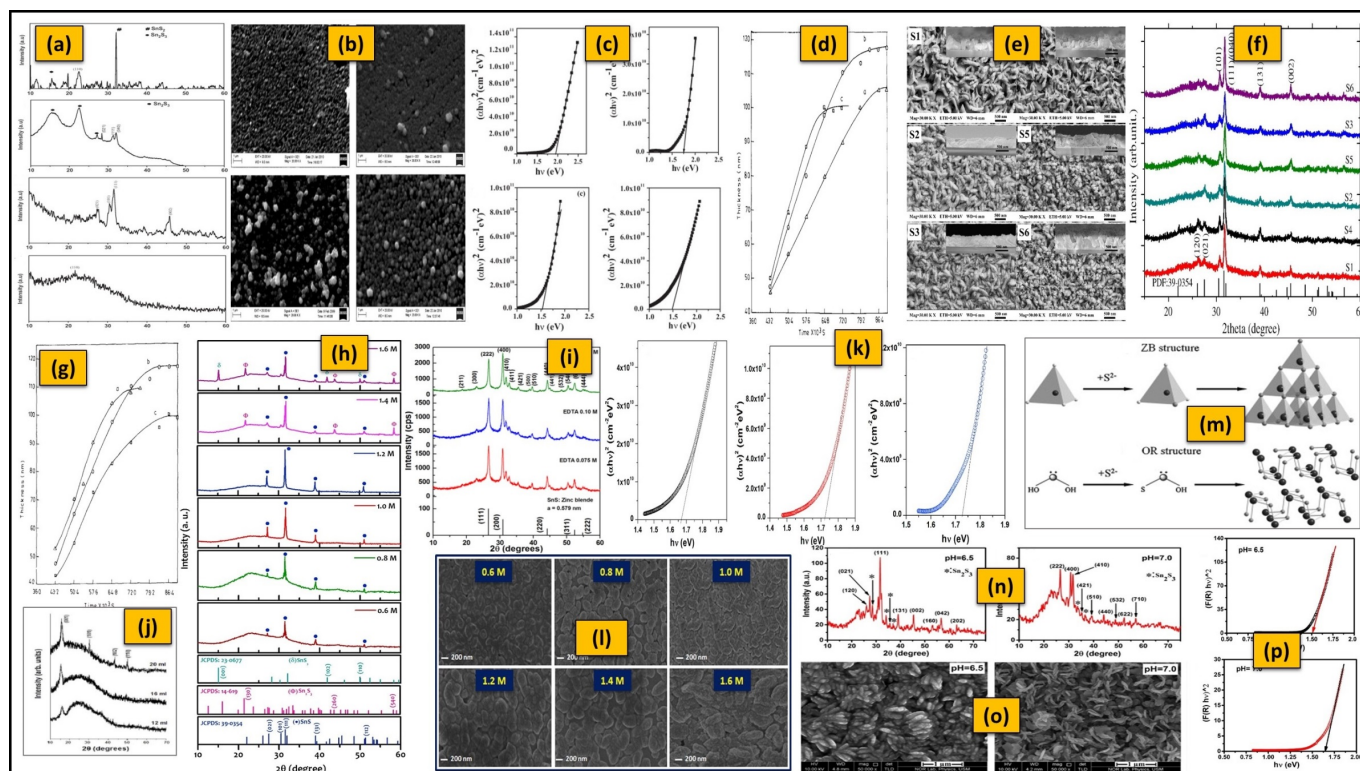


Figure 7. (a–c) XRD patterns, SEM images, and $(\alpha hv)^2$ versus (hv) graph of o-SnS films grown at various SnCl_2 concentrations (reprinted with permission [191]. © 2012, Elsevier), and variation in o-SnS film (d) thickness with different TA concentrations (reprinted with permission [145]. © 1987, Elsevier). (e,f) Morphology and crystallinity changes of o-SnS films with ST concentrations (reprinted with permission [187]. © 2012, Elsevier). (g) Variation in SnS film thickness with different TEA concentrations (reprinted with permission [145]. © 1987, Elsevier). (h,i) XRD patterns of the o-SnS films and c-SnS films deposited at different TTA (reprinted with permission [211]. © 2019, Elsevier) and EDTA concentrations, respectively (reprinted with permission [26]. © 2016, Elsevier). (j) XRD patterns of SnS_2 films deposited at various volumes of ammonia solution (reprinted with permission [41]. © 2012, Elsevier). (k) $(\alpha hv)^2$ versus (hv) for c-SnS films prepared using various EDTA amounts reprinted with permission [26]. © 2016, Elsevier). (l) SEM images of o-SnS films deposited with various TTA concentrations (reprinted with permission [211]. © 2019, Elsevier). (m,n) Scheme of the formation (reprinted with permission [185]. © 2011, Elsevier) and XRD patterns of o-SnS and c-SnS films (reprinted with permission [27]. © 2018, Elsevier). (o) Morphologies of o-SnS and c-SnS films (reprinted with permission [184]. © 2011, Elsevier), and (p) variation in the band gap o-SnS films at different pH values (reprinted with permission [27]. © 2018, Elsevier).

3.3. Complexing Agents and Their Concentration Effect

As stated in Section 3.1, in order to develop influential Sn_xS_y films, the control of the availability of Sn ions in the reaction bath is essential. It can be successfully attained by the addition of an appropriate concentration of a complexing agent [128,148]. Moreover, adhesion, morphology, crystallinity, and the deposition rate of Sn_xS_y films can be significantly affected by the concentration of the complexing agent [128]. Therefore, knowledge of the behavior of complexing agents in the bath can help to obtain good quality Sn_xS_y films. The behavior of complexing agents is described in terms of their stability constants (K_s), which is the equilibrium constant for the formation of a complex in a solution [252]. It is defined for the equilibrium between an Sn ion ($\text{Sn}^{2+/4+}$) and a ligand (L) as [148]

$$K_s = \frac{a_{\text{Sn}^{2+/4+}} - L}{a_{\text{Sn}^{2+/4+}} + a_L} \quad (1)$$

where a is the activity of subscripted species and can be approximated by its concentration. A large value of K_s implies a strong binding affinity for the metal (Sn) ion, while a small value of K_s implies a weak binding affinity [148]. Generally, complexing agents can prevent

the formation of powder/bulk precipitation of tin hydroxides in the reaction bath, and they can easily maintain the supersaturating condition. If a complexing agent has a weak binding affinity, it does not arrest the bulk precipitation of tin hydroxides. On the other hand, if it has an extremely strong binding affinity, it restricts the deposition of the desired film [253]. Therefore, in order to prevent powder/bulk precipitation of tin hydroxides, the complexing binding affinity must be intermediate.

Various complexing agents have been explored to control Sn ions depending on the bath conditions during the deposition of Sn_xS_y films (Tables 4 and 5). However, there are only a few reports on the study of complexing agent concentration. Initially, the influence of TEA complexing agent concentration on the thickness of o-SnS films was made in 1987 [145]. An optimized TEA complexing agent concentration controls the formation of o-SnS films, yielding a thick o-SnS film (Figure 7g). In addition to the growth (thickness), the change in TEA complexing agent concentration can also influence the phase formation and crystallinity of o-SnS, c-SnS, and SnS_2 films. The lower tartaric acid (TTA) complexing agent concentration creates the weak tin complexation, leading to partial homogeneous precipitation, resulting in low-crystalline o-SnS films. As the complexing agent concentration increases, the improved tin complexation controls the reaction, yielding the formation of better crystalline films o-SnS. Over the limit, the availability of free Sn ions is reduced due to strong complexation, resulting in the formation of sulfur-rich tin phases such as Sn_2S_3 and SnS_2 (Figure 7h) [211]. Single-phase, polycrystalline o-SnS films with (111) preferred orientation are produced at 1.85 M of TEA [191] and 1.4 M of TTA [211], while a c-SnS (222)/(400) is formed at 0.125 M of EDTA [26] concentrations (Figure 7i). The crystallinity of o-SnS films can be improved by replacing the lower stability (Sn^{2+} -TEA) complexing agent with the higher stability (Sn^{2+} -EDTA) one [198,254], due to the fact that EDTA (hexaligand) may generate a ligand more quickly than TEA (triligand) [255]. An increase in citric acid and ammonia concentration also improves the crystallinity in the case of SnS_2 films (Figure 7j) [41,131]. The concentration of the complexing agent similarly influences the morphological and optical properties of the o-SnS, c-SnS, and SnS_2 films. The direct optical energy gap for o-SnS films reduces with increasing complexing agent concentration (TSC, 0.06–0.08 M; TEA, 12.5–13 M; TTA, 0.6–1.4 M) from 2.16 eV to 1.17 eV [50,182,214], but rises from 1.67 eV to 1.73 eV [26] for c-SnS films with EDTA (0.075–0.125 M) (Figure 7l). The change in complexing agent concentration (TSC, TTA) improves the compactness and morphology of o-SnS films (Figure 7m). This may improve their electrical properties, such as electrical mobility ($\sim 228 \text{ cm}^2\text{V}^{-1}\text{s}^{-1}$) and carrier concentration ($\sim 4.1 \times 10^{15} \text{ cm}^{-3}$). No previous study has examined the effect of complexing agents on the formation and physical properties of Sn_2S_3 films.

3.4. Solution pH Effect

In CBD, solution pH/bath pH (a measure of the acidity or basicity of a solution) is an important parameter because it directly affects the growth mechanism as well as reaction rate. Therefore, it can influence the formation of phases and physical properties of films [27]. In addition, the bath pH must be at a specific optimum value to maintain supersaturation condition ($Q_{\text{ip}} > K_{\text{sp}}$, Figure 5c) for the formation of Sn_xS_y films. The preparation of Sn_xS_y films was reported both in acidic (pH < 7) and alkaline (pH > 7) baths (see Tables 4 and 5). When the bath pH is varied between 1 and 14, the concentration of OH^- ions increases, which results in a reduction in the concentration of free Sn^{2+} or Sn^{4+} ions in the solution. Thus, the hydroxide mechanism can predominate during film development, resulting in the creation of $\text{Sn}(\text{OH})_{2 \text{ or } 4}$ in addition to Sn_xS_y . A higher bath pH, on the other hand, encourages the hydrolysis of a sulfur source precursor.

A few researchers have investigated the bath pH effect on o-SnS and c-SnS films growth and their physical properties (Table 4). The bath pH effect on the adhesion and growth rate of o-SnS films was first reported in 1989 [36]. According to this report, the good adhesion of o-SnS films on glass can be obtained with a bath pH > 3. The growth rate is low at pH ~ 7 and high at pH ~ 10 for o-SnS films due to the formation of $\text{Sn}(\text{OH})_{2 \text{ or } 4}$ precipitate

from the hydrolysis of an Sn precursor because a part of $\text{Sn}(\text{OH})_{2 \text{ or } 4}$ precipitate turns into Na_2SnO_2 , which dissolves back in the solution. The change in growth rate by bath pH leads to the variation in grain size of o-SnS films [183]. The bath pH can also influence the growth mechanism, which leads to phase transformation [184,185]. An o-SnS forms at a lower pH of 6.5 via the cluster-by-cluster mechanism, whereas c-SnS forms at a higher pH of 7.0 through the ion-by-ion mechanism (Figure 7n,o) [27].

The phase transition caused by the change in bath pH leads to a change in the morphologies of the film surfaces (Figure 7o) and the energy band gaps (o-SnS: 1.51 eV and c-SnS: 1.64 eV) (Figure 7p) [27,184,185]. The increase in solution pH results in the decrease of free Sn^{2+} ion concentration as well as the concentration of OH^- ions, which are favorable for the hydrolysis of the S ion source [256], leading to the increase in the concentration of S^{2-} ions. Thus, the interaction of Sn^{2+} and S^{2-} ions can form the c-SnS via an ion-by-ion mechanism because the potential barrier of heterogeneous nucleation is lower than that of homogeneous nucleation [25,185]. However, these mechanisms are speculated, and direct in situ measurement evidence such as in situ quartz crystal microbalance and electrochemical impedance is lacking. Therefore, such studies are required for understanding the growth mechanism of Sn_xS_y films [257]. On the other hand, no studies in the literature have examined the effect of bath pH on the properties of SnS_2 and Sn_2S_3 films.

3.5. Solution Temperature (T_b) Effect

In CBD, solution temperature/bath temperature (T_b) also played a crucial role in the preparation of thin films with high quality and desired features. It critically enhances the rate of dissociation of the precursors and thus strongly affects the thickness, growth rate, type of nucleation, crystalline phase, crystallite size, morphology, and optoelectrical properties of thin films. The change in film growth rate as a function of T_b can be determined through the Arrhenius equation [258],

$$k(T) = A e^{\frac{-E_a}{RT}} \quad (2)$$

where $k(T)$ is the temperature-dependent growth rate for the given deposition conditions, A is a pre-exponential constant related to the initial reagent concentration, E_a is the activation energy (kJ/mol), and R is the gas constant ($R = 8.3145 \text{ J mol}^{-1} \text{ K}^{-1}$).

The deposition of Sn_xS_y films has been reported in the T_b range of room temperature (T_r)—90 °C (Tables 4 and 5). The effect of T_b on the formation of o-SnS, c-SnS films, and their properties (Table 4) was studied extensively. The T_b changes the growth rate due to the variation in the deposition mechanism, i.e., the ion-by-ion mechanism, which is less thermally activated with low activation energy (at lower bath temperatures). In contrast, cluster-by-cluster is believed to occur at relatively higher temperatures [259]. Thus, the thickness of a film has a close relationship with the T_b . First, it increases significantly with the T_b due to the increase in bath supersaturation [145,213] and reaches saturation point very quickly because the hydrolysis of the S precursor is greatly improved by the increase in T_b [182] (Figure 8a). Then, it decreases down to a terminal point because of the ion-ion condensation process and high homogeneous precipitation rate [145,146]. In addition, the T_b significantly affects the microstructures of o-SnS and c-SnS films.

Generally, the films prepared at lower T_b have smaller grains, and those grains increase in size with T_b due to the covering of voids by secondary nucleation (Figure 8b) [50,212]. The change in grain shape may indicate a change in the growth mechanism [146]. The T_b can also influence the composition of c-SnS films. The c-SnS films show a non-stoichiometric composition at higher and lower T_b values due to the relatively faster and slower release of Sn^{2+} ions from the tin complex due to the variation of thermal energy in the solution [50]. Single-phase, polycrystalline o-SnS films with (111) preferred orientation and c-SnS films with (222)/(400) preferred orientation are produced separately at T_b of 70 °C [212] and 65 °C [50] using a different source of materials (Table 4), respectively.

On the other hand, the T_b shows an impact on phase transformations when other bath parameters remained constant. The films predominantly exhibit the o-SnS phase

above the T_b range of 30–40 °C, whereas the c-SnS phase is below this range (20–30 °C) for particular deposition conditions [146]. The T_b can directly affect the crystallinity of both o-SnS and c-SnS films. The crystallinity of both films is improved with T_b due to the supply of sufficient thermal energy for further crystallization (Figure 8c) [50,212]. Thus, an average crystallite size is improved with T_b —however, up to a certain extent [212]. As the T_b improves the kinetic energy of the reactants and accelerates the interaction between all ions in the reaction bath, the nuclei formation (crystallite grow) is enhanced on the surface of the substrate [260]. However, at higher T_b , the crystallite size is decreased due to the dissolution of grown film.

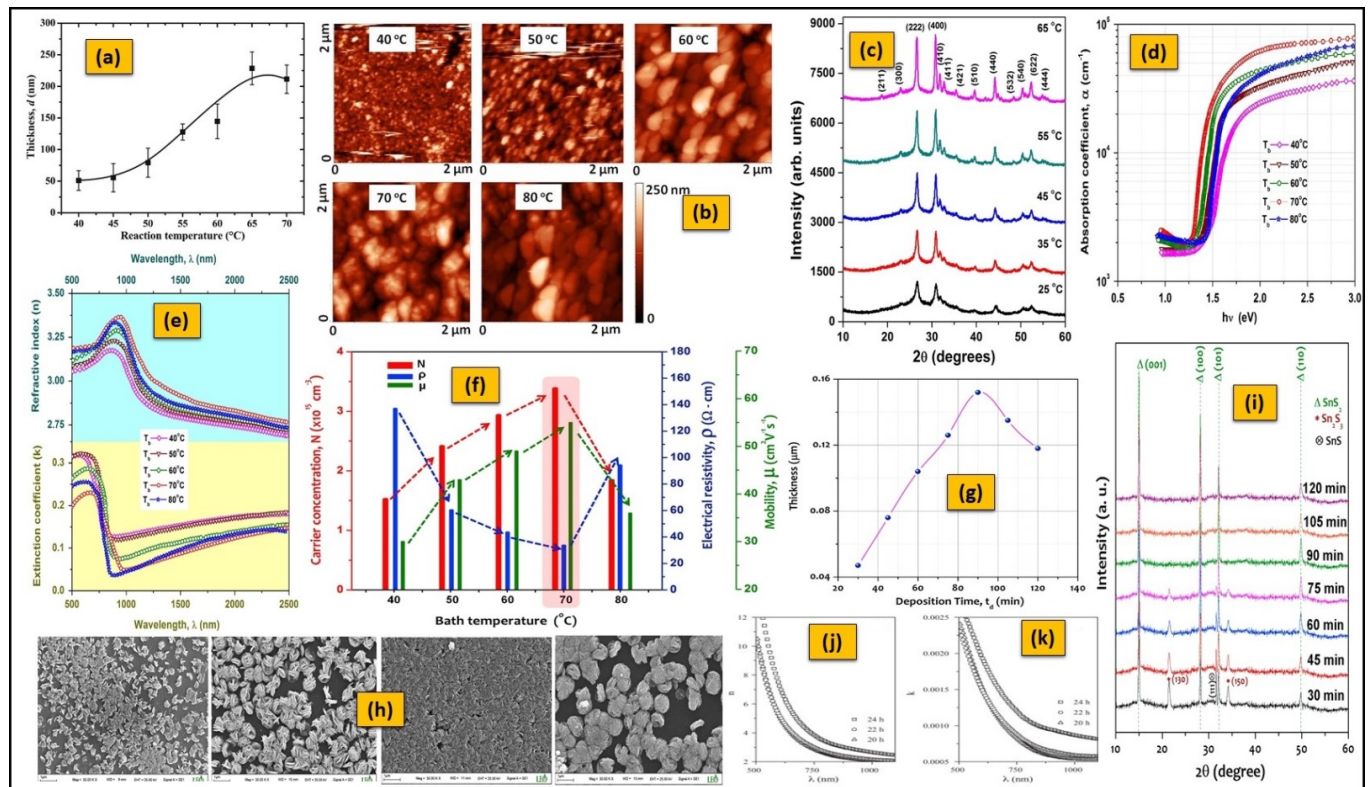


Figure 8. (a) Variation in o-SnS film thickness with bath temperature (reprinted with permission [213]. © 2019, Elsevier). (b,f) Morphological and electrical properties of o-SnS at different bath temperatures (reprinted with permission [212]. © 2019, Elsevier). (c) Change in crystallinity of c-SnS films with bath temperature (reprinted with permission [50]. © 2016, Elsevier). (d,e) Plots of absorption coefficient refractive index and extinction coefficient of o-SnS films (reprinted with permission [17]. © 2015, Elsevier). (g,i) Variation in thickness and crystallinity of SnS₂ films with deposition time (reprinted with permission [56]. © 2017, Elsevier). (h) Morphology of ORT-SnS thin films deposited at various times (reprinted with permission [177]. © 2010, Elsevier). (j) Variation in refractive index and (k) variation in extinction coefficient of Sn₂S₃ films with deposition time (reprinted with permission [34]. © 2012, Elsevier).

The T_b also influences the optical characteristics of the o-SnS and c-SnS films. In o-SnS films, the T_b improves the sharpness of the absorption edge with a high optical absorption coefficient ($>10^4 \text{ cm}^{-1}$) [17] (Figure 8d), which is suitable for PV devices. The optical energy gap of o-SnS and c-SnS films decreases from 1.41 eV to 1.30 eV and from 1.74 eV to 1.68 eV, respectively, with the increase in T_b (30–70 °C) [17,50]. As mentioned above, T_b can improve the grain size and simultaneously reduce height (smoothness of the surface) and the number of grain boundaries [261]; this minimizes imperfections in the film and enhances the quality of the film, which can lead to change in density of localized states within the energy gap [262]. Therefore, band gap tuning is easily possible in CBD deposited o-SnS and c-SnS films regarding T_b , which is essential for designing highly efficient solar cells [263]. The optical parameters, namely, refractive index (n), extinction coefficient (k), and real/imaginary dielectric constants of o-SnS films, are in ranges of 2.72–3.24, 0.24–0.13,

and 7.34–10.48/0.85–1.32 [17], respectively (Figure 8e). Here, the variation in the optical parameters may be arrived from the change in strain and packing density with T_b [264].

As previously mentioned, T_b improves the crystallinity along with grain size and thickness. Thus, the scattering of charge carriers by grain boundaries decreases with respect to T_b , which makes a significant change in the electrical characteristics of films [265]. These possible reasons may improve the carrier density and a consequent reduction in resistivity in both o-SnS and c-SnS films. The reduction of the dispersing effects of carriers can lead to an increase in the mobility of carriers in those films ($\sim 55 \text{ cm}^2 \text{ V}^{-1} \text{ s}^{-1}$ for o-SnS at 70°C [212] and $28 \text{ cm}^2 \text{ V}^{-1} \text{ s}^{-1}$ for c-SnS at 45°C [50]) (Figure 8f). However, the above-mentioned description confirms the importance of T_b in the CBD process until there are no reports on the T_b influence on both SnS_2 and Sn_2S_3 films.

3.6. Deposition Time Effect

Deposition time (t_d) is the most important bath parameter among the various deposition conditions. It affects the growth rate/thickness and properties of Sn_xS_y films. In CBD, the t_d period can be divided into three steps, namely, (i) nucleation or initiation, which requires high activation energy; (ii) linear growth, which includes heterogeneous growth of nuclei; and (iii) termination or saturation, in which chemical reagents become depleted and the reaction begins to slow down and eventually stops [266]. Thus, the rate of formation of nuclei can be in terms of t_d by the following Avrami equation (a conventional diffusion-controlled reaction model) [267]:

$$\alpha = 1 - e^{-(kt_d)^n} \quad (3)$$

where α is the fractional decomposition (or reaction), k is a rate constant, and n is the Avrami exponent.

There are a considerable number of reports on the study of the t_d effect on o-SnS films, but there are only a few reports for c-SnS [210,225], SnS_2 [56], and Sn_2S_3 [34] films (Tables 4 and 5). Typically, a t_d from a few minutes to several hours has been reported to prepare these Sn_xS_y films (Tables 4 and 5). The growth of Sn_xS_y films with t_d was simply described in terms of thickness. In the initial state, the change in film thickness is insignificant because of the requirement of long incubation time for nucleation [198], and the thickness increases linearly due to the availability of sufficient amounts of Sn^{2+} or Sn^{4+} and S^{2-} ions. Next, the film thickness increases faster, then decreases at a longer deposition time, and attains a maximum value as a terminal/final thickness. Here, the attained terminal thickness is not only t_d -dependent but also T_b -related [145]. Thus, a terminal thickness should be considered when the reaction undergoes at a constant temperature. A terminal thickness in the range of 120–900 nm can be obtained for different t_d varying from 1 h to 24 h at a constant range of T_b ($T_r=75^\circ \text{C}$) for o-SnS and c-SnS films [128,145,175,198,225], and a thickness of 152 nm can be attained at a t_d of 90 min for SnS_2 films (Figure 8g) [56]. The variation in the thickness (growth) of these films with respect to t_d can be explained by considering two competing processes taking place in the deposition bath. One process includes heterogeneous precipitation, which leads to film growth (thickness improves). The other involves the dissolution of the preformed film, which results in the decrease of film thickness.

The t_d has a significant impact on the surface morphology, crystallinity, crystallite size, and phase purity of Sn_xS_y films. As the t_d increases, the size and quantity of grains (or aggregations) can be improved to form a more homogeneous film [177] (Figure 8h). This indicates an occurrence of nucleation growth with t_d [56,190]. If t_d exceeds the optimum value, a non-uniform film with porous nature might be formed due to the dissolution of pre-adhered grains in the film [190]. This phenomenon can be experimentally observed for o-SnS, SnS_2 , and Sn_2S_3 films when the t_d varies between 2 and 10 h [177], 30–120 min [56], and 20–24 h [34], respectively. The t_d can considerably improve the crystallinity of the Sn_xS_y films and simultaneously enhance the crystallite size. However, beyond the limit of t_d , the crystallinity becomes poor, and the crystallite size decreases (Figure 8i) [56,146,177,190,225].

The reduction of crystallite size is due to the lowering of the van der Waals force in between crystallites because the substrate remained in the solution longer than necessary [177]. In addition to the crystallinity of films, the t_d also influences the phase purity of a film. At low t_d , the released Sn^{2+} or Sn^{4+} ions are relatively low in the reaction bath compared to the available S^{2-} ions. These available S^{2-} ions are not balanced by the all released Sn^{2+} or Sn^{4+} ions, leading to the development of other secondary phases, whereas at longer t_d they are counterbalanced, promoting the growth of the pure phase [56].

As mentioned previously, the t_d directly influences the thickness of Sn_xS_y films. Thus, it tremendously shows an impact on their optical transmittance/absorbance. Always, shorter t_d periods generate the thinnest film of high transmittance, which might be affected by abundant porosities [175,177]. Simultaneously, the more extended t_d periods produce thick films of high absorption [34,175,190], essential for solar cell application. The longer t_d period also improves the size of crystallites that can affect the optical absorption and the band gap energy of films [190].

The quantum size effect and changing barrier height (or variation in grain size) are also responsible for the variation in the band gap of films with t_d at other identical growth conditions [22,177]. The increase in t_d period reduces the band gap of o-SnS, SnS_2 , and Sn_2S_3 films from 1.83 eV to 1.30 eV [177], 2.95 eV to 2.80 eV [56], and 2.12 to 2.03 eV [34], respectively. In contrast, the longer t_d period generates greater compression impacts with the thickness in o-SnS films, which may enhance the band gap (0.82–1.22 eV) [175]. In addition to the optical gap, t_d shows a significant effect on the optical constants such as refractive index (n , SnS_2 : 2.57–2.63, Sn_2S_3 : 4.89–7.18) and extinction coefficient (k , SnS_2 : 0.69–0.61, Sn_2S_3 : 0.0015–0.0019) (Figure 8j,k) [34,56]. However, no previous studies had included the variations in optical constants of o-SnS and c-SnS films with t_d . On the other hand, the t_d reduces the electrical resistivity and improves the carrier density and mobility of carriers in the case of both o-SnS and SnS_2 films [56,177] due to the improved crystallinity and suppression of secondary phases with t_d period. In contrast, in the case of c-SnS and Sn_2S_3 films, there are no reports available in the literature.

3.7. Other Parameters

3.7.1. Substrate Nature and Its Cleaning Process Effect

Generally, thin films require proper mechanical support that provides sufficient adhesion. These supports are commonly called substrates. Substrates have a significant effect on the film properties in practice [268]. Therefore, the choice of a suitable substrate with a specific form for a thin film with a particular application is critical since the substrate must be structurally and chemically compatible with the thin film material in terms of thermal and mechanical stability [269,270]. Moreover, the substrate nature strongly affects the preferred orientation of a thin film, which plays a major role in device performance [271]. Therefore, currently, the exploration of feasible substrates has become an active research area. The CBD has the benefit of allowing thin film deposition on unevenly shaped surfaces. However, the substrate nature greatly affects the deposition process and film quality. Usually, substrates with rough surfaces have better anchoring of the initial deposit in the tiny valleys. Substrates such as glass, tin oxide (TO), indium tin oxide (ITO), and silica/quartz are relatively reactive, owing to the presence of hydroxyl surface groups. Furthermore, when the lattice of the deposited material matches well with that of the substrate, the free energy change is smaller; this facilitates fast nucleation with good morphology and structure. Although the substrate nature has more impact on the process of CBD and the deposited thin film characteristics, there are only a few studies on this area in the case of o-SnS and SnS_2 films and no reports for c-SnS and Sn_2S_3 films (Tables 4 and 5). The reports related to the effects of molybdenum (Mo), ITO, and TO and borosilicate glass substrates [204] on the properties of o-SnS films and the glass, TO, and titanium (Ti) substrates [130] on SnS_2 films are available in the literature. At 0.01 M of Sn and S sources concentrations, both Mo and TO substrates generate o-SnS films with a better surface coverage, whereas the borosilicate glass and ITO substrates produce a discontinuous film with separate agglomerated o-SnS

particles. When the concentration of sources is 0.03 M, all substrates except the borosilicate glass form a complete and uniform coverage of o-SnS films. At a high concentration of 0.09 M, all substrates produce a complete coverage of o-SnS films but with a lower adhesive nature [204]. In the case of SnS₂, the amorphous and n-type nature films formed on the glass and Ti substrates, respectively.

In addition to the substrate nature, the cleaning process of the substrate also significantly affects the quality of thin films. Improper cleaning of substrates results in the formation of pinholes in the film, which creates major issues on the fabrication of large-area devices and produces short circuits in solar cells [272]. Unfortunately, there is a lack of research on this area for CBD deposited o-SnS, c-SnS, SnS₂, and Sn₂S₃ thin films.

3.7.2. Stirring Speed and Humidity Effect

In the CBD, chemical solutions with a homogeneous distribution of precursors are necessary before starting the process. Continuous mixing of the reaction solution is mandatory for realizing a uniform thin film deposition [273]. This could be achieved by stirring the solutions at appropriate speeds. At the beginning of the deposition, the stirring speed does not have a significant impact on the growth rate of thin films. However, for longer deposition times, it directly affects the growth rate. In addition, stirring with uneven speed may produce a variation in thin film uniformity and improper diffusion of complex ions toward the substrate [274], and stirring provokes precipitation and reduces the final thickness of the film. Therefore, care must be taken in stirring the solution to obtain the desired quality of thin films.

On the other hand, environmental humidity also influences the formation and physical properties of CBD processed films [273] since the CBD can be performed in an open environment where the gas–liquid interface is influenced by moisture. Even after the deposition of films, they considerably degrade because of their colloidal nature [275]. Therefore, the maintenance of environmental humidity is vital for the deposition of defect-free films. Although the control of stirring speed and environmental humidity is essential for producing quality Sn_xS_y films, there is no systematic study on these effects in the literature.

3.8. Summary

Sn_xS_y are binary metal chalcogenides that have attracted considerable attention due to their abundant, low cost, and nontoxic constituent elements. In comparison to other vacuum and chemical approaches, they may be simply synthesized utilizing a simple non-vacuum CBD methodology. Sn precursors, S precursors, and complexing agents are ideally T(II)C, TA, and TEA, respectively. The following lines are made based on the examination of published data (Tables 4 and 5) and the explanation in Sections 3.1–3.7. Changes in Sn precursor concentration, complexing agent concentration, and T_b can be used to manipulate high-intensity plans and crystallinity. Maintaining complexing agent concentration, bath pH, and t_d, may regulate phase transition and growth rate. Controlling S precursor and complexing agent concentrations results in good morphological, optical, and electrical characteristics. As a result, optimizing each deposition parameter is critical for producing high-quality Sn_xS_y thin films for a variety of applications. However, no previous research has looked at the effect of S precursor concentration on c-SnS, SnS₂, and Sn₂S₃ films; complexing agent concentration on Sn₂S₃ films; bath pH on the properties of SnS₂ and Sn₂S₃ films; T_b on both SnS₂ and Sn₂S₃ films; and t_d on c-SnS and Sn₂S₃ films. Furthermore, for all o-SnS, c-SnS, SnS₂, and Sn₂S₃ thin films, there is a dearth of research on the substrate nature-cleaning procedure, stirring speed, and humidity influence.

According to the description in this part, it is confirmed that further research is required to improve the quality of Sn_xS_y films and more studies are necessary related to the optimization of all deposition parameters. Hence, research focusing on this area is essential.

4. Conclusions

Sn_xS_y thin films deposited with CBD are a relatively recent development, and their process–property correlations must be understood for the desired application. Further, the fabrication of single-phase o-SnS, c-SnS, SnS_2 , and Sn_2S_3 thin films in CBD is very condition-dependent. Additionally, it is crucial to identify and separate the o-SnS, c-SnS, SnS_2 , and Sn_2S_3 phases. However, until recently, there has been a dearth of detailed studies on the optimization of growth parameters. The present review outlined the background and basic properties of Sn_xS_y (o-SnS, c-SnS, SnS_2 , and Sn_2S_3) along with the principle, nucleation, growth, and growth mechanism of Sn_xS_y thin films by CBD. Furthermore, the influence of growth parameters such as precursor concentration (tin source, sulfur source, and complexing agent), bath pH, bath temperature (T_b), deposition time (t_d) on the phase formation, and physical properties of Sn_xS_y thin films were comprehensively described. As a result, the reader should be able to prepare single-phase tin sulfide materials with ease after studying the present article. Hence, the present review should motivate readers to conduct extensive investigations on Sn_xS_y films to develop cost-effective, eco-friendly, and earth-abundant tin sulfide materials to meet all future energy requirements. The connection between the physical properties of Sn_xS_y thin films and their photovoltaic application will be discussed in our subsequent article.

Author Contributions: Conceptualization, V.R.M.R.; writing—original draft preparation, S.G.; review, V.R.M.R., T.R.R.K., and C.P.; Writing final version—review and editing, W.K.K.; supervision, W.K.K. All authors have read and agreed to the published version of the manuscript.

Funding: This study was supported by Priority Research Centers Program through the National Research Foundation of Korea (NRF), funded by the Ministry of Education (2014R1A6A1031189) and the 2019 Yeungnam University Research Grant.

Data Availability Statement: Not applicable.

Conflicts of Interest: The authors declare no conflict of interest.

Abbreviations

Abbreviation	Chemical Name
A	Ammonia
AA	Acetic acid
AC	Ammonium citrate
ACE	Acetone
AF	Ammonium fluoride
AH	Ammonium hydroxide
ALD	Atomic layer deposition
AS	Ammonium sulfide
BT	Baking temperature
CA	Citric acid
CALPHAD	CALculation of PHase diagram
CBD	Chemical bath deposition
CBM	Conduction band minimum
CBO	Conduction band offset
CSS	Close space sublimation
CUB	Cubic
DDT	Dodecanethiol
DIW	Deionized water
DW	Distilled water

EDS	Energy-dispersive X-ray spectroscopy
EDTA	Ethylenediaminetetraacetic acid
EL	Electrolyte
FF	Fill factor
G	Glass
GA	Glacial acetic acid
GIXRD	Grazing incidence X-ray diffraction
HCL	Hydrochloric acid
HEX	Hexagonal
HH	Hydrazine hydrate
HWVD	Hot wall vapor deposition
ITO	Indium tin oxide
JCPDS	Joint committee on powder diffraction standards
Li	Lithium
MeOH	Methanol
Mo	Molybdenum
Na	Sodium
Na ₂ EDTA	Disodium ethylenediaminetetraacetate
NTA	Nitriloacetic acid
ODE	Octadecene
OLA	Oleylamine
ORT	Orthorhombic
PG	Propylene glycol
PL	Photoluminescence
QE	Quantum efficiency
RS	Rock salt
SAED	Selected area electron diffraction
SCR	Space charge region
SDS	Sodium sulfide
Si	Silicon
SILAR	Successive ionic layer adsorption and reaction
SIMS	Secondary ion mass spectrometry
SS	Stainless steel
SnS	Tin monosulfide
SnS ₂	Tin disulfide
Sn ₂ S ₃	Tin sesquisulfide
ST	Sodium thiosulfate
TA	Thioacetamide
T(II)C	Tin (II) chloride dehydrate
TC(IV)	Tin(IV) chloride pentahydrate
TEA	Triethanolamine
TEM	Transmission electron microscopy
Ti	Titanium
TO	Tin oxide
TOP	Trioctylphosphine oxide
T _r	Room temperature
TSC	Trisodium citrate
TTA	Tartaric acid
TU	Thiourea
UAED	Ultrasound-assisted electrodeposition
VBM	Valence band maximum
XRD	X-ray diffraction
ZB	Zinc blended

References

1. De Elisa, R. Cadmium telluride solar cells: Selenium diffusion unveiled. *Nat. Energy* **2016**, *1*, 16143–16146.
2. Solar Frontier Achieves World Record Thin-Film Solar Cell Efficiency of 23.35%. Available online: http://www.solar-frontier.com/eng/news/2019/0117_press.html (accessed on 14 July 2021).
3. Chen, X.; Hou, Y.; Zhang, B.; Yang, X.H.; Yang, H.G. Low-cost SnS_x counter electrodes for dye-sensitized solar cells. *Chem. Commun.* **2013**, *49*, 5793–5795. [[CrossRef](#)] [[PubMed](#)]
4. PV Division | Business Information | KITAGAWA SEIKI Co., Ltd. Available online: http://www.kitagawaseiki.co.jp/en/jigyo_pv.html (accessed on 14 July 2021).
5. Ge, J.; Zhang, Y.; Heo, Y.-J.; Park, S.-J. Advanced Design and Synthesis of Composite Photocatalysts for the Remediation of Wastewater: A Review. *Catalysts* **2019**, *9*, 122. [[CrossRef](#)]
6. Liao, C.-H.; Huang, C.-W.; Wu, J.C.S. Hydrogen Production from Semiconductor-based Photocatalysis via Water Splitting. *Catalysts* **2012**, *2*, 490–516. [[CrossRef](#)]
7. Zhao, Y.; Yang, Q.; Chang, Y.; Pang, W.; Zhang, H.; Duan, X. Novel Gas Sensor Arrays Based on High-Q SAM-Modified Piezotransduced Single-Crystal Silicon Bulk Acoustic Resonators. *Sensors* **2017**, *17*, 1507. [[CrossRef](#)]
8. Campaña, A.; Florez, S.; Noguera, M.; Fuentes, O.; Ruiz Puentes, P.; Cruz, J.; Osma, J. Enzyme-Based Electrochemical Biosensors for Microfluidic Platforms to Detect Pharmaceutical Residues in Wastewater. *Biosensors* **2019**, *9*, 41. [[CrossRef](#)] [[PubMed](#)]
9. Lee, S.-H.; Park, J.-U.; Kim, G.; Jee, D.-W.; Kim, J.H.; Kim, S. Rigorous Study on Hump Phenomena in Surrounding Channel Nanowire (SCNW) Tunnel Field-Effect Transistor (TFET). *Appl. Sci.* **2020**, *10*, 3596. [[CrossRef](#)]
10. Mohammed, M.; Chun, D.-M. Electrochemical Performance of Few-Layer Graphene Nano-Flake Supercapacitors Prepared by the Vacuum Kinetic Spray Method. *Coatings* **2018**, *8*, 302. [[CrossRef](#)]
11. Wang, Y.; Mao, Y.; Ji, Q.; Yang, M.; Yang, Z.; Lin, H. Electrostatic Discharge Characteristics of SiGe Source/Drain PNN Tunnel FET. *Electronics* **2021**, *10*, 454. [[CrossRef](#)]
12. Li, S.; Lam, K.H.; Cheng, K.W.E. The Thermoelectric Analysis of Different Heat Flux Conduction Materials for Power Generation Board. *Energies* **2017**, *10*, 1781. [[CrossRef](#)]
13. Kumar, S.G.; Rao, K.S.R.K. Physics and chemistry of CdTe/CdS thin film heterojunction photovoltaic devices: Fundamental and critical aspects. *Energy Environ. Sci.* **2014**, *7*, 45–102. [[CrossRef](#)]
14. Alzoubi, T.; Moustafa, M. Numerical optimization of absorber and CdS buffer layers in CIGS solar cells using SCAPS. *Int. J. Smart Grid Clean Energy* **2019**, *8*, 291–298. [[CrossRef](#)]
15. Bag, S.; Gunawan, O.; Gokmen, T.; Zhu, Y.; Todorov, T.K.; Mitzi, D.B. Low band gap liquid-processed CZTSe solar cell with 10.1% efficiency. *Energy Environ. Sci.* **2012**, *5*, 7060–7065. [[CrossRef](#)]
16. Jiang, F.; Shen, H.; Gao, C.; Liu, B.; Lin, L.; Shen, Z. Preparation and properties of SnS film grown by two-stage process. *Appl. Surf. Sci.* **2011**, *257*, 4901–4905. [[CrossRef](#)]
17. Sreedevi, G.; Vasudeva Reddy, M.; Park, C.; Jeon, C.W.; Ramakrishna Reddy, K.T. Comprehensive optical studies on SnS layers synthesized by chemical bath deposition. *Opt. Mater.* **2015**, *42*, 468–475. [[CrossRef](#)]
18. Koteeswara Reddy, N.; Ramakrishna Reddy, K.T. Preparation and characterisation of sprayed tin sulphide films grown at different precursor concentrations. *Mater. Chem. Phys.* **2007**, *102*, 13–18. [[CrossRef](#)]
19. Jiang, F.; Shen, H.; Wang, W.; Zhang, L. Preparation of SnS film by sulfurization and SnS/a-Si heterojunction solar cells. *J. Electrochem. Soc.* **2012**, *159*, H235. [[CrossRef](#)]
20. Devika, M.; Koteeswara Reddy, N.; Venkatramana Reddy, S.; Ramesh, K.; Gunasekhar, K.R. Influence of rapid thermal annealing (RTA) on the structural and electrical properties of SnS films. *J. Mater. Sci. Mater. Electron.* **2009**, *20*, 1129–1134. [[CrossRef](#)]
21. Noguchi, H.; Setiyadi, A.; Tanamura, H.; Nagatomo, T.; Omoto, O. Characterization of vacuum-evaporated tin sulfide film for solar cell materials. *Sol. Energy Mater. Sol. Cells* **1994**, *35*, 325–331. [[CrossRef](#)]
22. Ogah, O.E.; Zoppi, G.; Forbes, I.; Miles, R.W. Thin films of tin sulphide for use in thin film solar cell devices. *Thin Solid Films* **2009**, *517*, 2485–2488. [[CrossRef](#)]
23. Ragina, A.J.; Murali, K.V.; Preetha, K.C.; Deepa, K.; Remadevi, T.L. A Study of optical parameters of tin sulphide thin films using the swanepoel method. In *AIP Conference Proceedings*; American Institute of Physics: College Park, MD, USA, 2011; Volume 1391, pp. 752–754.
24. Mahdi, M.S.; Ibrahim, K.; Hmood, A.; Ahmed, N.M.; Mustafa, F.I.; Azzez, S.A. High performance near infrared photodetector based on cubic crystal structure SnS thin film on a glass substrate. *Mater. Lett.* **2017**, *200*, 10–13. [[CrossRef](#)]
25. Nair, P.K.; Garcia-Angelmo, A.R.; Nair, M.T.S. Cubic and orthorhombic SnS thin-film absorbers for tin sulfide solar cells. *Phys. Status Solidi Appl. Mater. Sci.* **2016**, *213*, 170–177. [[CrossRef](#)]
26. Chalapathi, U.; Poornaprakash, B.; Park, S.-H. Growth and properties of cubic SnS films prepared by chemical bath deposition using EDTA as the complexing agent. *J. Alloys Compd.* **2016**, *689*, 938–944. [[CrossRef](#)]
27. Mahdi, M.S.; Ibrahim, K.; Ahmed, N.M.; Hmood, A.; Azzez, S.A.; Mustafa, F.I.; Bououdina, M. Influence of pH value on structural, optical and photoresponse properties of SnS films grown via chemical bath deposition. *Mater. Lett.* **2018**, *210*, 279–282. [[CrossRef](#)]
28. Garcia-Angelmo, A.R.; Romano-Trujillo, R.; Campos-Álvarez, J.; Gomez-Daza, O.; Nair, M.T.S.; Nair, P.K. Thin film solar cell of SnS absorber with cubic crystalline structure. *Phys. Status Solidi* **2015**, *212*, 2332–2340. [[CrossRef](#)]
29. Chalapathi, U.; Poornaprakash, B.; Park, S.H. Effect of post-deposition annealing on the growth and properties of cubic SnS films. *Superlattices Microstruct.* **2017**, *103*, 221–229. [[CrossRef](#)]

30. Alpen, U.V.; Fenner, J.; Gmelin, E. Semiconductors of the type MeII MeIVS₃. *Strateg. Surv.* **1975**, *76*, 50–54. [[CrossRef](#)]
31. Lopez, S.; Ortiz, A. Spray pyrolysis deposition of Sn_xS_y thin films. *Semicond. Sci. Technol.* **1994**, *9*, 2130–2133. [[CrossRef](#)]
32. Godoy-Rosas, R.; Barraza-Felix, S.; Ramirez-Bon, R.; Ochoa-Landin, R.; Pineda-Leon, H.A.; Flores-Acosta, M.; Ruvalcaba-Manzo, S.G.; Acosta-Enriquez, M.C.; Castillo, S.J. Synthesis and characterization of Sn₂S₃ as nanoparticles, powders and thin films, using soft chemistry reactions. *Chalcogenide Lett.* **2017**, *14*, 365–371.
33. Koteeswara Reddy, N.; Ramakrishna Reddy, K.T. Optical behaviour of sprayed tin sulphide thin films. *Mater. Res. Bull.* **2006**, *41*, 414–422. [[CrossRef](#)]
34. Guneri, E.; Gode, F.; Boyarbay, B.; Gumus, C. Structural and optical studies of chemically deposited Sn₂S₃ thin films. *Mater. Res. Bull.* **2012**, *47*, 3738–3742. [[CrossRef](#)]
35. Kanevce, A.; Reese, M.O.; Barnes, T.M.; Jensen, S.A.; Metzger, W.K. The roles of carrier concentration and interface, bulk, and grain-boundary recombination for 25% efficient CdTe solar cells. *J. Appl. Phys.* **2017**, *121*, 214506. [[CrossRef](#)]
36. Ristov, M.; Sinadinovski, G.; Grozdanov, I.; Mitreski, M. Chemical deposition of Tin(II) sulphide thin films. *Thin Solid Films* **1989**, *173*, 53–58. [[CrossRef](#)]
37. Acharya, S.; Srivastava, O.N. Electronic behaviour of SnS₂ crystals. *Phys. Status Solidi* **1981**, *65*, 717–723. [[CrossRef](#)]
38. Varkey, A.J. Preparation of tin disulphide thin films by solution growth. *Int. J. Mater. Prod. Technol.* **1997**, *12*, 490–495. [[CrossRef](#)]
39. Shi, C.; Chen, Z.; Shi, G.; Sun, R.; Zhan, X.; Shen, X. Influence of annealing on characteristics of tin disulfide thin films by vacuum thermal evaporation. *Thin Solid Films* **2012**, *520*, 4898–4901. [[CrossRef](#)]
40. Fadavieslam, M.R.; Shahtahmasebi, N.; Rezaee-Roknabadi, M.; Bagheri-Mohagheghi, M.M. Effect of deposition conditions on the physical properties of Sn_xS_y thin films prepared by the spray pyrolysis technique. *J. Semicond.* **2011**, *32*, 113002. [[CrossRef](#)]
41. Ramakrishna Reddy, K.T.; Sreedevi, G.; Ramya, K.; Miles, R. Physical properties of nano-crystalline SnS₂ layers grown by chemical bath deposition. *Energy Procedia* **2012**, *15*, 340–346. [[CrossRef](#)]
42. Ghorpade, U.; Suryawanshi, M.; Shin, S.W.; Gurav, K.; Patil, P.; Pawar, S.; Hong, C.W.; Kim, J.H.; Kolekar, S. Towards environmentally benign approaches for the synthesis of CZTSSe nanocrystals by a hot injection method: A status review. *Chem. Commun.* **2014**, *50*, 11258. [[CrossRef](#)]
43. Avellaneda, D.; Nair, M.T.S.; Nair, P.K. Polymorphic tin sulfide thin films of zinc blende and orthorhombic structures by chemical deposition. *J. Electrochem. Soc.* **2008**, *155*, D517. [[CrossRef](#)]
44. Gode, F.; Guneri, E.; Baglayan, O. Effect of tri-sodium citrate concentration on structural, optical and electrical properties of chemically deposited tin sulfide films. *Appl. Surf. Sci.* **2014**, *318*, 227–233. [[CrossRef](#)]
45. Koteeswara Reddy, N.; Ramakrishna Reddy, K.T. Electrical properties of spray pyrolytic tin sulfide films. *Solid State Electron.* **2005**, *49*, 902–906. [[CrossRef](#)]
46. Sinsermuksakul, P.; Heo, J.; Noh, W.; Hock, A.S.; Gordon, R.G. Atomic layer deposition of tin monosulfide thin films. *Adv. Energy Mater.* **2011**, *1*, 1116–1125. [[CrossRef](#)]
47. Wangperawong, A.; Herron, S.M.; Runser, R.R.; Hagglund, C.; Tanskanen, J.T.; Lee, H.B.R.; Clemens, B.M.; Bent, S.F. Vapor transport deposition and epitaxy of orthorhombic SnS on glass and NaCl substrates. *Appl. Phys. Lett.* **2013**, *103*, 052105. [[CrossRef](#)]
48. Djessas, K.; Masse, G. SnS thin films grown by close-spaced vapor transport. *J. Mater. Sci. Lett.* **2000**, *19*, 2135–2137. [[CrossRef](#)]
49. Albers, W.; Haas, C.; Vink, H.J.; Wasscher, J.D. Investigations on SnS. *J. Appl. Phys.* **1961**, *32*, 2220–2225. [[CrossRef](#)]
50. Chalapathi, U.; Poornaprakash, B.; Park, S.H. Chemically deposited cubic SnS thin films for solar cell applications. *Sol. Energy* **2016**, *139*, 238–248. [[CrossRef](#)]
51. Skelton, J.M.; Burton, L.A.; Jackson, A.J.; Oba, F.; Parker, S.C.; Walsh, A. Lattice dynamics of the tin sulphides SnS₂, SnS and Sn₂S₃: Vibrational spectra and thermal transport. *Phys. Chem. Chem. Phys.* **2017**, *19*, 12452–12465. [[CrossRef](#)] [[PubMed](#)]
52. Kherchachi, I.B.; Attaf, A.; Saidi, H.; Bouhdjar, A.; Bendjidi, H.; Youcef, B.; Azizi, R. The synthesis, characterization and phase stability of tin sulfides (SnS₂, SnS and Sn₂S₃) films deposited by ultrasonic spray. *Main Group Chem.* **2016**, *15*, 231–242. [[CrossRef](#)]
53. Chen, B.; Xu, X.; Wang, F.; Liu, J.; Ji, J. Electrochemical preparation and characterization of three-dimensional nanostructured Sn₂S₃ semiconductor films with nanorod network. *Mater. Lett.* **2011**, *65*, 400–402. [[CrossRef](#)]
54. Julien, C.; Eddrief, M.; Samaras, I.; Balkanski, M. Optical and electrical characterizations of SnSe, SnS₂ and SnSe₂ single crystals. *Mater. Sci. Eng. B* **1992**, *15*, 70–72. [[CrossRef](#)]
55. Madelung, O. IV-VII₂ compounds. In *Semiconductors: Data Handbook*; Springer: Berlin/Heidelberg, Germany, 2004; pp. 606–612.
56. Sreedevi, G.; Vasudeva Reddy, M.R.; Babu, P.; Chinho, P.; Chan Wook, J.; Ramakrishna Reddy, K.T. Studies on chemical bath deposited SnS₂ films for Cd-free thin film solar cells. *Ceram. Int.* **2017**, *43*, 3713–3719. [[CrossRef](#)]
57. Chen, S.; Gong, X.G.; Walsh, A.; Wei, S.-H. Defect physics of the kesterite thin-film solar cell absorber Cu₂ZnSnS₄. *Appl. Phys. Lett.* **2010**, *96*, 021902. [[CrossRef](#)]
58. Ettema, A.R.H.F.; de Groot, R.A.; Haas, C.; Turner, T.S. Electronic structure of SnS deduced from photoelectron spectra and band-structure calculations. *Phys. Rev. B* **1992**, *46*, 7363–7373. [[CrossRef](#)]
59. Lippens, P.E.; El Khalifi, M.; Womes, M. Electronic structures of SnS and SnS₂. *Phys. Status Solidi* **2016**, *254*, 1600194. [[CrossRef](#)]
60. Skelton, J.M.; Burton, L.A.; Oba, F.; Walsh, A. Chemical and lattice stability of the tin sulfides. *J. Phys. Chem. C* **2017**, *121*, 6446–6454. [[CrossRef](#)] [[PubMed](#)]
61. Lindwall, G.; Shang, S.; Kelly, N.R.; Anderson, T.; Liu, Z.K. Thermodynamics of the S-Sn system: Implication for synthesis of earth abundant photovoltaic absorber materials. *Sol. Energy* **2016**, *125*, 314–323. [[CrossRef](#)]

62. Wang, W.; Winkler, M.T.; Gunawan, O.; Gokmen, T.; Todorov, T.K.; Zhu, Y.; Mitzi, D.B. Device characteristics of CZTSSe thin-film solar cells with 12.6% efficiency. *Adv. Energy Mater.* **2014**, *4*, 1–5. [CrossRef]
63. Loferski, J.J. Theoretical considerations governing the choice of the optimum semiconductor for photovoltaic solar energy conversion. *J. Appl. Phys.* **1956**, *27*, 777–784. [CrossRef]
64. Skelton, J.M.; Burton, L.A.; Oba, F.; Walsh, A. Metastable cubic tin sulfide: A novel phonon-stable chiral semiconductor. *APL Mater.* **2017**, *5*, 036101. [CrossRef]
65. Herzenbergite. Available online: <https://www.mindat.org/min-1880.html> (accessed on 13 February 2018).
66. Ottemannite: Ottemannite Mineral Information and Data. Available online: <https://www.mindat.org/min-3042.html> (accessed on 13 February 2018).
67. Berndtite: Berndtite Mineral Information and Data. Available online: <https://www.mindat.org/min-637.html> (accessed on 13 February 2018).
68. Anthony, J.W.; Bideaux, R.A.; Bladh, K.W.; Nichols, M.C. *Handbook of Mineralogy-Borates, Carbonates, Sulfates*; Mineral Data Publishing: Tucson, AZ, USA, 2004; Volume V, p. 221.
69. Eastaugh, N.; Walsh, V.; Chaplin, T.; Ruth, S. *Pigment Compendium: A Dictionary and Optical Microscopy of Historical Pigments*; Butterworth-Heinemann: Oxfordshire, UK, 2008; ISBN 0750689803.
70. Moh, G.H.; Berndt, F. Two new natural tin sulfides, Sn₂S₃ and SnS₂. *New Yearb. Mineral. Monatshefte* **1964**, *4*, 94–95.
71. Yao, K.; Li, J.; Shan, S.; Jia, Q. One-step synthesis of urchinlike SnS/SnS₂ heterostructures with superior visible-light photocatalytic performance. *Catal. Commun.* **2017**, *101*, 51–56. [CrossRef]
72. Jing, J.; Cao, M.; Wu, C.; Huang, J.; Lai, J.; Sun, Y.; Wang, L.; Shen, Y. Chemical bath deposition of SnS nanosheet thin films for FTO/SnS/CdS/Pt photocathode. *J. Alloys Compd.* **2017**, *726*, 720–728. [CrossRef]
73. Zhang, F.; Zhang, Y.; Zhang, G.; Yang, Z.; Dionysiou, D.D.; Zhu, A. Exceptional synergistic enhancement of the photocatalytic activity of SnS₂ by coupling with polyaniline and N-doped reduced graphene oxide. *Appl. Catal. B Environ.* **2018**, *236*, 53–63. [CrossRef]
74. Sun, Y.; Cheng, H.; Gao, S.; Sun, Z.; Liu, Q.; Leu, Q.; Lei, F.; Yao, T.; He, J.; Wei, S.; et al. Freestanding tin disulfide single-layers realizing efficient visible-light water splitting. *Angew. Chem. Int. Ed.* **2012**, *51*, 8727–8731. [CrossRef]
75. Chauhan, H.; Singh, M.K.; Kumar, P.; Hashmi, S.A.; Deka, S. Development of SnS₂/RGO nanosheet composite for cost-effective aqueous hybrid supercapacitors. *Nanotechnology* **2017**, *28*, 025401. [CrossRef] [PubMed]
76. Wang, Y.; Huang, L.; Wei, Z. Photoresponsive field-effect transistors based on multilayer SnS₂ nanosheets. *J. Semicond.* **2017**, *38*, 034001. [CrossRef]
77. Wu, Q.; Jiao, L.; Du, J.; Yang, J.; Guo, L.; Liu, Y.; Wang, Y. One-pot synthesis of three-dimensional SnS₂ architectures as anode material for lithium-ion batteries. *J. Power Source* **2013**, *239*, 89–93. [CrossRef]
78. Li, H.; Zhou, M.; Li, W.; Wang, K.; Cheng, S.; Jiang, K. Layered SnS₂ cross-linked by carbon nanotubes as a high performance anode for sodium ion batteries. *RSC Adv.* **2016**, *6*, 35197–35202. [CrossRef]
79. Ou, J.Z.; Ge, W.; Carey, B.; Daeneke, T.; Rotbart, A.; Shan, W.; Wang, Y.; Fu, Z.; Chrimes, A.F.; Wlodarski, W.; et al. Physisorption-based charge transfer in two-dimensional SnS₂ for selective and reversible NO₂ gas sensing. *ACS Nano* **2015**, *9*, 10313–10323. [CrossRef] [PubMed]
80. Sanchez-Juarez, A.; Tiburcio-Silver, A.; Ortiz, A. Fabrication of SnS₂/SnS heterojunction thin film diodes by plasma-enhanced chemical vapor deposition. *Thin Solid Films* **2005**, *480*, 452–456. [CrossRef]
81. Fan, C.; Li, Y.; Lu, F.Y.; Deng, H.X.; Wei, Z.M.; Li, J.B. Wavelength dependent UV-Vis photodetectors from SnS₂ flakes. *RSC Adv.* **2016**, *6*, 422–427. [CrossRef]
82. Singh, D.J. Optical and electronic properties of semiconducting Sn₂S₃. *Appl. Phys. Lett.* **2016**, *109*, 1–5. [CrossRef]
83. Li, Y.; Xie, H.; Tu, J. Nanostructured SnS/carbon composite for supercapacitor. *Mater. Lett.* **2009**, *63*, 1785–1787. [CrossRef]
84. Saito, W.; Hayashi, K.; Nagai, H.; Miyazaki, Y. Preparation and thermoelectric properties of mixed valence compound Sn₂S₃. *Jpn. J. Appl. Phys.* **2017**, *56*, 061201. [CrossRef]
85. Devika, M.; Koteeswara Reddy, N.; Sreekantha Reddy, D.; Ramesh, K.; Gunasekhar, K.; Raja Gopal, E.; Sung Ha, P. Metal-insulator-semiconductor field-effect transistors (MISFETs) using p-type SnS and nanometer-thick Al₂S₃ layers. *RSC Adv.* **2017**, *7*, 11111–11117. [CrossRef]
86. Wang, W.; Shi, L.; Lan, D.; Li, Q. Improving cycle stability of SnS anode for sodium-ion batteries by limiting Sn agglomeration. *J. Power Source* **2018**, *377*, 1–6. [CrossRef]
87. Lian, Q.; Zhou, G.; Liu, J.; Wu, C.; Wei, W.; Chen, L.; Li, C. Extrinsic pseudocapacitive Li-ion storage of SnS anode via lithiation-induced structural optimization on cycling. *J. Power Source* **2017**, *366*, 1–8. [CrossRef]
88. Afsar, M.F.; Rafiq, M.A.; Tok, A.I.Y. Two-dimensional SnS nanoflakes: Synthesis and application to acetone and alcohol sensors. *RSC Adv.* **2017**, *7*, 21556–21566. [CrossRef]
89. Chung, R.J.; Wang, A.N.; Peng, S.Y. An enzymatic glucose sensor composed of carbon-coated nano tin sulfide. *Nanomaterials* **2017**, *7*, 39. [CrossRef]
90. Wang, C.; Chen, Y.; Jiang, J.; Zhang, R.; Niu, Y.; Zhou, T.; Xia, J.; Tian, H.; Hu, J.; Yang, P. Improved thermoelectric properties of SnS synthesized by chemical precipitation. *RSC Adv.* **2017**, *7*, 16795–16800. [CrossRef]
91. Jayalakshmi, M.; Mohan Rao, M.; Choudary, B.M. Identifying nano SnS as a new electrode material for electrochemical capacitors in aqueous solutions. *Electrochem. Commun.* **2004**, *6*, 1119–1122. [CrossRef]

92. Nozaki, H.; Fukano, T.; Ohta, S.; Seno, Y.; Katagiri, H.; Jimbo, K. Crystal structure determination of solar cell materials: $\text{Cu}_2\text{ZnSnS}_4$ thin films using X-ray anomalous dispersion. *J. Alloys Compd.* **2012**, *524*, 22–25. [[CrossRef](#)]
93. Burton, L.A.; Walsh, A. Phase stability of the earth-abundant tin sulfides SnS , SnS_2 , and Sn_2S_3 . *J. Phys. Chem. C* **2012**, *116*, 24262–24267. [[CrossRef](#)]
94. Ahmet, I.Y.; Hill, M.S.; Johnson, A.L.; Peter, L.M. polymorph-selective deposition of high purity SnS thin films from a single source precursor. *Chem. Mater.* **2015**, *27*, 7680–7688. [[CrossRef](#)]
95. Ehm, L.; Knorr, K.; Dera, P.; Krimmel, A.; Bouvier, P.; Mezouar, M. Pressure-induced structural phase transition in the IV–VI semiconductor SnS . *J. Phys. Condens. Matter* **2004**, *16*, 3545–3554. [[CrossRef](#)]
96. Brownson, J.R.S.; Georges, C.; Larramona, G.; Jacob, A.; Delatouche, B.; Levy-Clement, C. Chemistry of tin monosulfide (δ - SnS) electrodeposition. *J. Electrochem. Soc.* **2008**, *155*, D40. [[CrossRef](#)]
97. Brownson, J.R.S.; Georges, C.; Levy-Clement, C. Synthesis of a δ - SnS polymorph by electrodeposition. *Chem. Mater.* **2006**, *18*, 6397–6402. [[CrossRef](#)]
98. Mariano, A.N.; Chopra, K.L. Polymorphism in some IV–VI compounds induced by high pressure and thin-film epitaxial growth. *Appl. Phys. Lett.* **1967**, *10*, 282–284. [[CrossRef](#)]
99. Rabkin, A.; Samuha, S.; Abutbul, R.E.; Ezersky, V.; Meshi, L.; Golan, Y. New nanocrystalline materials: A previously unknown simple cubic phase in the SnS binary system. *Nano Lett.* **2015**, *15*, 2174–2179. [[CrossRef](#)]
100. Biacchi, A.J.; Vaughn, D.D.; Schaak, R.E. Synthesis and crystallographic analysis of shape-controlled SnS nanocrystal photocatalysts: Evidence for a pseudotetragonal structural modification. *J. Am. Chem. Soc.* **2013**, *135*, 11634–11644. [[CrossRef](#)] [[PubMed](#)]
101. Wang, X.; Liu, Z.; Zhao, X.-G.; Lv, J.; Biswas, K.; Zhang, L. Computational design of mixed-valence tin sulfides as solar absorbers. *ACS Appl. Mater. Interfaces* **2019**, *11*, 24867–24875. [[CrossRef](#)] [[PubMed](#)]
102. Sugaki, A.; Kitakaze, A.; Kitazawa, H. Synthesized tin and tin-silver sulfide minerals: Synthetic sulfide minerals (XIII). *Sci. Rep.* **1985**, *3*, 199–211.
103. Guenter, J.R.; Oswald, H. New polytype form of tin (IV) sulfide. *Nat. Sci.* **1968**, *55*, 171–177. [[CrossRef](#)]
104. Mosburg, S.; Ross, D.R.; Bethke, P.M.; Toulmin, P. X-ray powder data for herzenbergite, teallite and tin trisulfide. *US Geol. Surv. Prof. Pap. C* **1961**, *424*, 347.
105. Babu, P.; Vasudeva Reddy, M.; Sreedevi, G.; Chinho, P. Review on earth-abundant and environmentally benign Cu-Sn-X ($X = \text{S}, \text{Se}$) nanoparticles by chemical synthesis for sustainable solar energy conversion. *J. Ind. Eng. Chem.* **2018**, *60*, 19–52. [[CrossRef](#)]
106. Nikolic, P.M.; Mihajlovic, P.; Lavrencic, B. Splitting and coupling of lattice modes in the layer compound SnS . *J. Phys. C Solid State Phys.* **1977**, *10*, L289–L292. [[CrossRef](#)]
107. Wiley, J.D.; Buckel, W.J.; Schmidt, R.L. Infrared reflectivity and Raman scattering in GeS . *Phys. Rev. B* **1976**, *13*, 2489–2496. [[CrossRef](#)]
108. Smith, A.J.; Meek, P.E.; Liang, W.Y. Raman scattering studies of SnS_2 and SnSe_2 . *J. Phys. C Solid State Phys.* **1977**, *10*, 1321–1323. [[CrossRef](#)]
109. Chandrasekhar, H.R.; Mead, D.G. Long-wavelength phonons in mixed-valence semiconductor $\text{Sn}_{1-x}\text{Sn}_{1+x}\text{S}_3$. *Phys. Rev. B* **1979**, *19*, 932–937. [[CrossRef](#)]
110. Gedi, S.; Reddy, V.R.M.; Kang, J.; Jeon, C.-W. Impact of high temperature and short period annealing on SnS films deposited by E-beam evaporation. *Appl. Surf. Sci.* **2017**, *402*, 463–468. [[CrossRef](#)]
111. Abutbul, R.E.; Segev, E.; Zeiri, L.; Ezersky, V.; Makov, G.; Golan, Y. Synthesis and properties of nanocrystalline π - SnS —A new cubic phase of tin sulphide. *RSC Adv.* **2016**, *6*, 5848–5855. [[CrossRef](#)]
112. Bharatula, L.D.; Erande, M.B.; Mulla, I.S.; Rout, C.S.; Late, D.J. SnS_2 nanoflakes for efficient humidity and alcohol sensing at room temperature. *RSC Adv.* **2016**, *6*, 105421–105427. [[CrossRef](#)]
113. Reddy, T.S.; Kumar, M.C.S. Effect of substrate temperature on the physical properties of co-evaporated Sn_2S_3 thin films. *Ceram. Int.* **2016**, *42*, 12262–12269. [[CrossRef](#)]
114. Kumagai, Y.; Burton, L.A.; Walsh, A.; Oba, F. Electronic structure and defect physics of tin sulfides: SnS , Sn_2S_3 , and SnS_2 . *Phys. Rev. Appl.* **2016**, *6*, 1–14. [[CrossRef](#)]
115. Burton, L.A.; Colombara, D.; Abellon, R.D.; Grozema, F.C.; Peter, L.M.; Savenije, T.J.; Dennler, G.; Walsh, A. Synthesis, characterization, and electronic structure of single-crystal SnS , Sn_2S_3 , and SnS_2 . *Chem. Mater.* **2013**, *25*, 4908–4916. [[CrossRef](#)]
116. Vasudeva Reddy, M.R.; Mohan Reddy, P.; Phaneendra Reddy, G.; Sreedevi, G.; Kishore Kumar, Y.B.R.; Babu, P.; Woo Kyoung, K.; Ramakrishna Reddy, K.T.; Chinho, P. Review on Cu_2SnS_3 , Cu_3SnS_4 , and Cu_4SnS_4 thin films and their photovoltaic performance. *J. Ind. Eng. Chem.* **2019**, *76*, 39–74. [[CrossRef](#)]
117. Khoa, D.Q.; Nguyen, C.V.; Phuc, H.V.; Ilyasov, V.V.; Vu, T.V.; Cuong, N.Q.; Hoi, B.D.; Lu, D.V.; Feddi, E.; El-Yadri, M.; et al. Effect of strains on electronic and optical properties of monolayer SnS : Ab-initio study. *Phys. B Condens. Matter* **2018**, *545*, 255–261. [[CrossRef](#)]
118. Segev, E.; Abutbul, R.E.; Argaman, U.; Golan, Y.; Makov, G. Surface energies and nanocrystal stability in the orthorhombic and π -phases of tin and germanium monochalcogenides. *CrystEngComm* **2018**, *20*, 4237–4248. [[CrossRef](#)]
119. Qiu, G.; Zhang, H.; Liu, Y.; Xia, C. Strain effect on the electronic properties of Ce-doped SnS_2 monolayer. *Phys. B Condens. Matter* **2018**, *547*, 1–5. [[CrossRef](#)]

120. Ullah, H.; Noor-A-Alam, M.; Kim, H.J.; Shin, Y.H. Influences of vacancy and doping on electronic and magnetic properties of monolayer SnS. *J. Appl. Phys.* **2018**, *124*. [CrossRef]
121. Zandalazini, C.I.; Navarro Sanchez, J.; Albanesi, E.A.; Gupta, Y.; Arun, P. Contribution of lattice parameter and vacancies on anisotropic optical properties of tin sulphide. *J. Alloys Compd.* **2018**, *746*, 9–18. [CrossRef]
122. Akhoundi, E.; Faghihnasiri, M.; Memarzadeh, S.; Firouzian, A.H. Mechanical and strain-tunable electronic properties of the SnS monolayer. *J. Phys. Chem. Solids* **2019**, *126*, 43–54. [CrossRef]
123. Sreedevi, G.; Vasudeva Reddy, M.; Babu, P.; Chan-Wook, J.; Chinho, P.; Ramakrishna Reddy, K.T. A facile inexpensive route for SnS thin film solar cells with SnS₂ buffer. *Appl. Surf. Sci.* **2016**, *372*, 116–124. [CrossRef]
124. Srivind, J.; Nagarethinam, V.S.; Balu, A.R. Optimization of S:Sn precursor molar concentration on the physical properties of spray deposited single phase Sn₂S₃ thin films. *Mater. Sci. Pol.* **2016**, *34*, 393–398. [CrossRef]
125. Von Schnering, H.G.; Wiedemeier, H. The high temperature structure of β-SnS and β-SnSe and the B16-to-B33 type λ-transition path. *J. Crystallogr. Cryst. Mater.* **1981**, *156*, 143–150. [CrossRef]
126. Hazen RM and Finger LW The crystal structures and compressibilities of layer minerals at high pressure. I SnS₂, berndite. *Am. Mineral.* **1978**, *63*, 289–292.
127. Park, H.K.; Jo, J.; Hong, H.K.; Song, G.Y.; Heo, J. Structural, optical, and electrical properties of tin sulfide thin films grown with electron-beam evaporation. *Curr. Appl. Phys.* **2015**, *15*, 964–969. [CrossRef]
128. Nair, M.T.S.; Nair, P.K. Simplified chemical deposition technique for good quality SnS thin films. *Semicond. Sci. Technol* **1991**, *6*, 132–134. [CrossRef]
129. Price, L.S.; Parkin, I.P.; Hardy, A.M.E.; Clark, R.J.H.; Hibbert, T.G.; Molloy, K.C. Atmospheric pressure chemical vapor deposition of tin sulfides (SnS, Sn₂S₃, and SnS₂) on glass. *Chem. Mater.* **1999**, *11*, 1792–1799. [CrossRef]
130. Lokhande, C.D. A chemical method for tin disulphide thin film deposition. *J. Phys. D Appl. Phys.* **1990**, *23*, 1703–1705. [CrossRef]
131. Li, J.; Zhang, Y.C.; Zhang, M. Preparation of SnS₂ thin films by chemical bath deposition. *Mater. Sci. Forum* **2010**, *663*, 104–107. [CrossRef]
132. Thangaraju, B.; Kaliannan, P. Spray pyrolytic deposition and characterization of SnS and SnS₂ thin films. *J. Phys. D Appl. Phys.* **2000**, *33*, 1054–1059. [CrossRef]
133. Gopalakrishnan, P.; Anbazhagan, G.; Vijayarajasekaran, J.; Vijayakumar, K. Effect of substrate temperature on tin disulphide thin films. *Int. J. Thin Film. Sci. Technol.* **2017**, *6*, 73–75. [CrossRef]
134. Tomas, R.; Lukas, S.; Libor, D.; Marek, B.; Milan, V.; Ludvik, B.; Tomas, W.; Roman, J. SnS and SnS₂ thin films deposited using a spin-coating technique from intramolecularly coordinated organotin sulfides. *Appl. Organomet. Chem.* **2015**, *29*, 176–180. [CrossRef]
135. Anitha, N.; Anitha, M.; Amalraj, L. Influence of precursor solution volume on the properties of tin disulphide (SnS₂) thin films prepared by nebulized spray pyrolysis technique. *Opt. Int. J. Light Electron Opt.* **2017**, *148*, 28–38. [CrossRef]
136. Vijayakumar, K.; Sanjeeviraja, C.; Jayachandran, M.; Amalraj, L. Characterization of tin disulphide thin films prepared at different substrate temperature using spray pyrolysis technique. *J. Mater. Sci. Mater. Electron.* **2011**, *22*, 929–935. [CrossRef]
137. Sanchez-Juarez, A.; Ortiz, A. Effects of precursor concentration on the optical and electrical properties of Sn_xS_y thin films prepared by plasma-enhanced chemical vapour deposition. *Semicond. Sci. Technol.* **2002**, *17*, 931–937. [CrossRef]
138. Amalraj, L.; Sanjeeviraja, C.; Jayachandran, M. Spray pyrolysed tin disulphide thin film and characterisation. *J. Cryst. Growth* **2002**, *234*, 683–689. [CrossRef]
139. Ragina, A.J.; Murali, K.V.; Preetha, K.C.; Deepa, K.; Remadevi, T.L. UV irradiated wet chemical deposition and characterization of nanostructured tin sulfide thin films. *J. Mater. Sci. Mater. Electron.* **2012**, *23*, 2264–2271. [CrossRef]
140. Joshua Gnanamuthu, S.; Johnson Jeyakumar, S.; Kartharinal Punithavathy, I.; Jobe Prabhakar, P.C.; Suganya, M.; Usharani, K.; Balu, A.R. Properties of spray deposited nano needle structured Cu-doped Sn₂S₃ thin films towards photovoltaic applications. *Optik* **2016**, *127*, 3999–4003. [CrossRef]
141. Khadraoui, M.; Benramdane, N.; Mathieu, C.; Bouzidi, A.; Miloua, R.; Kebbab, Z.; Sahraoui, K.; Desfeux, R.; Wang, M. Optical and electrical properties of Sn₂S₃ thin films grown by spray pyrolysis. *Solid State Commun.* **2010**, *150*, 297–300. [CrossRef]
142. Mnari, M.; Kamoun, N.; Bonnet, J.; Dachraoui, M. Chemical bath deposition of tin sulphide thin films in acid solution. *Comptes Rendus Chim.* **2009**, *12*, 824–827. [CrossRef]
143. David Smyth-Boyle's Homepage. Available online: <http://www.ch.ic.ac.uk/obrien/barton/dsb/dsbcbd.html> (accessed on 14 February 2018).
144. Sreedevi, G.; Vasudeva Reddy, M.; Ramakrishna Reddy, K.T.; Soo Hyun, K.; Chan Wook, J. Chemically synthesized Ag-doped SnS films for PV applications. *Ceram. Int.* **2016**, *42*, 19027–19035. [CrossRef]
145. Pramanik, P.; Basu, P.K.; Biswas, S. Preparation and characterization of chemically deposited tin(II) sulphide thin films. *Thin Solid Films* **1987**, *150*, 269–276. [CrossRef]
146. Garcia-Angelmo, A.R.; Nair, M.T.S.; Nair, P.K. Evolution of crystalline structure in SnS thin films prepared by chemical deposition. *Solid State Sci.* **2014**, *30*, 26–35. [CrossRef]
147. Lokhande, C.D.; Bhad, V.V.; Dhumure, S.S. Conversion of tin disulphide into silver sulphide by a simple chemical method. *J. Phys. D Appl. Phys.* **1992**, *25*, 315–318. [CrossRef]
148. Opananont, B.; Baxter, J.B. Dynamic speciation modeling to guide selection of complexing agents for chemical bath deposition: Case study for ZnS thin films. *Cryst. Growth Des.* **2015**, *15*, 4893–4900. [CrossRef]

149. Lokhande, C.D. Chemical deposition of metal chalcogenide thin films. *Mater. Chem. Phys.* **1991**, *27*, 1–43. [CrossRef]
150. Chopra, K.L.; Kainthla, R.C.; Pandya, D.K.; Thakoor, A.P. *Physics of Thin Films*; Francombe, M.H., Vossen, J.L., Eds.; Academic Press: New York, NY, USA, 1982; Volume 12, p. 201.
151. Chopra, K.L.; Kainthla, R.C.; Pandya, D.K.; Thakoor, A.P. Chemical solution deposition of inorganic films. In *Physics of Thin Films*; Elsevier: Amsterdam, The Netherlands, 1982; Volume 12, pp. 167–235. ISBN 0079-1970.
152. Savadogo, O.; Mandal, K.C. Studies on new chemically deposited photoconducting antimony trisulphide thin films. *Sol. Energy Mater. Sol. Cells* **1992**, *26*, 117–136. [CrossRef]
153. Licht, S.; Longo, K.; Peramunage, D.; Forouzan, F. Conductometric analysis of the second acid dissociation constant of H₂S in highly concentrated aqueous media. *J. Electroanal. Chem. Interfacial Electrochem.* **1991**, *318*, 111–129. [CrossRef]
154. Pentia, E.; Draghici, V.; Sarau, G.; Mereu, B.; Pintilie, L.; Sava, F.; Popescu, M. Structural, electrical, and photoelectrical properties of Cd_xPb_{1-x}S thin films prepared by chemical bath deposition. *J. Electrochem. Soc.* **2004**, *151*, G729. [CrossRef]
155. Wired Chemist, Solubility Product Constants, K_{sp}. Available online: <http://www.wiredchemist.com/chemistry/data/solubility-product-constants> (accessed on 30 April 2018).
156. Vaxasoftware, Solubility Product Constants. Available online: http://www.vaxasoftware.com/doc_eduen/qui/ks.pdf (accessed on 30 April 2018).
157. Engelken, R.D.; Ali, S.; Chang, L.N.; Brinkley, C.; Turner, K.; Hester, C. Study and development of a generic electrochemical ion-exchange process to form M_xS optoelectronic materials from ZnS precursor films formed by chemical-precipitation solution deposition. *Mater. Lett.* **1990**, *10*, 264–274. [CrossRef]
158. Nair, M.T.S.; Nair, P.K. SnS-Cu_xS thin film combination: A desirable solar control coating for architectural and automobile glazings. *J. Phys. D Appl. Phys.* **1991**, *24*, 450–453. [CrossRef]
159. Nair, P.K.; Nair, M.T.S. Chemically deposited SnS-Cu_xS thin films with high solar absorptance: New approach to all-glass tubular solar collectors. *J. Phys. D. Appl. Phys.* **1991**, *24*, 83–87. [CrossRef]
160. Nair, P.K.; Nair, M.T.S.; Campos, J.; Sanchez, A. SnS-SnO₂ conversion of chemically deposited SnS thin films. *Adv. Mater. Opt. Electron.* **1992**, *1*, 117–121. [CrossRef]
161. Nair, P.K. Photoconductive SnO₂ thin films from thermal decomposition of chemically deposited SnS thin films. *J. Electrochem. Soc.* **1993**, *140*, 539. [CrossRef]
162. Nair, P.K.; Nair, M.T.S.; Zingaro, R.A.; Meyers, E.A. XRD, XPS, optical and electrical studies on the conversion of SnS thin films to SnO₂. *Thin Solid Films* **1994**, *239*, 85–92. [CrossRef]
163. Ray, S.C.; Karanjai, M.K.; DasGupta, D. Structure and photoconductive properties of dip-deposited SnS and SnS₂ thin films and their conversion to tin dioxide by annealing in air. *Thin Solid Films* **1999**, *350*, 72–78. [CrossRef]
164. Ristov, M.; Sinadinovski, G.; Mitreski, M.; Ristova, M. Photovoltaic cells based on chemically deposited p-type SnS. *Sol. Energy Mater. Sol. Cells* **2001**, *69*, 17–24. [CrossRef]
165. Tanusevski, A. Optical and photoelectric properties of SnS thin films prepared by chemical bath deposition. *Semicond. Sci. Technol.* **2003**, *18*, 501–505. [CrossRef]
166. Nair, M.T.S.; Lopez-Mata, C.; GomezDaza, O.; Nair, P.K. Copper tin sulfide semiconductor thin films produced by heating SnS-CuS layers deposited from chemical bath. *Semicond. Sci. Technol.* **2003**, *18*, 755–759. [CrossRef]
167. Niinobe, D.; Wada, Y. Controlled deposition of SnS into/onto SnO₂ nano-particle film and application to photoelectrochemical cells. *Bull. Chem. Soc. Jpn.* **2006**, *79*, 495–497. [CrossRef]
168. Avellaneda, D.; Delgado, G.; Nair, M.T.S.; Nair, P.K. Structural and chemical transformations in SnS thin films used in chemically deposited photovoltaic cells. *Thin Solid Films* **2007**, *515*, 5771–5776. [CrossRef]
169. Ge, Y.H.; Guo, Y.Y.; Shi, W.M.; Qiu, Y.H.; Wei, G.P. Influence of In-doping on resistivity of chemical bath deposited SnS films. *J. Shanghai Univ.* **2007**, *11*, 403–406. [CrossRef]
170. Hankare, P.P.; Jadhav, A.V.; Chate, P.A.; Rathod, K.C.; Chavan, P.A.; Ingole, S.A. Synthesis and characterization of tin sulphide thin films grown by chemical bath deposition technique. *J. Alloys Compd.* **2008**, *463*, 581–584. [CrossRef]
171. Avellaneda, D.; Nair, M.T.S.; Nair, P.K. Photovoltaic structures using chemically deposited tin sulfide thin films. *Thin Solid Films* **2009**, *517*, 2500–2502. [CrossRef]
172. Turan, E.; Kul, M.; Aybek, A.S.; Zor, M. Structural and optical properties of SnS semiconductor films produced by chemical bath deposition. *J. Phys. D Appl. Phys.* **2009**, *42*, 245408. [CrossRef]
173. Mathews, N.R.; Avellaneda, D.; Anaya, H.B.M.; Campos, J.; Nair, M.T.S.; Nair, P.K. Chemically and electrochemically deposited thin films of tin sulfide for photovoltaic structures. *Mater. Res. Soc. Symp. Proc.* **2009**, *1165*, 367–373. [CrossRef]
174. Aksay, S.; Ozer, T.; Zor, M. Vibrational and X-ray diffraction spectra of SnS film deposited by chemical bath deposition method. *Eur. Phys. J. Appl. Phys.* **2009**, *47*, 30502. [CrossRef]
175. Wang, Y.; Reddy, Y.B.K.; Gong, H. Large-surface-area nanowall SnS films prepared by chemical bath deposition. *J. Electrochem. Soc.* **2009**, *156*, H157. [CrossRef]
176. Akkari, A.; Guasch, C.; Kamoun, T.N. Chemically deposited tin sulphide. *J. Alloys Compd.* **2010**, *490*, 180–183. [CrossRef]
177. Guneri, E.; Ulutas, C.; Kirmizigul, F.; Altindemir, G.; Gode, F.; Gumus, C. Effect of deposition time on structural, electrical, and optical properties of SnS thin films deposited by chemical bath deposition. *Appl. Surf. Sci.* **2010**, *257*, 1189–1195. [CrossRef]
178. Guneri, E.; Gode, F.; Ulutas, C.; Kirmizigul, F.; Altindemir, G.; Gumus, C. Properties of p-type SnS thin films prepared by chemical bath deposition. *Chalcogenide Lett.* **2010**, *7*, 685–694.

179. Gaied, I.; Akkari, A.; Yacoubi, N.; Kamoun, N. Influence of the triethanolamine concentration on the optical properties of tin sulphide thin films by the photothermal deflection spectroscopy. *J. Phys. Conf. Ser.* **2010**, *214*, 012128. [[CrossRef](#)]
180. Wang, Y.; Gong, H.; Fan, B.; Hu, G. Photovoltaic behavior of nanocrystalline SnS/TiO₂. *J. Phys. Chem. C* **2010**, *114*, 3256–3259. [[CrossRef](#)]
181. Ragina, A.J.; Preetha, K.C.; Murali, K.V.; Deepa, K.; Remadevi, T.L. Wet chemical synthesis and characterization of tin sulphide thin films from different host solutions. *Adv. Appl. Sci. Res.* **2011**, *2*, 438–444.
182. Kassim, A.; Min, H.S.; Sharif, A.; Haron, J.; Nagalingam, S. Chemical bath deposition of SnS thin films: AFM, EDAX and UV-Visible characterization. *Orient. J. Chem.* **2011**, *27*, 1375–1381.
183. Kassim, A.; Min, H.S.; Shariff, A.; Haron, M.J. The effect of the pH value on the growth and properties of chemical bath deposited SnS thin films. *Mater. Chem. Phys.* **2011**, *15*, 45–48. [[CrossRef](#)]
184. Gao, C.; Shen, H.; Sun, L.; Shen, Z. Chemical bath deposition of SnS films with different crystal structures. *Mater. Lett.* **2011**, *65*, 1413–1415. [[CrossRef](#)]
185. Gao, C.; Shen, H.; Sun, L. Preparation and properties of zinc blende and orthorhombic SnS films by chemical bath deposition. *Appl. Surf. Sci.* **2011**, *257*, 6750–6755. [[CrossRef](#)]
186. Herron, S.M.; Wangperawong, A.; Bent, S.F. Chemical bath deposition and microstructuring of tin (II) sulfide films for photo-voltaics. In Proceedings of the 37th IEEE Photovoltaic Specialists Conference, Seattle, WA, USA, 19–24 June 2011; pp. 368–371.
187. Gao, C.; Shen, H. Influence of the deposition parameters on the properties of orthorhombic SnS films by chemical bath deposition. *Thin Solid Films* **2012**, *520*, 3523–3527. [[CrossRef](#)]
188. Xia, D.L.; Xu, J.; Shi, W.Q.; Lei, P.; Zhao, X.J. Synthesis and properties of SnS thin films by chemical bath deposition. *Eng. Mater.* **2012**, *509*, 333–338. [[CrossRef](#)]
189. Martinez, H.; Avellaneda, D. Modifications in SnS thin films by plasma treatments. *Nucl. Instrum. Methods Phys. Res. Sect. B Beam Interact. Mater. Atoms* **2012**, *272*, 351–356. [[CrossRef](#)]
190. Patel, T.H. Influence of deposition time on structural and optical properties of chemically deposited SnS thin films. *Open Surf. Sci. J.* **2012**, *4*, 6–13. [[CrossRef](#)]
191. Jayasree, Y.; Chalapathi, U.; Uday Bhaskar, P.; Raja, V.S. Effect of precursor concentration and bath temperature on the growth of chemical bath deposited tin sulphide thin films. *Appl. Surf. Sci.* **2012**, *258*, 2732–2740. [[CrossRef](#)]
192. Avellaneda, D.; Krishnan, B.; Das Roy, T.K.; Castillo, G.A.; Shaji, S. Modification of structure, morphology and physical properties of tin sulfide thin films by pulsed laser irradiation. *Appl. Phys. A* **2013**, *110*, 667–672. [[CrossRef](#)]
193. Sreedevi, G.; Ramakrishna Reddy, K.T. Properties of tin monosulphide films grown by chemical bath deposition. *Conf. Pap. Energy* **2013**, *2013*, 528724. [[CrossRef](#)]
194. Soonmin, H.; Kassim, A.; Weetee, T. Thickness dependent characteristics of chemically deposited tin sulfide films. *Univ. J. Chem.* **2013**, *1*, 170–174. [[CrossRef](#)]
195. Osuwa, J.C.; Ugochukwu, J. Effects of aluminum and manganese impurity concentrations on optoelectronic properties of thin films of tin sulfide (SnS) using CBD method. *IOSR J. Environ. Sci. Toxicol. Food Technol.* **2013**, *5*, 32–36. [[CrossRef](#)]
196. Onwuemeka, J.I.; Ezike, F.M.; Nwulu, N.C. The effect of annealing temperature and time on the optical properties of SnS thin films prepared by chemical bath deposition. *Int. J. Innov. Educ. Res.* **2013**, *1*, 121–130. [[CrossRef](#)]
197. Reghima, M.; Akkari, A.; Guasch, C.; Castagné, M.; Kamoun-Turki, N. Synthesis and characterization of Fe-doped SnS thin films by chemical bath deposition technique for solar cells applications. *J. Renew. Sustain. Energy* **2013**, *5*, 063109. [[CrossRef](#)]
198. Jayasree, Y.; Chalapathi, U.; Raja, V.S. Growth and characterization of tin sulphide thin films by chemical bath deposition using ethylene diamine tetra-acetic acid as the complexing agent. *Thin Solid Films* **2013**, *537*, 149–155. [[CrossRef](#)]
199. Dhanya, A.C.; Deepa, K.; Geetanjali, P.M.; Anupama, M.; Remadevi, T.L. Effect of post deposition by UV irradiation on chemical bath deposited tin sulfide thin films. *Appl. Phys. A* **2014**, *116*, 1467–1472. [[CrossRef](#)]
200. He, H.Y.; Fei, J.; Lu, J. Optical and electrical properties of pure and Sn⁴⁺-doped n-SnS films deposited by chemical bath deposition. *Mater. Sci. Semicond. Process.* **2014**, *24*, 90–95. [[CrossRef](#)]
201. Safonova, M.; Nair, P.K.; Mellikov, E.; Garcia, A.R.; Kerm, K.; Revathi, N.; Romann, T.; Mikli, V.; Volobujeva, O. Chemical bath deposition of SnS thin films on ZnS and CdS substrates. *J. Mater. Sci. Mater. Electron.* **2014**, *25*, 3160–3165. [[CrossRef](#)]
202. Avellaneda, D.; Krishnan, B.; Rodriguez, A.C.; Das Roy, T.K.; Shaji, S. Heat treatments in chemically deposited SnS thin films and their influence in CdS/SnS photovoltaic structures. *J. Mater. Sci. Mater. Electron.* **2015**, *26*, 5585–5592. [[CrossRef](#)]
203. Joshi, L.P.; Risal, L.; Shrestha, S.P. Effects of concentration of triethanolamine and annealing temperature on band gap of thin film of tin sulphide prepared by chemical bath deposition method. *J. Nepal Phys. Soc.* **2016**, *3*, 1–5. [[CrossRef](#)]
204. Safonova, M.; Mellikov, E.; Mikli, V.; Kerm, K.; Revathi, N.; Volobujeva, O. Chemical bath deposition of SnS thin films from the solutions with different concentrations of tin and sulphur. *Adv. Mater. Res.* **2015**, *1117*, 183–186. [[CrossRef](#)]
205. Mahdi, M.S.; Ibrahim, K.; Hmood, A.; Ahmed, N.M.; Azzez, S.A.; Mustafa, F.I. A highly sensitive flexible SnS thin film photodetector in the ultraviolet to near infrared prepared by chemical bath deposition. *RSC Adv.* **2016**, *6*, 114980–114988. [[CrossRef](#)]
206. Chaki, S.H.; Chaudhary, M.D.; Deshpande, M.P. SnS thin films deposited by chemical bath deposition, dip coating and SILAR techniques. *J. Semicond.* **2016**, *37*, 1–9. [[CrossRef](#)]
207. Mahdi, M.S.; Ibrahim, K.; Hmood, A.; Ahmed, N.M.; Mustafa, F.I. Control of phase, structural and optical properties of tin sulfide nanostructured thin films grown via chemical bath deposition. *J. Electron. Mater.* **2017**, *46*, 4227–4235. [[CrossRef](#)]

208. Avellaneda, D.; Sánchez-Orozco, I.; Martínez, J.A.A.; Shaji, S.; Krishnan, B. Thin films of tin sulfides: Structure, composition and optoelectronic properties. *Mater. Res. Express* **2018**, *6*, 016409. [[CrossRef](#)]
209. Cao, M.; Wu, C.; Yao, K.; Jing, J.; Huang, J.; Cao, M.; Zhang, J.; Lai, J.; Ali, O.; Wang, L.; et al. Chemical bath deposition of single crystal SnS nanobelts on glass substrates. *Mater. Res. Bull.* **2018**, *104*, 244–249. [[CrossRef](#)]
210. Patil, A.M.; Lokhande, V.C.; Patil, U.M.; Shinde, P.A.; Lokhande, C.D. High performance all-solid-state asymmetric supercapacitor device based on 3D nanospheres of β -MnO₂ and Nanoflowers of O-SnS. *ACS Sustain. Chem. Eng.* **2018**, *6*, 787–802. [[CrossRef](#)]
211. Gedi, S.; Minnam Reddy, V.R.; Kotte, T.R.R.; Park, Y.; Kim, W.K. Effect of C₄H₆O₆ concentration on the properties of SnS thin films for solar cell applications. *Appl. Surf. Sci.* **2019**, *465*, 802–815. [[CrossRef](#)]
212. Gedi, S.; Minnam Reddy, V.R.; Alhammadi, S.; Reddy Guddeti, P.; Kotte, T.R.R.; Park, C.; Kim, W.K. Influence of deposition temperature on the efficiency of SnS solar cells. *Sol. Energy* **2019**, *184*, 305–314. [[CrossRef](#)]
213. Cabrera-German, D.; García-Valenzuela, J.A.; Cota-Leal, M.; Martínez-Gil, M.; Aceves, R.; Sotelo-Lerma, M. Detailed characterization of good-quality SnS thin films obtained by chemical solution deposition at different reaction temperatures. *Mater. Sci. Semicond. Process.* **2019**, *89*, 131–142. [[CrossRef](#)]
214. Mallika Bramaramba Devi, P.; Phaneendra Reddy, G.; Ramakrishna Reddy, K.T. Structural and optical studies on PVA capped SnS films grown by chemical bath deposition for solar cell application. *J. Semicond.* **2019**, *40*, 052101. [[CrossRef](#)]
215. Mahdi, M.S.; Hmood, A.; Ibrahim, K.; Ahmed, N.M.; Bououdina, M. Dependence of pH on phase stability, optical and photoelectrical properties of SnS thin films. *Superlattices Microstruct.* **2019**, *128*, 170–176. [[CrossRef](#)]
216. Huang, J.; Ma, Y.; Yao, K.; Wu, C.; Cao, M.; Lai, J.; Zhang, J.; Sun, Y.; Wang, L.; Shen, Y. Chemical bath deposition of SnS:In thin films for Pt/CdS/SnS:In/Mo photocathode. *Surf. Coat. Technol.* **2019**, *358*, 84–90. [[CrossRef](#)]
217. Gonzalez-Flores, V.E.; Mohan, R.N.; Ballinas-Morales, R.; Nair, M.T.S.; Nair, P.K. Thin film solar cells of chemically deposited SnS of cubic and orthorhombic structures. *Thin Solid Films* **2019**, *672*, 62–65. [[CrossRef](#)]
218. Mallika Bramaramba Devi, P.; Reddy, G.P.; Reddy, K.T.R. Optical investigations on PVA capped SnS nanocrystalline films deposited by CBD process. *Mater. Res. Express* **2019**, *6*, 115523. [[CrossRef](#)]
219. John, S.; Geetha, V.; Francis, M. Effect of pH on the optical and structural properties of SnS prepared by chemical bath deposition method. *IOP Conf. Ser. Mater. Sci. Eng.* **2020**, *872*, 012139. [[CrossRef](#)]
220. Muthalif, M.P.A.; Choe, Y. Control of the interfacial charge transfer resistance to improve the performance of quantum dot sensitized solar cells with highly electrocatalytic Cu-doped SnS counter electrodes. *Appl. Surf. Sci.* **2020**, *508*, 145297. [[CrossRef](#)]
221. Ben Mbarek, M.; Reghima, M.; Yacoubi, N.; Barradas, N.; Alves, E.; Bundaleski, N.; Teodoro, O.; Kunst, M.; Schwarz, R. Microwave transient reflection in annealed SnS thin films. *Mater. Sci. Semicond. Process.* **2021**, *121*, 105302. [[CrossRef](#)]
222. Marquez, I.G.; Romano-Trujillo, R.; Gracia-Jimenez, J.M.; Galeazzi, R.; Silva-González, N.R.; García, G.; Coyopol, A.; Nieto-Caballero, F.G.; Rosendo, E.; Morales, C. Cubic, orthorhombic and amorphous SnS thin films on flexible plastic substrates by CBD. *J. Mater. Sci. Mater. Electron.* **2021**, 1–9. [[CrossRef](#)]
223. Cao, M.; Zhang, X.; Ren, J.; Sun, Y.; Cui, Y.; Zhang, J.; Ling, J.; Huang, J.; Shen, Y.; Wang, L.; et al. Chemical bath deposition of SnS:Cu/ZnS for solar hydrogen production and solar cells. *J. Alloys Compd.* **2021**, *863*, 158727. [[CrossRef](#)]
224. Higareda-Sanchez, A.; Mis-Fernandez, R.; Rimmaudo, I.; Camacho-Espinosa, E.; Pena, J.L. Evaluation of pH and deposition mechanisms effect on tin sulfide thin films deposited by chemical bath deposition. *Superlattices Microstruct.* **2021**, *151*, 106831. [[CrossRef](#)]
225. Akkari, A.; Regima, M.; Guasch, C.; Kamoun Turki, N. Effect of deposition time on physical properties of nanocrystallized SnS zinc blend thin films grown by chemical bath deposition. *Adv. Mater. Res.* **2011**, *324*, 101–104. [[CrossRef](#)]
226. Akkari, A.; Guasch, C.; Castagne, M.; Kamoun-Turki, N. Optical study of zinc blend SnS and cubic In₂S₃:Al thin films prepared by chemical bath deposition. *J. Mater. Sci.* **2011**, *46*, 6285–6292. [[CrossRef](#)]
227. Akkari, A.; Reghima, M.; Guasch, C.; Kamoun-Turki, N. Effect of copper doping on physical properties of nanocrystallized SnS zinc blend thin films grown by chemical bath deposition. *J. Mater. Sci.* **2012**, *47*, 1365–1371. [[CrossRef](#)]
228. Reghima, M.; Akkari, A.; Guasch, C.; Kamoun-Turki, N. Effect of indium doping on physical properties of nanocrystallized SnS zinc blend thin films grown by chemical bath deposition. *J. Renew. Sustain. Energy* **2012**, *4*, 011602. [[CrossRef](#)]
229. Reghima, M.; Akkari, A.; Guasch, C.; Kamoun, N. Structural, optical, and electrical properties of SnS:Ag thin films. *J. Electron. Mater.* **2015**, *44*, 4392–4399. [[CrossRef](#)]
230. Barrios-Salgado, E.; Rodríguez-Guadarrama, L.A.; Garcia-Angelmo, A.R.; Campos Álvarez, J.; Nair, M.T.S.; Nair, P.K. Large cubic tin sulfide–tin selenide thin film stacks for energy conversion. *Thin Solid Films* **2016**, *615*, 415–422. [[CrossRef](#)]
231. Nair, P.K.; Barrios-Salgado, E.; Nair, M.T.S. Cubic-structured tin selenide thin film as a novel solar cell absorber. *Phys. Status Solidi Appl. Mater. Sci.* **2016**, *213*, 2229–2236. [[CrossRef](#)]
232. Abutbul, R.E.; Garcia-Angelmo, A.R.; Burshtein, Z.; Nair, M.T.S.; Nair, P.K.; Golan, Y. Crystal structure of a large cubic tin monosulfide polymorph: An unraveled puzzle. *CrystEngComm* **2016**, *18*, 5188–5194. [[CrossRef](#)]
233. Sanal, K.C.; Nair, P.K.; Nair, M.T.S. Band offset in zinc oxy-sulfide/cubic-tin sulfide interface from X-ray photoelectron spectroscopy. *Appl. Surf. Sci.* **2017**, *396*, 1092–1097. [[CrossRef](#)]
234. Mahdi, M.S.; Ibrahim, K.; Ahmed, N.M.; Hmood, A.; Mustafa, F.I.; Azzez, S.A.; Bououdina, M. High performance and low-cost UV–Visible–NIR photodetector based on tin sulphide nanostructures. *J. Alloys Compd.* **2018**, *735*, 2256–2262. [[CrossRef](#)]
235. Javed, A.; Bashir, M. Controlled growth, structure and optical properties of Fe-doped cubic π -SnS thin films. *J. Alloys Compd.* **2018**, *759*, 14–21. [[CrossRef](#)]

236. Flores, V.E.G.; Nair, M.T.S.; Nair, P.K. Thermal stability of “metastable” cubic tin sulfide and its relevance to applications. *Semicond. Sci. Technol.* **2018**, *33*. [[CrossRef](#)]
237. Abutbul, R.E.; Golan, Y. Chemical epitaxy of π -phase cubic tin monosulphide. *CrystEngComm* **2020**, *22*, 6170–6181. [[CrossRef](#)]
238. Mahdi, M.S.; Al-Arab, H.S.; Al-Salman, H.S.; Ibrahim, K.; Ahmed, N.M.; Hmood, A.; Bououdina, M. A high-performance near-infrared photodetector based on π -SnS phase. *Mater. Lett.* **2020**, *273*, 127910. [[CrossRef](#)]
239. Javed, A.; Khan, N.; Bashir, S.; Ahmad, M.; Bashir, M. Thickness dependent structural, electrical and optical properties of cubic SnS thin films. *Mater. Chem. Phys.* **2020**, *246*, 122831. [[CrossRef](#)]
240. Barrios Salgado, E.; Lara Llanderal, D.E.; Nair, M.T.S.; Nair, P.K. Thin film thermoelectric elements of p–n tin chalcogenides from chemically deposited SnS–SnSe stacks of cubic crystalline structure. *Semicond. Sci. Technol.* **2020**, *35*, 045006. [[CrossRef](#)]
241. Chalapathi, U.; Poornaprakash, B.; Choi, W.J.; Park, S.-H. Ammonia(aq)-enhanced growth of cubic SnS thin films by chemical bath deposition for solar cell applications. *Appl. Phys. A* **2020**, *126*, 583. [[CrossRef](#)]
242. Rodriguez-Guadarrama, L.A.; Escorcía-García, J.; Alonso-Lemus, I.L.; Campos-Álvarez, J. Synthesis of π -SnS thin films through chemical bath deposition: Effects of pH, deposition time, and annealing temperature. *J. Mater. Sci. Mater. Electron.* **2021**, *32*, 7464–7480. [[CrossRef](#)]
243. Gaitan-Arevalo, J.R.; Gonzalez, L.A.; Escorcía-García, J. Cubic tin sulfide thin films by a Sn-NTA system based chemical bath process. *Mater. Lett.* **2021**, *286*, 129222. [[CrossRef](#)]
244. Eswar Neerugatti, K.; Shivaji Pawar, P.; Heo, J. Differential growth and evaluation of band structure of π -SnS for thin-film solar cell applications. *Mater. Lett.* **2021**, *284*, 129026. [[CrossRef](#)]
245. Ramakrishna Reddy, K.T.; Sreedevi, G.; Miles, R.W. Thickness effect on the structural and optical properties of SnS₂ films grown by CBD process. *J. Mater. Sci. Eng. A* **2013**, *3*, 182–186. [[CrossRef](#)]
246. Chalapathi, U.; Poornaprakash, B.; Purushotham Reddy, B.; Si Hyun, P. Preparation of SnS₂ thin films by conversion of chemically deposited cubic SnS films into SnS₂. *Thin Solid Films* **2017**, *640*, 81–87. [[CrossRef](#)]
247. Zhou, P.; Huang, Z.; Sun, X.; Ran, G.; Shen, R.; Ouyang, Q. Saturable absorption properties of the SnS₂/FTO thin film. *Optik* **2018**, *171*, 839–844. [[CrossRef](#)]
248. Joshi, M.P.; Khot, K.V.; Patil, S.S.; Mali, S.S.; Hong, C.K.; Bhosale, P.N. Investigating the light harvesting capacity of sulfur ion concentration dependent SnS₂ thin films synthesized by self-assembled arrested precipitation technique. *Mater. Res. Express* **2019**, *6*, 086467. [[CrossRef](#)]
249. Noppakudrittidej, P.; Vailikhit, V.; Teesetsopon, P.; Chooon, S.; Tubtimtae, A. Copper incorporation in Mn²⁺ doped Sn₂S₃ nanocrystals and the resultant structural, optical, and electrochemical characteristics. *Ceram. Int.* **2018**, *44*, 13973–13985. [[CrossRef](#)]
250. Mohan, R.N.; Nair, M.T.S.; Nair, P.K. Thin film Sn₂S₃ via chemical deposition and controlled heating—Its prospects as a solar cell absorber. *Appl. Surf. Sci.* **2020**, *504*, 144162. [[CrossRef](#)]
251. Liu, T.; Ke, H.; Zhang, H.; Duo, S.; Sun, Q.; Fei, X.; Zhou, G.; Liu, H.; Fan, L. Effect of four different zinc salts and annealing treatment on growth, structural, mechanical and optical properties of nanocrystalline ZnS thin films by chemical bath deposition. *Mater. Sci. Semicond. Process.* **2014**, *26*, 301–311. [[CrossRef](#)]
252. Salh, A.; Kyeongchan, M.; Hyeonwook, P.; Woo Kyoung, K. Effect of different cadmium salts on the properties of chemical-bath-deposited CdS thin films and Cu(InGa)Se₂ solar cells. *Thin Solid Films* **2017**, *625*, 56–61. [[CrossRef](#)]
253. Hodes, G. *Chemical Solution Deposition of Semiconductor Films*, 1st ed.; Marcel Dekker: New York, NY, USA, 2002; ISBN 0824708512.
254. Jeffery, G.H.; Bassett, J.; Mendham, J.; Denney, R.C. *Vogel's Textbook of Quantitative Inorganic Analysis*; ELBS Publ.: London, UK, 1989.
255. Flaschka, H.A. *EDTA Titrations. An Introduction to Theory and Practice*; Macmillan: New York, NY, USA, 1959.
256. Kaur, I. Growth kinetics and polymorphism of chemically deposited CdS films. *J. Electrochem. Soc.* **1980**, *127*, 943. [[CrossRef](#)]
257. Donna, J.M. Chemical bath deposition of CdS thin films: Electrochemical in situ kinetic studies. *J. Electrochem. Soc.* **1992**, *139*, 2810. [[CrossRef](#)]
258. Gonzalez Panzo, I.J.; Martin Varguez, P.E.; Oliva, A.I. Role of thiourea in the kinetic of growth of the chemical bath deposited ZnS films. *J. Electrochem. Soc.* **2014**, *161*, D761–D767. [[CrossRef](#)]
259. Kumarage, W.G.C.; Wijesundara, L.B.D.R.P.; Seneviratne, V.A.; Jayalath, C.P.; Dassanayake, B.S. Influence of bath temperature on CBD-CdS thin films. *Procedia Eng.* **2016**, *139*, 64–68. [[CrossRef](#)]
260. Bayon, R.; Hernandez-Mayoral, M.; Herrero, J. Growth mechanism of CBD-In(OH)_xS_y thin films. *J. Electrochem. Soc.* **2002**, *149*, C59–C67. [[CrossRef](#)]
261. Cortes, A.; Gómez, H.; Marotti, R.E.; Riveros, G.; Dalchiale, E.A. Grain size dependence of the bandgap in chemical bath deposited CdS thin films. *Sol. Energy Mater. Sol. Cells* **2004**, *82*, 21–34. [[CrossRef](#)]
262. Balasubramanian, V.; Suriyanarayanan, N.; Prabakar, S. Thickness-dependent structural properties of chemically deposited Bi₂S₃ thin films. *Adv. Applied Sci. Res.* **2012**, *3*, 2369–2373.
263. Patil, S.A.; Mengal, N.; Memon, A.A.; Jeong, S.H.; Kim, H.S. CuS thin film grown using the one pot, solution-process method for dye-sensitized solar cell applications. *J. Alloys Compd.* **2017**, *708*, 568–574. [[CrossRef](#)]
264. Gupta, V.; Mansingh, A. Influence of postdeposition annealing on the structural and optical properties of sputtered zinc oxide film. *J. Appl. Phys.* **1996**, *80*, 1063–1073. [[CrossRef](#)]
265. Jin Hong, L.; Byung Ok, P. Transparent conducting In₂O₃ thin films prepared by ultrasonic spray pyrolysis. *Surf. Coat. Technol.* **2004**, *184*, 102–107. [[CrossRef](#)]

266. Brien, P.O.; Mcaleese, J. bath deposition of ZnS and CdS. *Technology* **1998**, *8*, 2309–2314. [[CrossRef](#)]
267. Avrami, M. Granulation, phase change, and microstructure kinetics of phase change. III. *J. Chem. Phys.* **1941**, *9*, 177–184. [[CrossRef](#)]
268. Phillips, J.M. Substrate selection for thin-film growth. *MRS Bull.* **1995**, *20*, 35–39. [[CrossRef](#)]
269. Vasudeva Reddy, M.; Sreedevi, G.; Chinho, P.; Miles, R.W.; Ramakrishna Reddy, K.T. Development of sulfurized SnS thin film solar cells. *Curr. Appl. Phys.* **2015**, *15*, 588–598. [[CrossRef](#)]
270. Devika, M.; Koteeswara Reddy, N.; Ramesh, K.; Ganesan, V.; Gopal, E.S.R.; Ramakrishna Reddy, K.T. Influence of substrate temperature on surface structure and electrical resistivity of the evaporated tin sulphide films. *Appl. Surf. Sci.* **2006**, *253*, 1673–1676. [[CrossRef](#)]
271. Vasudeva Reddy, M.; Sreedevi, G.; Babu, P.; Ramakrishna Reddy, K.T.; Guillaume, Z.; Chinho, P. Influence of different substrates on the properties of sulfurized SnS films. *Sci. Adv. Mater.* **2016**, *8*, 247–251. [[CrossRef](#)]
272. Camacho Espinosa, E.; Oliva Aviles, A.I.; Oliva, A.I. Effect of the substrate cleaning process on pinhole formation in sputtered CdTe films. *J. Mater. Eng. Perform.* **2017**, *26*, 4020–4028. [[CrossRef](#)]
273. Tarkeshwar, S.; Devjyoti, L.; Ayush, K. Effects of various parameters on structural and optical properties of CBD-grown ZnS thin films: A review. *J. Electron. Mater.* **2018**, *47*, 1730–1751. [[CrossRef](#)]
274. Hubert, C.; Naghavi, N.; Roussel, O.; Etcheberry, A.; Hariskos, D.; Menner, R.; Powalla, M.; Kerrec, O.; Lincot, D. The Zn(S,O,OH)/ZnMgO buffer in thin film Cu(In,Ga)(S,Se)₂-based solar cells part I: Fast chemical bath deposition of Zn(S,O,OH) buffer layers for industrial application on co-evaporated Cu(In,Ga)Se₂ and electrodeposited CuIn(S,Se)₂ solar cells. *Prog. Photovolt. Res. Appl.* **2009**, *17*, 470–478. [[CrossRef](#)]
275. Li, Z.Q.; Shi, J.H.; Liu, Q.Q.; Wang, Z.A.; Sun, Z.; Huang, S.M. Effect of [Zn]/[S] ratios on the properties of chemical bath deposited zinc sulfide thin films. *Appl. Surf. Sci.* **2010**, *257*, 122–126. [[CrossRef](#)]